



Bergische Universität Wuppertal
Fachbereich C - Mathematik und Naturwissenschaften

Chlorine Activation and Heterogeneous Chemistry in the Polar Stratosphere: Model Simulations, In-Situ- and Satellite Observations

Dissertation zur Erlangung des Grades
“Doktor der Naturwissenschaften”
(Dr. rer. nat.)

vorgelegt von Tobias Wegner
geboren am 31.10.1983 in Essen

Die Dissertation kann wie folgt zitiert werden:

urn:nbn:de:hbz:468-20130607-103013-5

[<http://nbn-resolving.de/urn/resolver.pl?urn=urn%3Anbn%3Ade%3Ahbz%3A468-20130607-103013-5>]

Eidesstattliche Erklärung

Hiermit versichere ich, die Arbeit selbständig verfasst zu haben, nur die in der Dissertation angegebenen Hilfsmittel benutzt und alle wörtlich oder inhaltlich übernommenen Stellen als solche gekennzeichnet zu haben, und dass die Dissertation in der gegenwärtigen oder einer anderen Fassung noch keinem anderen Fachbereich, keiner Gesamthochschule und keiner anderen wissenschaftlichen Hochschule vorgelegen hat.

Tobias Wegner

Abstract

This work examines heterogeneous processes in climate models, in-situ- and satellite observations, with focus on chemical reactions that lead to activation of chlorine in the polar stratosphere. Parameterizations for these heterogeneous reactions are validated against in-situ measurements for atmospheric conditions where either the availability of a reaction partner or the prevailing temperature controls the extent of observed levels of active chlorine. The parameterizations for heterogeneous chemistry are shown to give an excellent representation of processes in the atmosphere, but the surfaces these reactions occur on are subject to some uncertainty. Heterogeneous reactions in the polar stratosphere take place on either Polar Stratospheric Clouds (PSCs) or the background sulfate aerosol, with the surface area of solid PSC particles contributing most to overall uncertainty. However, this work shows that PSC only have a minor effect on chlorine activation, and satellite observations from seven years of the entire polar vortex indicate no correlation between PSC coverage and the rate of chlorine activation.

The representation of PSCs is further investigated with the coupled-climate model SD-WACCM and satellite observations. Best representation of PSC processes in SD-WACCM is achieved when the amount of gas-phase HNO_3 allowed to form solid PSC particles is limited. This and other changes lead to an improved representation of the temperature-dependence of PSCs in SD-WACCM, compared to satellite observations.

Although PSCs and heterogeneous reactions are accurately represented in SD-WACCM, the development of gas-phase HCl , a proxy for chlorine activation, is substantially slower in the model than observations suggest. Established and novel processes that lead to removal of gas-phase HCl are examined, and the only process capable of reproducing the observations is the uptake of HCl into liquid PSC particles. A parameterization for the solubility of HCl in liquid PSC particles gives a very good representation of the temperature-dependence of removal of gas-phase HCl , but is very sensitive to temperature and ambient water vapor. Since the removal of HCl from the gas-phase by PSC particles presents a major, although temporary sink during the polar night, removal of gas-phase HCl cannot serve as an indicator for chlorine activation. This presents a major change in paradigm regarding chlorine chemistry in the polar vortex.

Zusammenfassung

Diese Arbeit befasst sich mit heterogenen Reaktionen, welche zur Aktivierung von Chlor in der polaren Stratosphäre führen. Hierzu werden Atmosphärenmodelle, In-situ- und Satellitendaten betrachtet. Parametrisierungen für diese Reaktionen werden mit In-situ Messungen validiert. Die Messungen wurden unter atmosphärischen Bedingungen durchgeführt, bei denen entweder die Verfügbarkeit von einem Reaktionspartner oder die Temperatur das Ausmaß der beobachteten Chloraktivierung kontrollierte. Es kann gezeigt werden, dass die Parametrisierungen der heterogenen Chemie die Prozesse in der Atmosphäre sehr gut wiedergeben können. Allerdings sind die Oberflächen, auf denen die heterogene Reaktionen ablaufen, großer Unsicherheit unterworfen. Die Oberfläche in der polaren Stratosphäre wird von Polaren Stratosphärenwolken (PSCs) und dem Hintergrundaerosol bestimmt, wobei die größte Unsicherheit von festen PSC Partikeln ausgeht. Diese Arbeit zeigt, dass PSCs nur geringen Einfluss auf Chloraktivierung haben und Satellitenbeobachtungen des polaren Vortex über den Zeitraum von sieben Jahren zeigen keine Korrelation zwischen dem Auftreten von PSCs und Chloraktivierung.

Des Weiteren wird die Darstellung von PSCs mit dem gekoppelten Klimamodell SD-WACCM und Satellitenbeobachtungen untersucht. Die beste Darstellung von PSC Prozessen in SD-WACCM wird erreicht, wenn die Menge an HNO_3 welche feste PSCs formen kann limitiert wird. Diese und weitere Änderungen führen, im Vergleich mit Satellitendaten, zu einer verbesserten Darstellung der Temperaturabhängigkeit von PSCs in SD-WACCM.

Obwohl SD-WACCM PSCs und heterogene Reaktionen korrekt wiedergibt, ist die Entwicklung von Gasphasen HCl, einem Indikator für Chloraktivierung, im Modell wesentlich langsamer als in den Beobachtungen. Bewährte und neue Prozessen, welche HCl aus der Gasphase entfernen können, werden untersucht. Der einzige Prozess, welcher die Entfernung von HCl aus der Gasphase erklären kann, ist die Aufnahme von HCl in flüssige PSC Teilchen. Die Parametrisierung der Löslichkeit von HCl in PSC Teilchen zeigt sehr gute Übereinstimmung mit der beobachteten Temperaturabhängigkeit. Allerdings ist dieser Prozess äußerst sensitiv auf Wasserdampf und Temperatur. Da die Löslichkeit von HCl in PSC Teilchen während der Polarnacht die größte, wenn auch temporäre Senke für HCl darstellt, kann eine Abnahme von HCl in der Gasphase nicht als Indikator für Chloraktivierung herangezogen werden. Dieses stellt einen Paradigmenwechsel für die Betrachtung von Chlorchemie im polaren Vortex dar.

Contents

1. Introduction	8
2. Halogen Chemistry	11
2.1. Gas-Phase Chemistry	11
2.2. Chlorine Activation and Deactivation	14
3. Polar Stratospheric Clouds and Stratospheric Aerosol	16
3.1. Background Aerosol	16
3.2. Polar Stratospheric Clouds	17
3.2.1. Supercooled Ternary Solutions	17
3.2.2. Nitric Acid Trihydrate	19
3.2.3. Ice Clouds	20
4. Heterogeneous Chemistry	21
4.1. Introduction to Heterogeneous Chemistry	21
4.2. Modeling γ for Stratospheric Aerosols	23
4.3. Heterogeneous Reaction Rates	25
5. The Influence of PSCs and the Background Aerosol on Chlorine Activation	28
5.1. In-situ Observations from March 2005	29
5.1.1. Deriving the Initialization	29
5.1.2. Estimating the Temperature Error	30
5.1.3. Modeling PSCs along Trajectories	31
5.1.4. Estimating the Influence of PSCs on Chlorine Activation	33
5.2. In-Situ Observations from the RECONCILE Campaign	34
5.3. Intra- and Interannual Variability of Chlorine Activation and PSC Occurrence	36
5.3.1. Variability of HCl and HNO ₃ Loss	36

5.3.2. Probability Density Distribution of Maximum Surface Area Enhancement by PSCs	38
5.4. Conclusions	40
6. Polar Stratospheric Clouds in SD-WACCM	42
6.1. Type I Polar Stratospheric Clouds	42
6.1.1. Observations and Reference Simulation	42
6.1.2. Test Simulation	47
6.2. Type II PSCs	52
6.2.1. Observations and Reference Simulation	52
6.2.2. Test Simulation	54
6.3. Conclusions	56
7. Chlorine Partitioning in SD-WACCM	58
7.1. Description of SD-WACCM Simulations	58
7.2. Depletion of Gas-Phase HCl	60
7.2.1. Observations and the BASE Simulation	60
7.2.2. Photolysis of Gas-Phase HNO ₃	65
7.2.3. Galactic Cosmic Rays	65
7.2.4. Photolysis of Condensed Phase HNO ₃	66
7.2.5. Constraining HCl Solubility from Observations	68
7.3. Modeling HCl Solubility in STS	72
7.4. The Combined Effect of J _{HNO₃(c)} , H _{HCl} and the Temperature Bias	75
7.4.1. Observations of Active Chlorine	76
7.5. Ozone Loss	78
7.6. Conclusions	79
8. Summary	82
A. Appendix	84
A.1. Model Descriptions	84
A.1.1. Chemical Lagrangian Model of the Stratosphere	84
A.1.2. Specified Dynamics - Whole Atmosphere Community Climate Model	84
A.2. Instrument Descriptions	87
A.2.1. Microwave Limb Sounder	87
A.2.2. Atmospheric Chemistry Experiment - Fourier Transform Spectrometer	87

List of Figures	89
List of Tables	94
Glossary	95
Bibliography	97

1. Introduction

The discovery of the Antarctic “ozone hole” by Farman et al. (1985) marked a key event for the atmospheric sciences. Ozone absorbs radiation in the ultraviolet, effectively shielding the surface of the Earth. The impact of halogenated, aliphatic hydrocarbons on ozone was already discussed in the landmark publication by Molina and Rowland (1974). Nevertheless, the magnitude of ozone loss discovered in the Antarctic stratosphere in 1985 was unexpected. Space-borne observations (Stolarski et al., 1986) quickly confirmed the observations by Farman et al. (1985), and revealed the spatial extent of the ozone hole, which in polar spring covers the entire Antarctic continent. Subsequent research revealed the mechanisms responsible for the destruction of stratospheric ozone over Antarctica (Solomon, 1999). A complex interplay of meteorology, radiative transfer, gas- and heterogeneous chemistry and aerosol micro-physics is necessary to produce the ozone hole. However, the primary culprit for the formation of the ozone hole was the unregulated emission of Chlorofluorocarbons (CFCs)

CFCs themselves are practically chemically inert in the troposphere. This allows these compounds to penetrate high into the stratosphere. The long atmospheric lifetime of several decades is determined by the photochemical loss in the stratosphere (World Meteorological Organization, 2011). The ultraviolet radiation in the middle atmosphere finally breaks the CFC bond, releasing Cl radicals. However, these radicals are quickly converted into the chlorine reservoir species HCl and ClONO₂. Under the conditions prevailing in the polar vortex, these reservoir gases are converted back into photo-labile chlorine species, which then drive the catalytic ozone loss cycles. During the polar night inside the polar vortex, temperatures can drop to below 195 K (−78°C), allowing the formation of Polar Stratospheric Clouds (PSCs). HCl and ClONO₂ become highly soluble in stratospheric aerosols at such low temperatures, allowing for heterogeneous reactions on the surfaces and inside the bulk of PSCs, followed by the release of Cl₂ (Solomon et al., 1986). At the same time HNO₃ nucleates to solid particles (Nitric Acid Trihydrate, NAT), that are large enough to sediment and denitrify the lower stratosphere (Fahey et al., 2001).

Once the sun illuminates the polar regions again in spring, Cl_2 is photolyzed to Cl radicals, which drive the catalytic ozone loss cycles, mainly via the ClO-dimer cycle (Molina and Molina, 1987). This cycle can be terminated by the reaction of ClO with NO_2 . But as HNO_3 has been effectively removed from the lower stratosphere by PSCs, NO_2 is not available, and the ClO-Dimer cycle can continue until it is terminated through the reaction of Cl with CH_4 (Douglass et al., 1995; Grooß et al., 2011). However, this reaction does not occur until ozone is almost completely depleted. All these processes take place inside the polar vortex which presents a transport barrier, and prevents mixing of polar and mid-latitude air. After the vortex breaks up, usually in late spring, the ozone poor air masses are transported to lower latitudes and mixed in, which results in a decrease of hemispheric mid-latitude ozone in the stratosphere.

The research of the ozone hole showed for the first time that anthropogenic emissions of trace gases have the potential to globally alter the composition of the atmosphere, and negatively impact the biosphere (e.g. Sweet et al., 2012). The risk of increased ultraviolet radiation on the surface prompted the ratification of the Montreal protocol in 1987 and its later amendments and adjustments (London (1990), Copenhagen (1992), Vienna (1995), Montreal (1997) and Beijing (1999)). Until today it is the most successful multilateral agreement for the protection of Earth's atmosphere. Its aim "*... to protect the ozone layer by taking precautionary measures to control equitably total global emissions of substances that deplete it, with the ultimate objective of their elimination on the basis of developments in scientific knowledge...*" led to the ban of CFCs and related compounds. Thanks to this agreement, the stratospheric chlorine burden peaked in the middle of the nineties and started to decrease since then (World Meteorological Organization, 2011). Newman et al. (2009) have shown what the atmosphere of the Earth would have looked like if CFC emission were allowed to rise unrestricted. Their model predicts almost complete, global destruction of the ozone layer by the middle of this century. A "World Avoided" owing to the Montreal protocol.

During the past decade the annual occurrence of the "ozone hole" over the Antarctic continent was mostly unnoticed by the public, but the record ozone depletion over the Arctic in 2010/11 (Manney et al., 2011) brought the "ozone hole" once again back into public focus. The increase in ozone depletion over the Arctic was connected to the increase in global mean temperature (Rex et al., 2006). While the basic processes behind the "ozone hole" are well understood, some questions remain open. The EU-FP7 project RECONCILE was established in 2008 to better constrain important parameters responsible for ozone depletion.

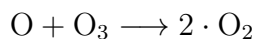
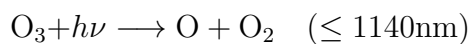
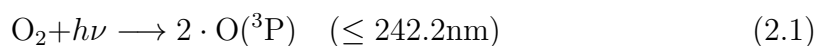
The purpose of this work is to gain a better understanding of the heterogeneous processes and the aerosols these occur on. The prevailing opinion is that heterogeneous reactions mainly occur on the surfaces of PSCs, but recently Drdla and Müller (2012) concluded that chlorine activation through heterogeneous chemistry is dominated by reactions on the background aerosol. With the current high chlorine loading in the stratosphere and a deliberate enhancement of the stratospheric aerosol layer being discussed to counter a temperature increase at the surface (Crutzen, 2006), understanding the role of the background aerosol for chlorine activation is essential.

Thus, in Chapters 4 and 5 the parameterizations for heterogeneous reactions in atmospheric models are discussed and validated against in-situ measurements. In addition, the influence of the various aerosols in the stratosphere on chlorine activation is analyzed, with special focus on the background aerosol and its potential for chlorine activation. Chapters 6 and 7 extend this analysis to the Whole Atmosphere Community Climate Model (WACCM), a coupled climate model. Chapter 6 discusses the representation of PSCs and improvements of the PSC scheme in WACCM done in this work. Chapter 7 then focuses on chlorine activation in the Antarctic vortex 2005. This analysis will show that the decrease in chlorine reservoir species cannot be explained with chlorine activation alone. Chapter 7 will discuss the impact of NO_x sources in the stratosphere, and offer an alternate explanation, beside chlorine activation, for the observed decrease in chlorine reservoir species.

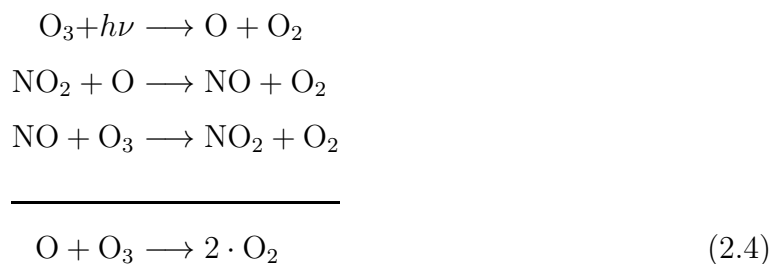
2. Halogen Chemistry

2.1. Gas-Phase Chemistry

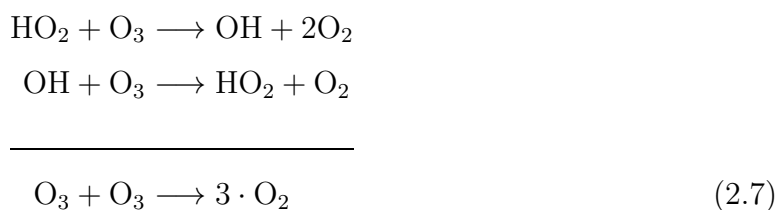
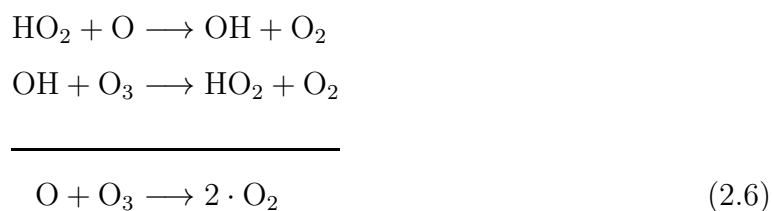
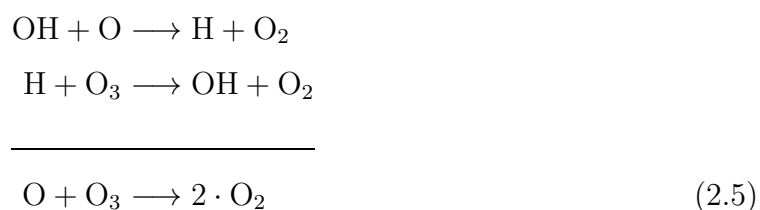
Stratospheric ozone is primarily produced by the photo-dissociation of molecular oxygen and subsequent recombination of atomic with molecular oxygen. Production of ozone has its maximum in the tropics where solar radiation is strongest. The first cycle describing production and depletion for ozone was formulated in 1930 by Chapman (1930), the so called “Chapman-cycle”



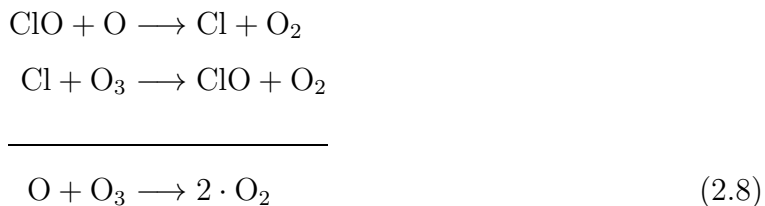
In the 1970s additional ozone loss cycles were discovered. The most important reactions are catalytic cycles involving NO_x ($\text{NO}+\text{NO}_2$), HO_x ($\text{OH}+\text{HO}_2$) and halogen radicals. Crutzen (1970) discovered the NO_x cycle, which is the most important ozone loss cycle above 40 km



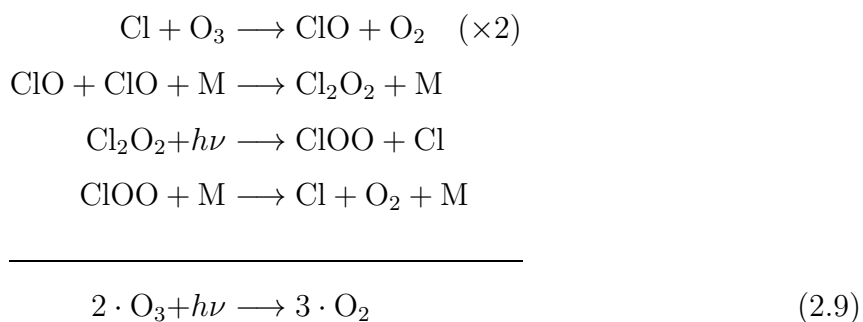
Ozone loss below 45 km is dominated by the HO_x cycles (Bates and Nicolet, 1950).



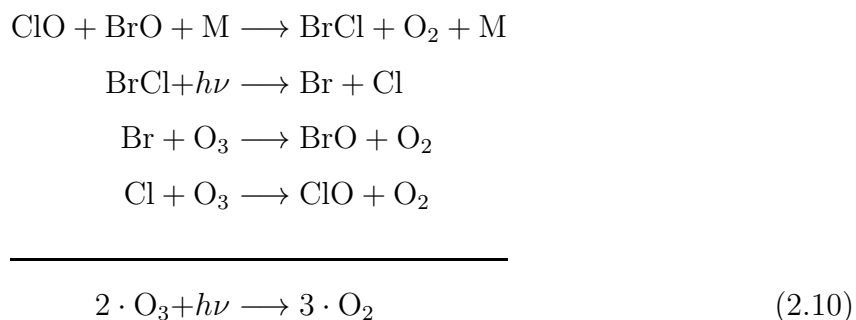
The chlorine cycle is most important at altitudes between 25-35 km (Molina and Rowland, 1974).



Molina and Rowland (1974) correctly predicted the ozone budget in the upper stratosphere, but none of these cycles could explain the occurrence of the “ozone hole”. Only with the discovery of the ClO-Dimer cycle could the ozone loss in the polar regions be explained (Molina and Molina, 1987).



The rate limiting step of this cycle is the photolysis of Cl_2O_2 , which is still subject to some uncertainty and ongoing research (von Hobe et al., 2007; Kawa et al., 2009; Sumińska-Ebersoldt et al., 2012). However, today it is established that this cycle is the main driving factor behind the “ozone hole”. Similar cycles exist for other halogen oxides like BrO (McElroy et al., 1986).



However, halogen oxides (e.g. ClO_x) do not readily occur in the stratosphere. The main reservoir species for halogens in the stratosphere are hydrogen (HX) and nitrate compounds (XONO_2). Only during the polar night inside the vortex are these reservoir species converted to halogen oxides, a process referred to as chlorine activation.

2.2. Chlorine Activation and Deactivation

Solomon et al. (1986) proposed that chlorine reservoir species are heterogeneously converted into ClO_x on the surfaces of PSCs. Overviews of chlorine partitioning can be found in Portmann et al. (1996), Solomon et al. (1996) and Solomon (1999). Three reactions proved to be the main pathway from inorganic to active chlorine.

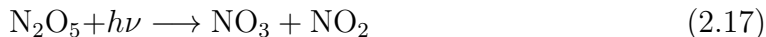


Reaction 2.11 is the most important pathway for chlorine activation. Assuming all HOCl is produced via reaction 2.12, the stoichiometric of chlorine activation would be 1:1 in HCl:ClONO₂. Although HCl is by up to a factor of three more abundant than ClONO₂ in the lower stratosphere, complete depletion of HCl is regularly observed in the Antarctic and for very cold winters in the Arctic polar vortex (Manney et al., 2011; Brakebusch et al., 2012).

The regeneration of the reservoir species occurs by the reaction of ClO with NO₂.



The limiting factor in the regeneration of ClONO₂ is the availability of NO_x, which is primarily formed through the photolysis of HNO₃ and the reaction with OH. The nighttime reservoir for NO_x is N₂O₅, and its formation is limited during the polar night depending on the air parcel's residence in dark regions.



N_2O_5 can also react heterogeneously with H_2O ; thus, remove NO_x , or directly with HCl resulting in additional chlorine activation.



A detailed discussion of ClONO_2 regeneration and HCl sinks may be found in chapter 7. Reaction 2.14 also presents a pathway to deactivate active chlorine (Müller et al., 1994; Douglass et al., 1995). At higher temperatures, when reaction 2.14 is faster than reaction 2.11 and 2.12 a net deactivation occurs. This usually occurs in the Arctic vortex, which generally is dynamically more active and warmer than its Antarctic counterpart. In the Antarctic, once ozone reaches very low values, the abundance of Cl -radicals increases, causing deactivation into HCl (Grooß et al., 2011).



The main open questions regarding heterogeneous chemistry in the polar vortex concerns the composition of the aerosols these reactions occur on. The impact of an unperturbed aerosol layer on heterogeneous processing was first discussed by Rodriguez et al. (1988), and recently Drdla and Müller (2012) proposed that the surface area provided by Polar Stratospheric Clouds is not needed to cause chlorine activation, but that the background aerosol alone is sufficient to explain the observed activation of chlorine.

3. Polar Stratospheric Clouds and Stratospheric Aerosol

The main aerosols in the stratosphere are the ubiquitous sulfate background aerosol and Polar Stratospheric Clouds (PSCs). In contrast to the background aerosol, PSCs only occur over the pole of the winter hemisphere when temperatures drop below a certain threshold.

3.1. Background Aerosol

First direct observational evidence for an aerosol layer in the stratosphere was obtained by Junge et al. (1961). From in-situ samples Junge et al. (1961) concluded that this aerosol layer is composed of sulfuric acid - water droplets. A thorough review of stratospheric aerosol can be found in the SPARC - Assessment of Stratospheric Aerosol Properties (ASAP; WMO/ICSU/IOC World Climate Research Programme, 2006). The stratospheric aerosol layer extends through the middle atmosphere up to 35 km. At greater altitudes, the higher temperatures and lower pressure cause complete evaporation of the aerosol particles. Only large scale volcanic eruptions, reaching up into the stratosphere, can cause significant short-term perturbations of the aerosol layer. In the absence of such eruptions the stratospheric aerosol is assumed to be in background conditions. Deshler (2008) shows that the integrated backscatter from ground based LIDAR measurements increased by two orders of magnitude after the eruptions of El Chichón in 1982 and Mt. Pinatubo in 1991. After such eruptions the return to background levels takes about 5 years. However, since the last decade was volcanically quiescent, the background aerosol layer is close to background conditions. Nevertheless, observations show a small positive trend of the stratospheric aerosol layer which is attributed to a series of minor volcanic eruptions (Solomon et al., 2011; Vernier et al., 2011).

The importance of the stratospheric aerosol layer on Earth's climate is twofold. First, the sulfuric acid aerosol reflects sunlight, impacting the radiative balance. The high

reflectivity results in a net cooling of the atmosphere (IPCC; Working Group I, 2007). Second, the background aerosol provides surface area for heterogeneous reactions, which play a major role in the depletion of stratospheric ozone. The impact of a volcanically enhanced aerosol layer on ozone was especially visible after the eruptions of El Chichón (Hofmann and Solomon, 1989) and Mt. Pinatubo (Portmann et al., 1996; Tilmes et al., 2008).

3.2. Polar Stratospheric Clouds

Polar Stratospheric Clouds (PSCs) are a unique feature of the polar vortex. Here, temperatures are low enough to cause condensation and nucleation of HNO_3 and H_2O . PSCs are principally divided into two categories. First, liquid particles which form when HNO_3 starts to condense on the background aerosol to create Supercooled Ternary Solution droplets (STS; Type Ib). Second, solid particles composed of Nitric Acid Trihydrate (NAT; Type Ia) and water ice (Type II). PSC micro-physics and chemistry were reviewed by Lowe and MacKenzie (2008) and more recently by Peter and Grooß (2012). Satellite and ground-based LIDAR observations show that PSCs are usually composed of mixtures of the various particle types (Pitts et al., 2009, 2011; Khosrawi et al., 2011; Lambert et al., 2012).

3.2.1. Supercooled Ternary Solutions

Supercooled Ternary Solutions (STS) are liquid aerosols composed of a temperature-dependent mixture of H_2SO_4 , HNO_3 and H_2O . Dye et al. (1990, 1992) reported in-situ measurements of HNO_3 containing particles at higher temperatures than the nucleation of NAT is expected, concluding that these particles must be liquid. This conclusion was corroborated by Carslaw et al. (1994); Drdla et al. (1994), who could reproduce the observed temperature-dependence of particle volume with a thermodynamic model for STS. This thermodynamic model for STS is described in detail in Carslaw et al. (1995a). However, the iteration procedure is computationally costly so CTMs and CCMs use analytic expressions that are valid for the typical range of stratospheric conditions (Tabazadeh et al., 1994b; Carslaw et al., 1995b).

Current models assume an instantaneous thermodynamic equilibrium between gas and condensed phase and a log-normal size distribution of STS particles. Figure 3.1 shows the composition of STS predicted by the Carslaw et al. (1995b) parameterization.

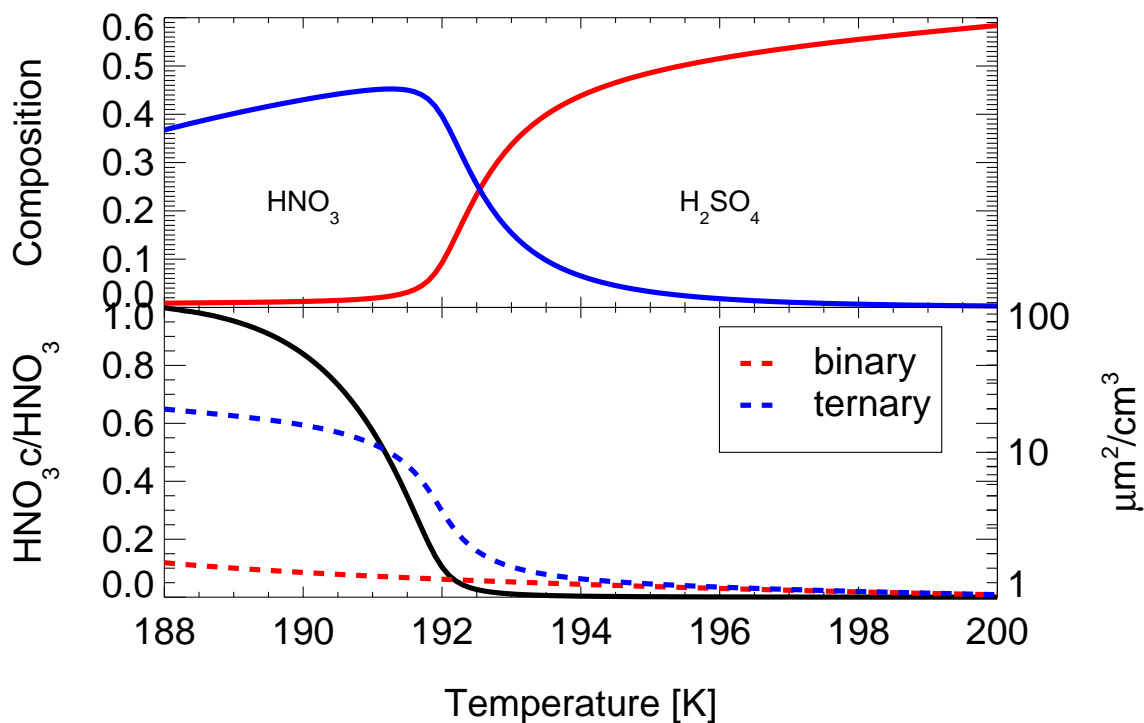


Figure 3.1.: Top: STS composition as function of temperature; Solid red marks the fraction of H₂SO₄ and solid blue the fraction of HNO₃. Bottom: Surface area density as function of temperature; Dashed red line marks the SAD for binary aerosol and blue dashed for STS. Solid black line marks the condensed fraction of HNO₃. Composition and SAD are calculated with the thermodynamic model of Carslaw et al. (1995b) for typical stratospheric conditions (50 hPa, 15 ppbv HNO₃, 4.5 ppbv H₂O and 0.15 ppbv H₂SO₄).

The aerosol consists of about 50% H₂O with varying fractions of HNO₃ and H₂SO₄ throughout the entire temperature range. At about 193 K HNO₃ starts to condense on the background aerosol, and below 192 K HNO₃ and H₂O have become the major constituents of STS. At these temperatures the fraction of H₂SO₄ becomes negligible. The formation of STS is accompanied by a drastic increase in surface area density (SAD, Figure 3.1, lower panel). Compared to the background aerosol, SAD increases tenfold with the uptake of HNO₃. The impact of this increase on heterogeneous activation of chlorine is further discussed in Chapter 5. This increase occurs over the very narrow temperature range between 193 and 191 K, which illustrates the temperature sensitivity of STS formation. Despite this large increase in SAD, STS droplets are assumed to be too small to be affected by gravitational settling; thus, do not lead to a vertical redistribution of HNO₃.

3.2.2. Nitric Acid Trihydrate

Nitric Acid Trihydrate (NAT, Voigt et al., 2000; Spang et al., 2005) and ice particles are the solid constituents of PSCs. These particles can form once the temperature drops below the respective thermodynamic equilibrium temperature. The thermodynamic equilibrium temperature for NAT (T_{NAT}) is reported, based on laboratory measurements, by Hanson and Mauersberger (1988), and at 20 km it corresponds to about 195 K. However, the formation of NAT is usually not observed at T_{NAT} , but observations suggest that a certain supersaturation is needed before NAT nucleates (Dye et al., 1990, 1992).

Modeling the nucleation of NAT particles presents a major challenge for current atmospheric models, since the nucleation mechanism itself is still subject to great uncertainty. The most primitive approach assumes thermodynamic equilibrium for NAT particles. Once a certain supersaturation is reached, NAT is assumed to be formed instantly at a prescribed number density and size distribution. Variations of this approach are described in Considine et al. (2000) and Davies et al. (2003). A more sophisticated approach explicitly models the nucleation and growth of NAT particles. Typically in this approach, a fixed nucleation rate is assumed (Voigt et al., 2005), and growth and evaporation is simulated as a function of supersaturation (Carslaw et al., 2002). Since this approach is computationally more costly, it is usually only used in CTMs (Grooß et al., 2005; Davies et al., 2006; Feng et al., 2011). A third approach, currently in development (Hoyle et al., 2012; Engel et al., 2012), describes the nucleation rate as function of condensation nuclei and supersaturation. From all approaches the last one is in best agreement with CALIPSO observations in terms of PSC composition. Chapter 6 describes the PSC scheme in the Whole Atmosphere Community Climate Model (WACCM) in more detail, and discusses how the scheme could be further improved in this work.

The challenge for models is not only to give a representation of PSC composition, but also to model the vertical distribution of odd nitrogen (NO_y). NAT particles can grow to such large sizes that their sedimentation causes a rapid removal of HNO_3 from the lower stratosphere, so-called denitrification. First observational evidence of these NAT “rocks” is described in Fahey et al. (2001). The correct representation of denitrification is a necessity for correctly modeling ozone depletion, since denitrification will suppress chlorine deactivation. With less NO_2 becoming available through the photolysis of HNO_3 (reaction 2.15), chlorine deactivation via reaction 2.14 is slowed down, which results in more ozone depletion through the ClO-Dimer and ClO-BrO cycles (Reactions 2.9 and 2.10).

NAT particles also provide surface area for heterogeneous reactions. However, the surface area computed from observed NAT particle number densities is small compared to STS and the background aerosol. Furthermore, there is considerable uncertainty about the temperature-dependent γ -value for important heterogeneous reactions on NAT (Peter, 1997). This suggests a negligible role of NAT for the activation rate of chlorine. The importance of NAT in terms of chlorine activation compared to STS and the background aerosol is elucidated in detail in Chapter 5.

3.2.3. Ice Clouds

Ice clouds present another major PSC type. The thermodynamic equilibrium temperature for ice, the frost point (T_{ICE}), is about 188 K at 20 km altitude. Murphy and Koop (2005) present an overview of parameterizations for the frost point, dated between 1946 (Goff and Gratch, 1946) and 2005 (Murphy and Koop, 2005). Differences between the frost point parameterization for stratospheric conditions are less than 0.2 K. These low temperatures usually only occur in the Antarctic stratosphere. However, some winters in the Arctic, e.g. 2009/2010, also exhibited temperatures below the frost point, leading to the formation of ice PSCs (e.g., Pitts et al., 2011; Khosrawi et al., 2011). Ice clouds are further distinguished into synoptic scale clouds and wave ice. Wave ice occurs when air masses are adiabatically lifted by mountains, which induces dramatic cooling rates (Carslaw et al., 1998; Luo et al., 2003), while synoptic scale ice clouds form when air masses are cooled below the frost point over a period of days. Analogous to NAT causing denitrification, ice PSCs lead to a severe dehydration of the stratosphere (Kelly et al., 1989). While ice PSCs do provide additional surface area for heterogeneous reactions, by the time this type of cloud forms, heterogeneous chemistry on other PSC types is already fast enough, so that the additional surface area has no significant effect on reaction rates. This is further discussed in Chapter 5. The representation of ice clouds in WACCM and the impact of dehydration on chlorine partitioning is presented in Chapters 6 and 7.

4. Heterogeneous Chemistry

Heterogeneous chemistry describes reactions that occur at the interface between phases. In the stratosphere these reactions occur on the surfaces of stratospheric aerosols and in their bulk phase, thus on the gas/liquid and gas/solid interface. Heterogeneous reactions in the stratosphere were unknown prior to the discovery of the ozone hole, but were rapidly recognized as a crucial element necessary to explain polar ozone depletion (Solomon et al., 1986). This chapter gives an introduction to heterogeneous chemistry and its incorporation into atmospheric models.

4.1. Introduction to Heterogeneous Chemistry

Numerous processes are involved in the interaction between gaseous molecules and liquid particles (Figure 4.1). Following the collision of a gas molecule with the liquid interface, the gas molecule can be adsorbed on the surface. The probability of a collision leading to adsorption is described by the mass accommodation coefficient α .

$$\alpha = \frac{\text{collisions leading to adsorption}}{\text{total collisions}} \quad (4.1)$$

Further possible interactions of a gas molecule with the liquid particle after adsorption are:

- chemical reactions at the surface
- diffusion into the bulk
- chemical reactions in the bulk
- solvation in the liquid phase
- segregation, removal of the solvation-cage on the way back to the interface
- desorption

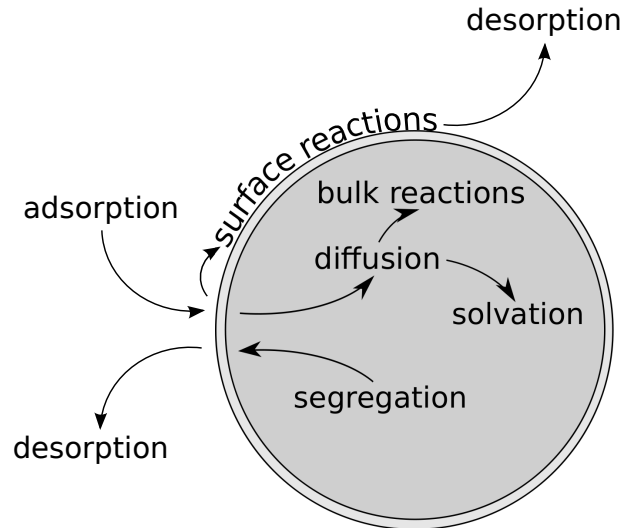


Figure 4.1.: Schematic of the heterogeneous processes between a gas molecule and a liquid droplet.

For solid particles, these processes are reduced to interactions at the surface. The irreversible removal of gaseous molecules due to these processes is described by the uptake coefficient γ .

$$\gamma = \frac{\text{collisions leading to reactions}}{\text{total collisions}} \quad (4.2)$$

Following Hanson et al. (1994) the bulk uptake coefficient Γ_b can be described as a function of mass accommodation coefficient α , Henry's law solubility H , diffusion constant D and reaction rate constant k^I :

$$\frac{1}{\gamma} = \frac{1}{\alpha} + \frac{\omega}{4HRT\sqrt{k^I D_l}} \quad (4.3)$$

where ω describes the mean molecular velocity, T the temperature and R the universal gas constant. The mass accommodation coefficient α for stratospheric aerosols is essentially unity (Hanson and Lovejoy, 1996; Robinson et al., 1998), and the uptake due to bulk processes can be written as:

$$\Gamma_b = \frac{4HRT\sqrt{k^I D_l}}{\omega} \quad (4.4)$$

where Γ_b describes the uptake coefficient due to bulk processes. If a surface reaction exist this can be described by the surface uptake coefficient Γ_s (Shi et al., 1999):

$$\Gamma_s = \frac{4(n_s/n_g)k_{surf}}{\omega} \quad (4.5)$$

where n_g and n_s describe the reactant concentrations in the gas-phase and on the surface, and k_{surf} the pseudo-first-order loss rate at the interface. For reactions on stratospheric aerosols these parameters are unknown; therefore, assumed to be linearly proportional to their bulk-phase counterparts (Swartz et al., 1999; Shi et al., 2001). Following a resistor model (Shi et al., 1999), the overall uptake coefficient γ can then be written as:

$$\frac{1}{\gamma} = 1 + \frac{1}{\Gamma_s + \frac{1}{\frac{k_{des}}{k_{sol}} + \frac{1}{\Gamma_b}}} \quad (4.6)$$

With γ known, the loss of a gaseous species to a heterogeneous reaction can be described by:

$$\frac{d[\text{spec}]}{dt} = 0.25 \cdot \omega \cdot [\text{spec}] \cdot SAD \cdot \gamma \quad (4.7)$$

where $[\text{spec}]$ describes the species concentration in the gas-phase in $\text{molec}\cdot\text{cm}^{-3}$, $0.25\cdot\omega\cdot[\text{spec}]$ the collision factor derived from the kinetic gas theory, and SAD the surface area density of the aerosol in $\text{cm}^2\text{cm}^{-3}$.

4.2. Modeling γ for Stratospheric Aerosols

Several parameterizations exist to calculate the uptake coefficient for the three most important heterogeneous reactions (Reactions 2.11 to 2.13) on stratospheric aerosols and PSC particles (Figure 4.2). The different parameterizations are based on various laboratory measurements for the parameters described in the previous section (Diffusivity, Solubility, etc.). This section will give an overview over the various parameterizations. Generally, the increase in γ -values with decreasing temperature follows the increase in solubility of trace gases.

First, the uptake coefficients for NAT particles are discussed. Two parameterizations, compiled by Carslaw and Peter (1997) based on the work by Hanson and Ravishankara (1993) (HR93) and Abbatt and Molina (1992) (AM92), have found use in atmospheric models. HR93 γ -values are significantly higher than AM92, while AM92 exhibits a greater temperature dependence, that causes the γ -values to increase above HR93 at temperatures below the frost point (~ 188 K). From the three reactions, the hydrolysis

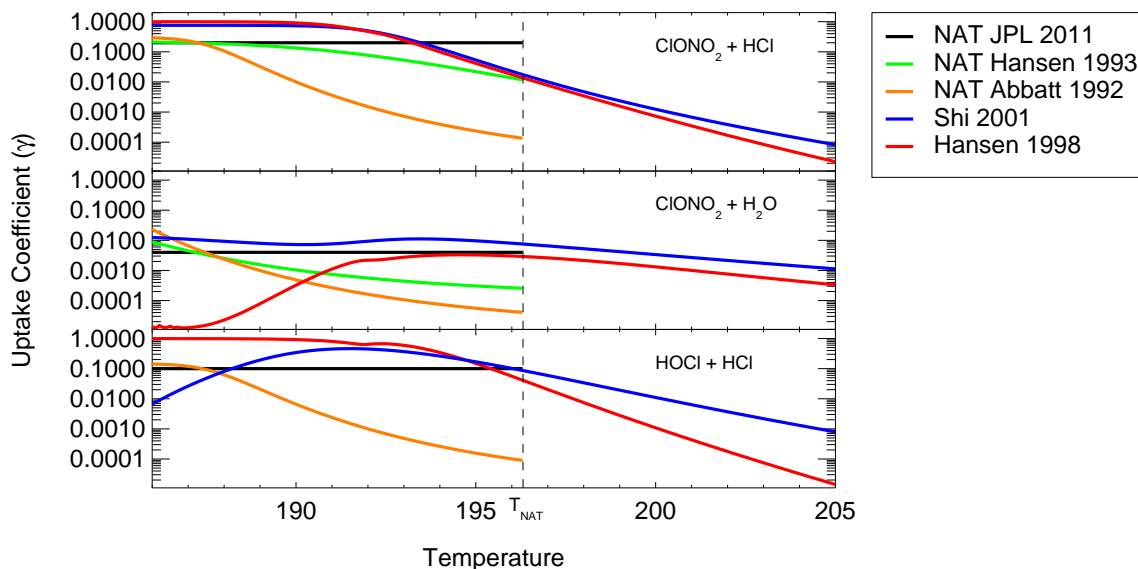


Figure 4.2.: γ -values calculated with parameterizations by Shi et al. (2001) (blue) and Hanson (1998) (red) for liquid aerosols. γ for NAT by Hanson and Ravishankara (1993) (green) and Abbatt and Molina (1992) (orange) as formulated by Carslaw and Peter (1997). Current JPL recommendations (Sander et al., 2011) are fixed γ -values for NAT (black).

of ClONO_2 has the lowest γ -value on NAT. The uptake coefficients for the reactions of HCl with $\text{ClONO}_2/\text{HOCl}$ are by about a magnitude larger than the ClONO_2 hydrolysis. In contrast to these parameterizations, JPL 2011 (Sander et al., 2011) recommends constant γ -values for all three reactions, which are, except for temperatures below the frost point, significantly larger than the parameterizations. The validity of either of the parameterizations or the constant γ -values has yet to be confirmed, though most atmospheric models either use HR93 or the JPL recommendations, since AM92 results in reaction rates too low for any significant chlorine activation on NAT. Since the abundance of HOCl is very small in the stratosphere compared to HCl and ClONO_2 , the most important heterogeneous reaction on NAT for chlorine activation is reaction 2.11.

Two parameterizations exist to compute γ -values on liquid aerosols, Hanson (1998) and Shi et al. (2001). Shi et al. (2001) represents the recommendation by JPL 2011. These two parameterizations result in similar γ -values for reaction 2.11, but differ significantly for 2.12 and 2.13. In addition to the bulk reaction, it is assumed that a fast surface reaction exists for the reaction of HCl with ClONO_2 . The fast surface reaction leads to a competition between reactions in the bulk and on the surface. This becomes visible in the hydrolysis of ClONO_2 for the parameterization by Hanson (1998), and in

the reaction HOCl+HCl for Shi et al. (2001), where the fast surface reaction depletes one species inside the bulk phase, slowing down the bulk reaction.

For the hydrolysis of ClONO₂, the γ -value computed with Shi et al. (2001) is consistently higher than Hanson (1998), with Hanson (1998) exhibiting a sharp drop at 193 K due to the fast surface reaction of ClONO₂ with HCl. Shi et al. (2001) introduced a flux correction to account for the depletion of HCl in the bulk phase due to the fast surface reaction. Therefore, the γ -value for the hydrolysis of ClONO₂ stays fairly constant for Shi et al. (2001), while the γ -value for ClONO₂+HCl never quite reaches unity. The flux correction in the Shi et al. (2001) parameterization also causes the drop in γ for HOCl+HCl due to the depletion of HCl in the bulk. Hanson (1998) did not account for depletion of bulk phase HCl; thus, γ shows a steady increase and reaches unity around 190 K. Compared to the γ -values on NAT, the liquid γ -values are generally higher.

4.3. Heterogeneous Reaction Rates

This section discusses the reaction rates calculated based on equation 4.7, taking into account the uptake coefficients described section 4.2 and the surface area density (SAD) provided by stratospheric aerosols (Chapter 3). SAD for the liquid aerosol is calculated assuming a log-normal size distribution with a particle number density of 10 cm⁻³ (Curtius et al., 2005), and taking into account the swelling of the aerosol due to uptake of H₂O and subsequent substantial increase in surface area due to the uptake of HNO₃ and H₂O when STS forms (Figure 3.1). NAT SAD is calculated assuming a uniform size distribution, and a range of particle number densities between 10⁻¹ and 10⁻⁴ cm⁻³. This range of particle number densities is derived from CALIPSO observations (Pitts et al., 2009, 2011) and represents the upper and lower limit for observations of NAT in the stratosphere.

Figure 4.3 shows the first order loss rates in HCl and ClONO₂ for typical stratospheric conditions for reactions 2.11 and 2.12 on liquid aerosols and NAT particles. When the hydrolysis of ClONO₂ is assumed to be the main production channel for HOCl, the overall activation rate of chlorine can be described by reactions 2.11 and 2.12. The various heterogeneous chemistry parameterizations and possible particle number densities for NAT particles cover several orders of magnitude in first order loss rates, which indicates a large uncertainty concerning their ability to act as reaction sites for chlorine activation. The sharp increase for liquid particles at 192 K is caused by the uptake of HNO₃ onto the background aerosol, which increases the surface area density and with it the reaction

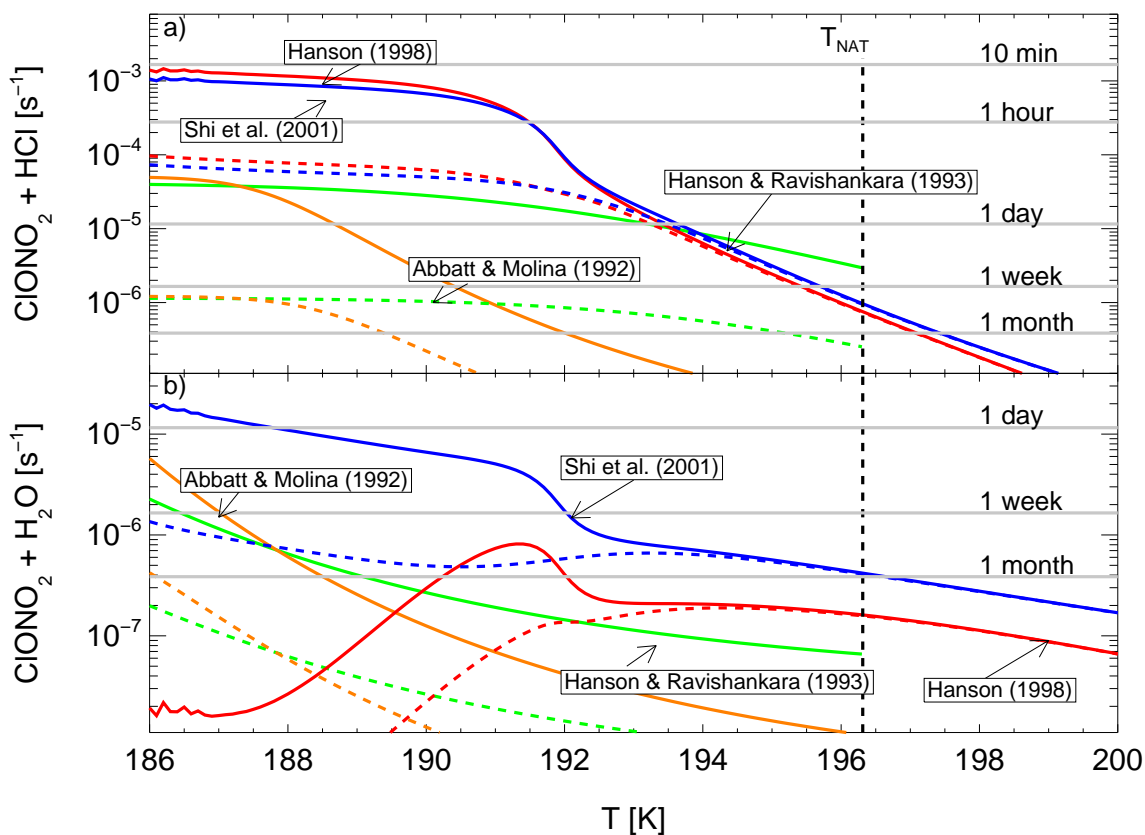


Figure 4.3.: First order loss rates for $\text{HCl} + \text{ClONO}_2$ and $\text{ClONO}_2 + \text{H}_2\text{O}$ for typical stratospheric conditions (50 hPa, 2 ppbv HCl, 1 ppbv ClONO_2 , 15 ppbv HNO_3 , 5 ppmv H_2O and 0.15 ppbv H_2SO_4).

rate about tenfold. In addition, Figure 4.3 shows the calculated reaction rate in the absence of any HNO_3 uptake (dashed red/blue lines). Over most of the temperature range heterogeneous reaction rates on NAT are slower than on the background aerosol, even when a high NAT particle number density of 10^{-1} cm^{-3} is assumed. Only at temperatures around the thermodynamic equilibrium temperature for NAT can reaction rates on NAT be faster than on the background aerosol. With the formation of STS or a NAT particle number density lower than 10^{-1} cm^{-3} , reaction rates on the liquid aerosol are always faster than on NAT.

While chlorine activation on liquid aerosols is not sensitive to the parameterization used, it is sensitive to temperature. The reaction rate doubles for every Kelvin and increases tenfold over a 2 K temperature range with the uptake of HNO_3 on the background aerosol. This causes high sensitivity of simulated chlorine activation to small variabilities in the temperature field. Therefore, even a small error in the temperature

fields has a larger effect than the uncertainty of the uptake coefficients. Heterogeneous processing on NAT, on the other hand, is very sensitive to the used parameterization and assumed particle number density, but less to temperature.

When considering these reaction rates, chlorine activation on the binary aerosol typically exceeds that on NAT by at least a factor of three, even when the highest observed particle number density for NAT is used. As observed NAT particle number densities are usually less than 10^{-1} cm^{-3} , chlorine activation rates on the binary aerosol exceed those on NAT by at least an order of magnitude. The formation of STS increases activation rates by another order of magnitude over the background aerosol. However, once STS forms the activation rate on the background aerosol is already fast enough to cause complete activation in a matter of hours. It is therefore unlikely that the increase in activation rate caused by STS is important for overall chlorine activation in the polar vortex. But it may be visible on short timescales (hours) and small spatial scale (hundreds of kilometers), which are usually probed with in-situ observations. The next section will discuss several in-situ observations of chlorine activation in the Arctic and analyze the impact of the various aerosol types.

5. The Influence of PSCs and the Background Aerosol on Chlorine Activation

This chapter will discuss the influence of the various aerosols in the stratosphere on chlorine activation, with focus on the hypothesis by Drdla and Müller (2012) that the reactivity of heterogeneous reactions on cold binary aerosol is sufficiently large to explain the greatest part of the observed chlorine activation, and that an enhancement of the reactivity by uptake of HNO_3 on the particles is not necessary for chlorine activation.

The impact of an unperturbed background aerosol layer on heterogeneous processing was first discussed by Rodriguez et al. (1988), and later developed by Hofmann and Solomon (1989); Cox et al. (1994); Hanson et al. (1994); Portmann et al. (1996). But Drdla and Müller (2012) concluded that even during volcanic quiescent times chlorine activation during the polar night is dominated by reactions on cold binary sulfate aerosol. However, elevated levels of active chlorine usually coincide with the presence of PSCs, which makes it difficult to attribute chlorine activation to heterogeneous processing on a particular aerosol or cloud type. Kawa et al. (1997) reported in-situ measurements of active chlorine from the Antarctic during the ASHOE/MAESA campaign in 1994, where back-trajectories indicated that during ten days prior to the measurement temperatures were too high for PSC formation; therefore, concluded that the observed chlorine activation must have occurred on the background aerosol. Here, the focus will be on in-situ observations, which allow chlorine activation on very small time and spatial scales to be assessed. These observations also allow a validation of the parameterizations for heterogeneous chemistry described in Chapter 4. Second, satellite measurements are used to assess chlorine activation on a vortex wide scale.

5.1. In-situ Observations from March 2005

During a flight into the Arctic vortex by the high-altitude research aircraft Geophysica on 7th March 2005, high concentrations of active chlorine compounds were observed by the HALOX instrument (von Hobe et al., 2006), with back-trajectories from the flightpath indicating that chlorine in the observed air masses was reactivated just 24 hours prior to the measurements. For the analysis of chlorine activation, chemistry and PSC microphysics are simulated along trajectories starting on 3rd March 2005 and ending on the flightpath. Trajectory and chemistry simulations are performed with the CLaMS Model (McKenna et al., 2002a,b), driven by ERA-INTERIM wind fields (Dee et al., 2011). To calculate reaction rates, JPL 2006 (Sander et al., 2006) recommendations are used (for heterogeneous chemistry JPL 2006 and 2011 recommendations are identical). STS growth is simulated with the thermodynamic model developed by Carslaw et al. (1995b), dynamic NAT growth with the model of Carslaw et al. (2002) and the NAT nucleation rate is taken from Voigt et al. (2005).

5.1.1. Deriving the Initialization

The initialization of these trajectories is based on in-situ measurements of N_2O and CH_4 from HAGAR (Homan et al., 2010; Werner et al., 2010), H_2O from the FISH instrument (Zöger et al., 1999) and aerosol particle number density (size range: 10nm- $5\mu\text{m}$ in diameter) from the COPAS instrument (Weigel et al., 2009). Additional details of this flight can be found in von Hobe et al. (2006).

CH_4 observations by HAGAR indicate that a homogeneous air mass was sampled although the flight covered 65° - 85°N equivalent latitude (Figure 5.1 top panel). From these measurements we derive the total inorganic chlorine loading Cl_y , with the CH_4 - Cl_y tracer correlation described in Groöß et al. (2002), as a function of potential temperature (Θ) and equivalent latitude (Φ). Concentrations of ClONO_2 , HCl and HNO_3 are taken from ACE – FTS v2.2update (Bernath et al., 2005) observations on 3rd and 4th March, interpolated onto the trajectory positions on 3rd March 12 UTC as a function of potential temperature and equivalent latitude. The difference between the concentrations of Cl_y and the sum of ClONO_2 + HCl is initialized as ClO_x (Figure 5.1 bottom panel).

For most of the flightpath, HNO_3 values initialized from ACE-FTS are between 6 and 7 ppbv. With the passive tracer subtraction method, this yields a denitrification of 50%, corroborating the conclusion by von Hobe et al. (2006) that the observed air masses were highly denitrified. All other chemical species are interpolated from the hemispheric

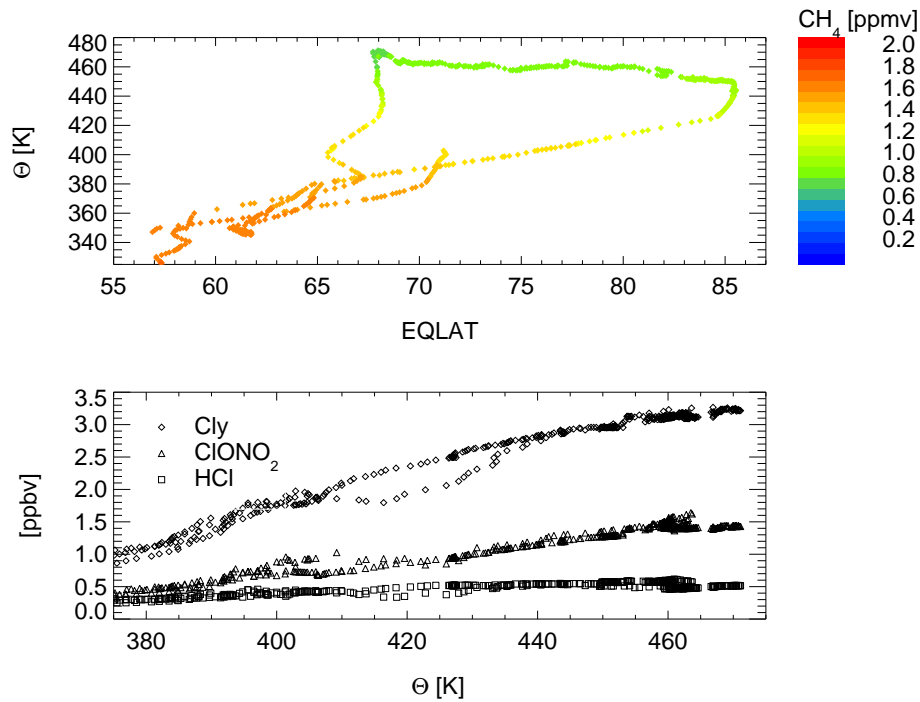


Figure 5.1.: Top: HAGAR CH_4 as function of potential temperature and equivalent latitude. Bottom: Derived initialization of chlorine species as function of potential temperature.

CLaMS simulation (Grooß and Müller, 2007), and the background aerosol surface area is taken from the climatology compiled by David Considine (Eyring et al., 2010). The error for the initialization of HNO_3 and the chlorine species is estimated by interpolating the satellite measurements onto the potential temperature of the observations, and subsequently calculating the range of observations of the three nearest neighbors in the equivalent latitude space. Typically, this results in an error of less than 0.2 ppbv.

5.1.2. Estimating the Temperature Error

Since heterogeneous chemistry is highly sensitive to temperature, accurate knowledge of temperature is necessary to model the activation of chlorine on stratospheric aerosols. Brakebusch et al. (2012) have shown that temperatures in the specified dynamics version of the Whole Atmosphere Community Climate Model tend to be warm biased compared to MLS observations, and that applying a -1.5 K temperature bias to the heterogeneous chemistry calculations improves the agreement between model and satellite observations.

Ambient temperature on board Geophysica is measured by the Thermodynamic Com-

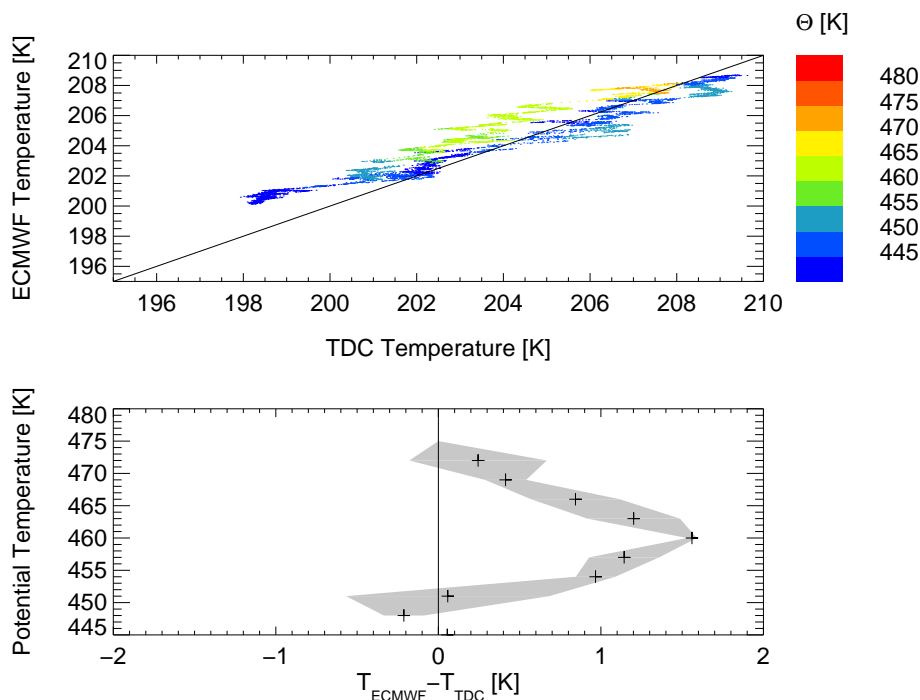


Figure 5.2.: Temperatures interpolated from ERA-INTERIM data on the flightpath versus TDC temperature measurements on board the Geophysica as function of potential temperature.

plex (TDC, Shur et al., 2006). These measurements similarly show a ~ 1.5 K bias when compared to ERA-INTERIM temperatures (Figure 5.2). Between 455-470 K ERA-INTERIM temperatures are consistently higher than observations. ERA-INTERIM shows agreement with observations at higher temperatures, but shows a warm bias at temperatures below 205 K. The lower panel in Figure 5.2 shows the vertical profile for the temperature bias. The highest warm bias is located at 460 K with 1.5 K. No in-situ temperature measurements exist over the course of the trajectories, so we assume the warm bias exists for the whole trajectory length and adjust the temperatures below 205 K according to the kernel shown in Figure 5.2.

5.1.3. Modeling PSCs along Trajectories

With adjusted temperatures the formation of PSCs is modeled along the trajectories (Figure 5.3). The model indicates presence of NAT and STS about 24 hours prior to the measurements. On the trajectories ending between 8:45 and 9:30 UTC, typically less than 0.1 ppbv HNO_3 condenses on STS. This enhances the surface area density by

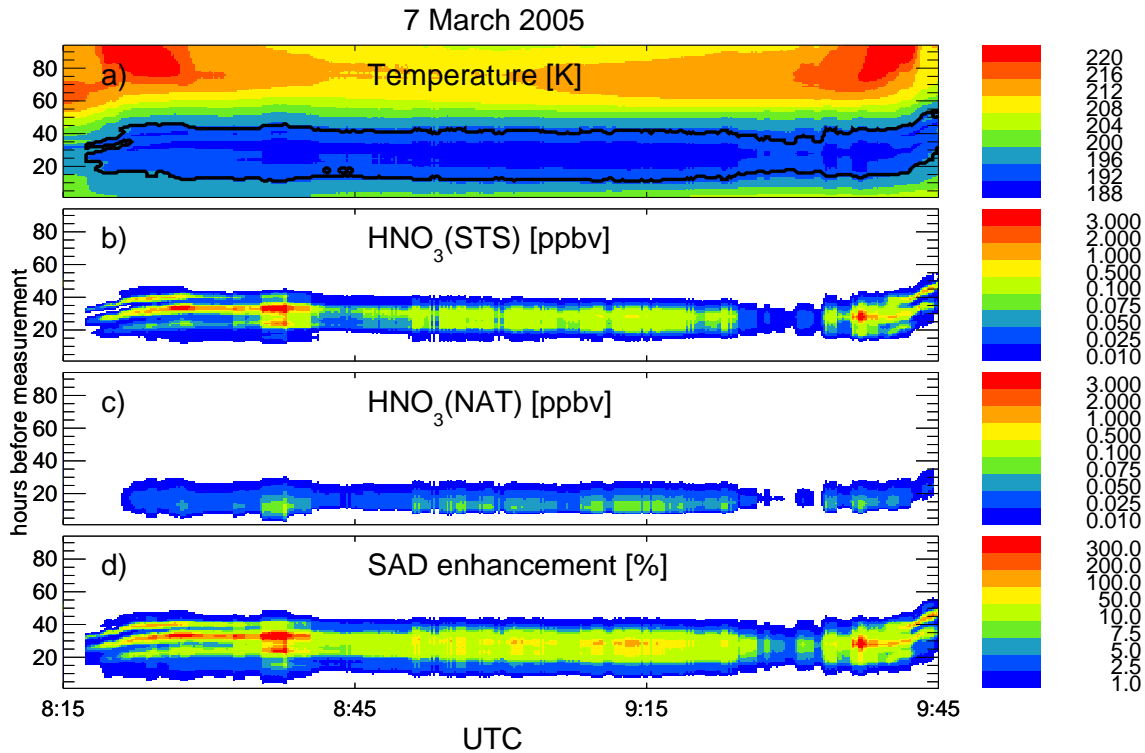


Figure 5.3.: Temperature history (a), simulated condensation of HNO₃ on STS (b), NAT (c) and corresponding enhancement of the surface area density over the background aerosol (d) along 92 h back-trajectories ending on the Geophysica flightpath. Areas under T_{NAT} are enclosed by the black line.

about a factor of 1.5 compared to the background aerosol. The maximum calculated enhancement is about a factor of 2. For trajectories ending before 8:45 and after 9:30, all available HNO₃ is predicted to condense to STS which maximally enhances the surface area density by a factor of 5. However, these maximum enhancements only occur for a few hours. For most of the time when temperatures along the trajectories are below T_{NAT} , NAT and STS enhance the surface area by less than 10% compared to the background aerosol.

As temperatures are below T_{NAT} for only about 20 hours, NAT particles cannot reach thermodynamic equilibrium and NAT particle number density is on the order of 10^{-3} cm^{-3} . Such a low particle number density leads to a negligible increase in surface area density. Therefore, any modeled increase in surface area density is caused by STS.

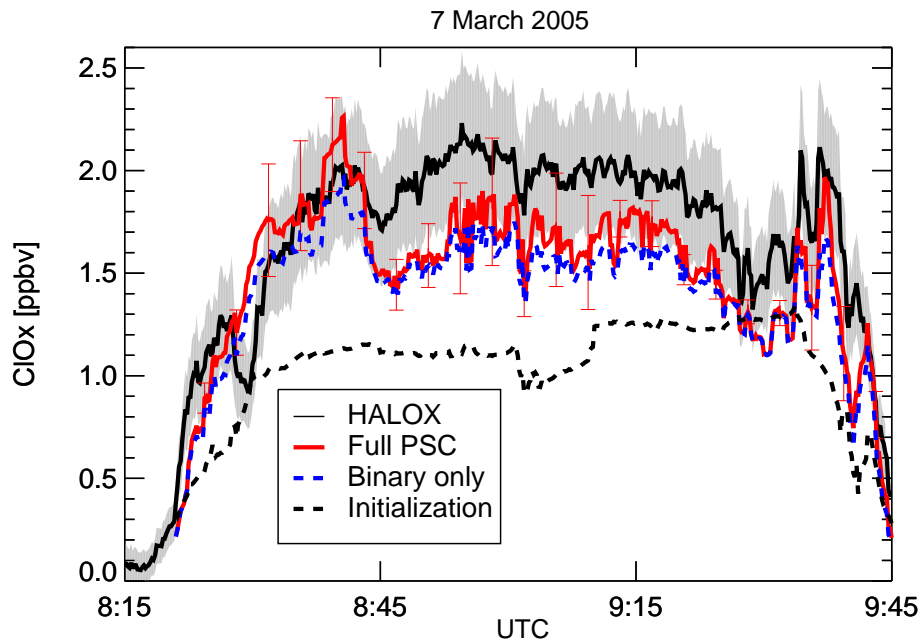


Figure 5.4.: Comparison of HALOX in-situ data and CLaMS simulations. Solid black line marks the HALOX ClO_x measurement with its accuracy shaded gray and the dashed black line initial ClO_x . Solid red line marks results from the “Full PSC” and dashed blue from the “Binary only” simulation. Error bars show model uncertainty.

5.1.4. Estimating the Influence of PSCs on Chlorine Activation

Two simulations are performed to assess the model’s ability to reproduce the measured extent of chlorine activation. In the first simulation heterogeneous reaction rates are calculated with a surface area density that includes all PSCs (Full PSC). In the second simulation only the surface area density of the background aerosol without any enhancement due to STS or NAT (Binary only) is used to derive heterogeneous reaction rates.

Figure 5.4 shows initialized, measured and modeled ClO_x for the Geophysica flight. Maximum activation is simulated for trajectories ending before 8:45 and after 9:30 UTC. These trajectories also exhibit the maximum uptake of HNO_3 on PSCs, as minimum temperatures are about 1-2 K lower than in the other trajectories. For trajectories ending between 8:45 and 9:30 UTC about 0.7 ppbv additional chlorine is activated within 92 h. The model cannot reproduce all of the fine structures of the measurements, which is most likely due to the coarse initialization and resolution of the ERA-INTERIM wind fields. However, both model simulations show good agreement with measured ClO_x ,

within the uncertainty of initialization and measurements. For trajectories ending before 8:45 modeled chlorine activation tends to be on the upper limit of uncertainty of the observations and afterwards at the lower limit.

The difference between both simulations is minimal, with the “Full PSC” activating slightly more chlorine than the “Binary only” simulation. However, this difference is on the order of 10%, which indicates that most of the observed activation of chlorine, within the considered time-frame, can be attributed to heterogeneous chemistry on a surface area density equivalent to background aerosol levels. Even though modeled PSCs increase the surface area density by up to 500%, the effect on chlorine activation is limited, as this maximum increase only lasts for a short time. In the model neither HCl nor ClONO₂ are completely depleted; thus, chlorine activation along the trajectories is limited by the heterogeneous reaction rates and not by the availability of either reservoir species. As the model results overlap with the observations, within the uncertainties of this simulation and measurements, the temperature dependence of the current parameterizations for heterogeneous chlorine activation is in agreement with the processes in the real atmosphere.

5.2. In-Situ Observations from the RECONCILE Campaign

In addition to the Geophysica flight from 7th March 2005, three Geophysica flights in January 2010 from the RECONCILE campaign in the Arctic (Figure 5.5) are examined. The temperature histories along seven-day trajectories ending on the flightpath of these flights show temperatures low enough for efficient heterogeneous chemistry. Temperatures are below T_{NAT} at the beginning of the trajectories and during the flights. In between temperatures are greater than 200 K; hence, all PSCs that formed initially most likely completely evaporated. Prior to the flights, temperatures for most trajectories are consecutively below T_{NAT} for about 30 h, with some trajectories during flight 2 residing below T_{NAT} for over 50 h. Trajectories for flight 3 are below T_{NAT} for the longest time. Here, temperatures are below T_{NAT} for 40 h at the beginning of the trajectories and again for 30 h when the flight occurred. In contrast to the 2005 flight, minimum temperatures for all three flights are below 190 K, low enough for extensive PSC formation. Measurements from the up- and downward facing LIDAR MAL 1 and MAL 2 (Matthey et al., 2003) on-board Geophysica show that backscatter ratios are elevated by a factor of 3-4 and a depolarization of less than 4%. These measurements suggest that no solid

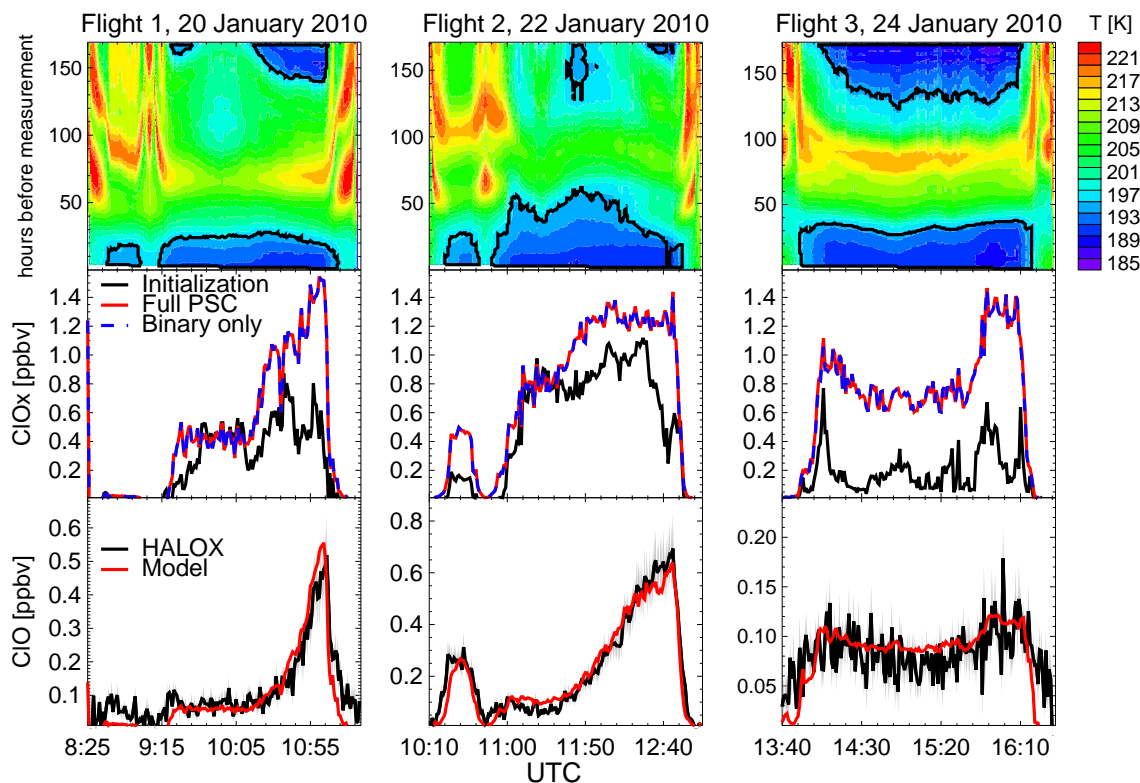


Figure 5.5.: Top: Temperature history along seven-day backward trajectories from HALOX measurements for 3 flights in January 2010. Middle: ClO_x initialization (black) and modeled ClO_x on the flightpath with full PSC surface area density (red) and background aerosol only (blue dashed). Bottom: Measured (black) and modeled values of ClO (red).

particles were present in the air masses which have been probed during the flight.

Chlorine activation is simulated by running box-model calculations along these seven day trajectories. The initialization is taken directly from a hemispheric 3D-CLaMS simulation. Total Cl_y is estimated from measured CH_4 by HAGAR via the CH_4 - Cl_y correlation (Groß et al., 2002). Model HCl and ClONO_2 are then scaled accordingly, so that model Cl_y agrees with observations. Generally model Cl_y is scaled up by about 15% to agree with observations. For all three flights the model activates significant amounts of chlorine over the seven day period considered. For flights 1 and 2 additional chlorine is activated along the majority of trajectories during the seven days of simulation, generally around 0.4 ppbv with some trajectories showing up to 0.8 ppbv additional ClO_x . Only a minor fraction of the trajectories shows no additional chlorine activation. The trajectories for flight 3 all show additional chlorine activation, generally, around 0.5 ppbv

with maximum additional ClO_x of 1.2 ppbv. The limiting factor for chlorine activation for these three flights is the availability of ClONO_2 . The model simulates that ClONO_2 is completely depleted at the time of the flights; hence, the additionally available surface area density provided by PSCs cannot have an effect on ClO_x levels. Consequently the “Binary only” simulation produces the same results as the “Full PSC” simulation.

In contrast to the flight on 7th March 2005, no reliable Cl_2O_2 measurements exist for the flights in January 2010, limiting the comparison to modeled and measured ClO . ClO possesses a distinct diurnal cycle, and the parameters describing the equilibrium between ClO and Cl_2O_2 are still subject to some uncertainty (von Hobe et al., 2007). To calculate ClO from simulated ClO_x the results from Sumińska-Ebersoldt et al. (2012), who constrained the $\text{ClO}/\text{Cl}_2\text{O}_2$ equilibrium parameters to in-situ observations, are used. The thermal equilibrium constant is taken from Plenge et al. (2005) and the Cl_2O_2 absorption cross-section from von Hobe et al. (2009) scaled to the absolute measurements of Lien et al. (2009). Figure 5.5 shows modeled and measured ClO for the three flights in January 2010. The first two flights have decreasing solar zenith angles leading to increasing ClO values and the third flight was carried out in darkness. Overall, the model shows excellent agreement with the measurements with flights 1 and 2 showing the dependence of ClO on the solar zenith angle and flight 3 showing nighttime, thermal equilibrium measurements.

5.3. Intra- and Interannual Variability of Chlorine Activation and PSC Occurrence

To examine whether heterogeneous processing on the background aerosol is also sufficient to describe vortex average chlorine activation, MLS observations for the Arctic winters 2004/05 to 2010/11 are investigated. The focus is on the intra- and inter-annual variability of chlorine activation and PSC occurrence to identify a possible correlation between the chlorine activation rate and the surface area provided by PSCs.

5.3.1. Variability of HCl and HNO_3 Loss

This analysis focuses on the vortex core, described by equivalent latitudes poleward of 75°N . A high inter-annual variability, common for the Arctic, is evident in the observations of HCl and HNO_3 (Figure 5.6). The winters 2004/05, 2007/08 and 2010/11 had very cold and stable vortices leading to strong denitrification, and depressed values

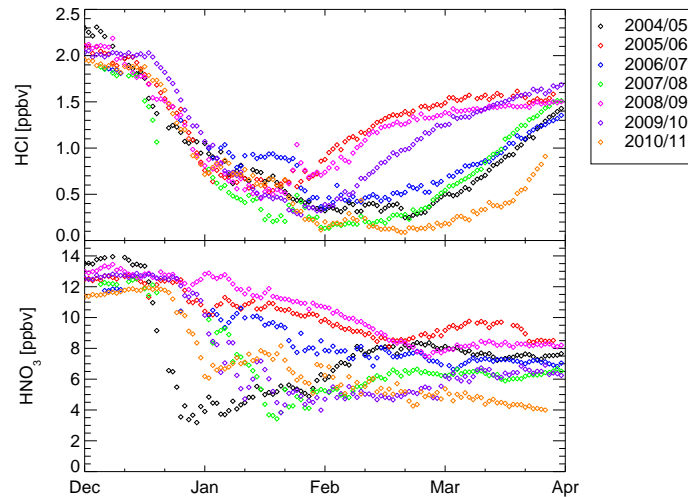


Figure 5.6.: HCl and HNO₃ observations by MLS for the Arctic winters 2004/05 to 2010/11 on 500 K potential temperature in the vortex core (equivalent latitude > 75°N).

of gas-phase HCl extending into spring. The observations for the winters 2005/06 and 2008/09, on the other hand, show hardly any denitrification, and HCl starts increasing in the middle of January.

The onset of chlorine activation at the beginning of winter is controlled by the quantitative titration of the available ClONO₂ through heterogeneous reaction 2.11. Thus, a decrease in gas-phase HCl can serve as an indicator for chlorine activation.

$$\frac{d[ClO_x]}{dt} \approx -\frac{d[HCl]}{dt} - \frac{d[ClONO_2]}{dt} \approx -2 \times \frac{d[HCl]}{dt} \quad (5.1)$$

Although HCl shows high inter-annual variability for the period of January to April, observations show only little variability in December when chlorine begins to become activated. At the end of December HCl has decreased by about 1 ppbv, 50% of the initially available HCl. Significant differences in HCl depletion between the different winters do not emerge until the middle of January. In winters 2005/06 and 2008/09 HCl starts recovering in January, while in winters 2004/05 and 2007/08 the final recovery does not begin until the middle of February. This corresponds to observations of HNO₃. A decrease in gas-phase HNO₃ is an indicator for PSC formation and irreversible denitrification. Pitts et al. (2009, 2011) have shown that the first PSCs forming in Arctic winter are mainly composed of STS and low particle number density NAT (<10⁻³

cm^{-3}). Therefore, the observed decrease in gas-phase HNO_3 in December can mostly be attributed to condensation of HNO_3 on STS and a lesser extent to NAT and irreversible denitrification.

In early winter HNO_3 shows, in contrast to HCl , high inter-annual variability indicating that the additional surface area provided by PSCs has no detectable direct influence on the rate of chlorine activation on a vortex wide scale. For the winters 2004/05 and 2009/10, 75% of gas-phase HNO_3 are removed throughout the winter. In 2004 gas-phase HNO_3 shows a steep decline in the middle of December and in 2009 at the end of December. For 2004 we can assume that the surface area density was significantly enhanced through HNO_3 uptake throughout December, while for 2009 surface area density was for most of the time at background levels. In winters 2005/06 and 2008/09 observations show only a gradual decrease of gas-phase HNO_3 . This decrease of gas-phase HNO_3 indicates that PSCs formed only to a minor extent compared to the winters 2004/05 and 2009/10. Pitts et al. (2011) show that maximum PSC coverage in the winter 2008/09 was only one third of the maximum coverage in 2009/10. Still, the decrease of HCl in December is very similar for all winters despite the high variability in gas-phase HNO_3 .

5.3.2. Probability Density Distribution of Maximum Surface Area Enhancement by PSCs

Figure 5.7 shows the probability density distribution of the maximum enhancement of the surface area by STS in the absence of NAT formation for the winters 2004/05, 2008/09 and 2009/10. These three winters cover the whole spectrum in HCl and HNO_3 variability. STS formation is calculated according to Carslaw et al. (1995b) along seven-day back-trajectories from MLS observations in December 2005, 2008 and 2009 poleward of 75°N equivalent latitude, assuming that no irreversible denitrification or dehydration has occurred yet. The trajectories are divided into 6 different bins. The first bin contains the fraction of trajectories with a maximum enhancement of the surface area density of less than 1.1; i.e. showing no significant enhancement over background aerosol levels. For the next two bins (maximum enhancement factor 1.1-1.5 and 1.5-2) only a small fraction of gas-phase HNO_3 has condensed on STS but has already significantly enhanced the surface area density. In the bins with an enhancement factor of 2-5 and 5-10 most available gas-phase HNO_3 is condensed on STS, and in the last bin virtually all HNO_3 is in STS leading to an increase of surface area density over the background aerosol of more than a factor of 10.

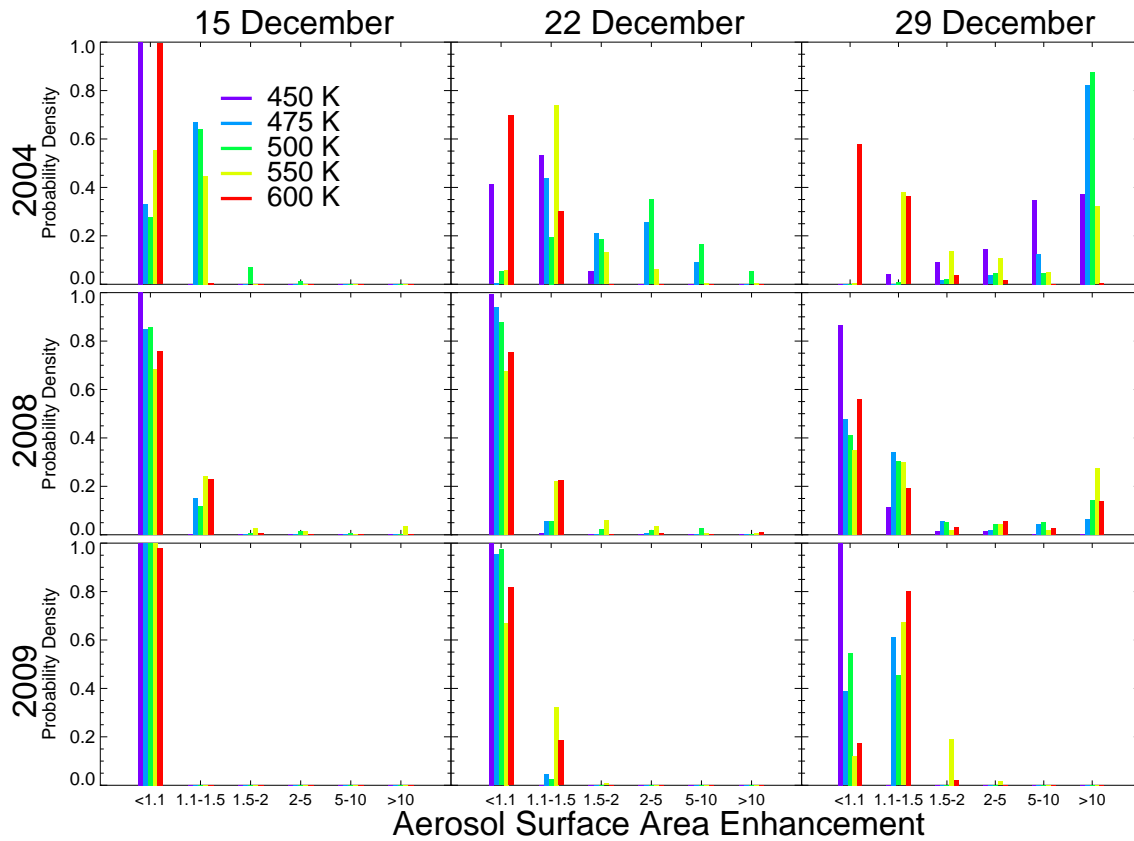


Figure 5.7.: Probability density distribution of maximum surface area density enhancement by STS along seven-day back-trajectories starting on MLS observations poleward of 75°N equivalent latitude in 2004, 2008 and 2009.

Figure 5.7 shows this distribution on three different days in December and for five altitudes. The trajectories ending 15th December show no or only a minor increase of surface area density, but already some differences emerge between the different winters. In 2009 none of the trajectories show any increase in SAD, and for 2008 less than 20% show a small enhancement. In 2004, however, only less than 30% between 475 and 550 K show no increase in surface area density.

Differences between the winters become more apparent for 22nd December. For 2008 and 2009 the distribution hardly changes compared to 15th December. Most trajectories still show little enhancement of surface area density. In 2004, however, most trajectories show some enhancement of surface area density, and between 475 and 550 K all do. At 500 K more than 50% of the trajectories already show an enhanced surface area density by more than a factor of 2. The difference between these three winters becomes most obvious for the trajectories started on 29th December. In 2004 the distribution

has completely shifted from trajectories only showing minor enhancement of surface area density on 15th December to the majority showing an enhancement of a factor greater than 10. On the 450 and 475 K isentropes more than 80% of the backward trajectories exhibit temperatures which lead to a more than tenfold increase in surface area density. This is also visible in the sharp drop in MLS gas-phase HNO_3 at the end of December 2004 (Figure 5.6). Nonetheless, MLS HCl measurements show no drastic change in the loss rate, suggesting that the heterogeneous loss of HCl is not connected to the available surface area density. The change in probability density for 2008 and 2009 towards the end of December is less pronounced. Most trajectories show only a minor increase in surface area density, but still their distribution is shifted towards higher surface area densities. This is more apparent in 2008 than in 2009. On 29th December 2009 the maximum increase in surface area density for almost all trajectories was less than a factor 1.5.

These three winters show the huge variability in PSC occurrence and HNO_3 uptake for December in the Arctic. Nevertheless, HCl loss rates observed by MLS are fairly constant throughout December with little inter- and intra-annual variability. Only the vertical extent of HCl loss shows inter-annual variability which is correlated with the vertical extent of the low temperatures necessary for efficient heterogeneous chemistry.

5.4. Conclusions

The importance of the stratospheric background aerosol for chlorine activation has been examined in this chapter. The evaluation of heterogeneous chemistry parameterizations has shown that uncertainties in NAT microphysics contribute most to the overall uncertainty in modeling heterogeneous chemistry. The uncertainties for NAT reactivity cover several orders of magnitude. However, using the most commonly observed NAT particle number densities, heterogeneous processing on these particles is significantly slower than on the background aerosol. For modeling chemistry on the binary background aerosol the greatest uncertainty results from temperature uncertainties, as the reaction rate doubles for every Kelvin and increases tenfold with the formation of STS over a 2 K temperature range.

To study heterogeneous chemistry on a synoptic timescale backtrajectories from the flightpath of the Geophysica flight on 7th March 2005 were analyzed. These trajectories show chlorine reactivation about 30 hours before the flight. With the initialization derived from satellite data, simulating chlorine activation along trajectories ending on

the flightpath allows the influence of the various aerosols on modeled chlorine activation to be assessed. Even though NAT and STS could form under the prevailing conditions, the additional surface area provided by PSCs in the model does not significantly enhance chlorine activation. 90% of additionally activated chlorine during this time-frame originates from heterogeneous chemistry on a surface area provided by the background aerosol. This shows that for modeling heterogeneous chemistry the increase in γ -values with decreasing temperature is more important than the increase of surface area density, and that to correctly model heterogeneous chemistry on synoptic timescales accurate knowledge about the prevailing temperatures is essential. This flight also showed that a considerable amount of chlorine can be activated on a timescale of hours when both HCl and ClONO₂ are available.

The three flights from January 2010 corroborate these results, albeit under very different ambient conditions. For the 2005 flight neither HCl nor ClONO₂ is completely depleted in the model; therefore, the temperature is the decisive factor determining the level of chlorine activation. In 2010, however, ClONO₂ is the limiting factor, since it is completely depleted while temperatures remain low enough for efficient heterogeneous chemistry. Thus, heterogeneous chemistry on the background aerosol surface area yields identical results as calculations with full PSC surface area, and both simulations show excellent agreement with observations.

Not only can heterogeneous processing on the background aerosol surface area explain the bulk of chlorine activation on synoptic timescales along individual trajectories, but satellite observations show that the vortex-average chlorine activation rate for the last seven Arctic winters is not correlated with the occurrence of PSCs and the associated uptake of HNO₃ from the gas-phase. The observed HCl loss rate in December is similar for all considered Arctic winters despite their high variability in PSC occurrence. Even intra-annual variability of gas-phase HNO₃ is not reflected in observed HCl. During December 2004 gas-phase HNO₃ dropped sharply while the HCl loss rate remained constant. Thus, the vortex-average observations confirm the findings from the in-situ observations that the surface area provided by PSCs does not significantly impact chlorine activation rates.

6. Polar Stratospheric Clouds in SD-WACCM

In this chapter the representation of Polar Stratospheric Clouds in a coupled-climate Model is analyzed. The previous chapters already discussed the impact of PSCs on chlorine activation. Despite their importance for ozone depletion, the simulation of PSCs still presents a major challenge for state of the art climate models. The simulation of PSCs in the Specified Dynamics version of the Whole Atmosphere Community Climate Model (SD – WACCM) is investigated, and the PSC scheme is improved to give a better representation of satellite observations of PSCs. SD-WACCM is described in detail in the Appendix. To simulate PSCs, the reference SD-WACCM simulation uses an equilibrium approach to simulate NAT particles (compare Chapter 3.2). STS is simulated according to the thermodynamic equilibrium model by Tabazadeh et al. (1994b). NAT is simulated to form at a supersaturation of 10, about 3 K below its thermodynamic equilibrium temperature (Hanson and Mauersberger, 1988), at a prescribed particle number density of 10^{-1} cm^{-3} . The thermodynamic equilibrium temperature for NAT is referred to as T_{NAT} and the temperature at a supersaturation of 10 $T_{\text{S,NAT}}$. In the reference case, it is assumed that if atmospheric conditions allow the presence of either particle type, HNO_3 is first partitioned into STS. This analysis focuses on the Antarctic winter 2005, which can be regarded as a typical Antarctic winter season.

6.1. Type I Polar Stratospheric Clouds

6.1.1. Observations and Reference Simulation

Figure 6.1 shows the typical development of HNO_3 containing species in the reference simulation on the 475 K potential temperature surface. The initial increase in gas-phase HNO_3 is caused by descent of HNO_3 -rich air masses, but with decreasing temperatures the model forms PSCs which rapidly deplete gas-phase HNO_3 .

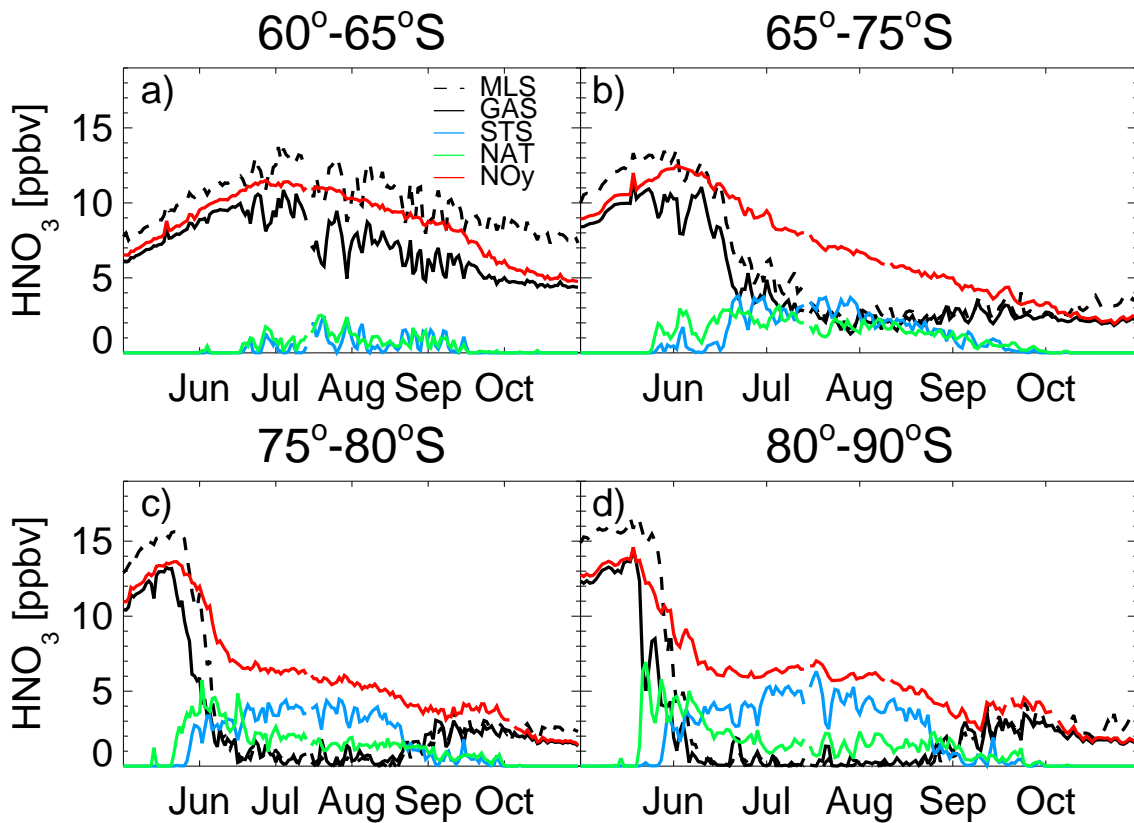


Figure 6.1.: Observations of gas-phase HNO_3 and modeled partitioning of HNO_3 between the gas-phase and PSCs on 475 K over Antarctica 2005 for four equivalent latitude regions. Dashed line are observations of gas-phase HNO_3 by MLS and solid lines model output from the reference simulation.

In the model NAT is formed first and then transitions into STS as temperatures cool down. This is most evident in the vortex core (Figure 6.1d). As soon as the temperature threshold, T_{S_NAT} , for NAT is reached, gas-phase HNO_3 drops sharply as HNO_3 is partitioned into NAT. As temperatures cool down further, STS starts to form and quickly becomes the prevalent PSC type. This indicates that in the model HNO_3 transitions from the solid to the liquid phase with decreasing temperature. Throughout the entire winter HNO_3 is completely removed from the gas-phase poleward of 80°S and strongly depleted between 65° - 80°S . With this approach most of the irreversible denitrification, through the sedimentation of NAT particles, occurs in early winter as can be seen by the steep decline of NO_y . By the middle of June about 50% of total denitrification in the vortex core has already occurred. Once HNO_3 is partitioned into STS denitrification becomes a more gradual process. At very low temperatures, when

almost all available HNO_3 is partitioned into STS, denitrification is shut off, as shown by constant NO_y values in July in the vortex core (Figure 6.1d). Farther away from the vortex core the formation of NAT is less abrupt. STS and NAT start to form at about the same time, and HNO_3 is equally distributed between STS, NAT and the gas-phase. This leads to more gradual denitrification, but reaches the same extent as simulated in the vortex core.

CALIPSO observations (Pitts et al., 2009) on the other hand indicate that the first PSCs formed are predominantly STS rather than NAT, and that mixed phase PSCs exist through the entire winter. This suggests that denitrification probably is a more gradual process. The reference simulation cannot represent this gradual denitrification process in the vortex core. In the vortex edge region, between 60° - 65°S equivalent latitude (Figure 6.1a), PSCs only form to a minor extent and most HNO_3 remains in the gas-phase so that only minor denitrification occurs. Nonetheless, the overall modeled gas-phase HNO_3 and denitrification at the end of polar winter are in excellent agreement with observations of gas-phase HNO_3 by MLS. Poleward of 75°S , observations also show total depletion of gas-phase HNO_3 and in the vortex edge region, between 65° - 75°S , gas-phase HNO_3 stays constant at low values.

Lambert et al. (2012) have shown that MLS observations of gas-phase HNO_3 as a function of temperature can be used to evaluate the PSC type. In Figure 6.2, observations of gas-phase HNO_3 are correlated with temperature and compared to MLS observations. The observations shown are limited to May and June 2005 poleward of 80°S on 475 K in the Antarctic. During this time the vortex starts to form, gradually cools down and observations indicate a decrease of gas-phase HNO_3 with decreasing temperatures (Figure 6.2a). In the observations gas-phase HNO_3 starts to decrease at $T_{\text{S_NAT}}$, and is completely depleted when temperatures reach the frost point. This decrease appears to follow the STS equilibrium function (Figure 6.2a, red line), with the scatter around this function indicative of mixed PSCs.

The reference simulation of SD-WACCM differs significantly from the observations (Figure 6.2b). In the model HNO_3 is completely removed from the gas-phase at $T_{\text{S_NAT}}$, and only the partitioning of HNO_3 between the different PSC types changes as temperatures decrease further. Lambert et al. (2012) have shown that mixed clouds occur over the whole temperature range, simultaneous with residual gas-phase HNO_3 . In the model, mixed PSCs only occur between T_{ICE} and $T_{\text{ICE}+2}$ K, and gas-phase HNO_3 is completely depleted. At higher temperatures modeled PSCs contain only NAT and at lower only STS particles. Lambert et al. (2012) have also shown that CALIPSO observa-

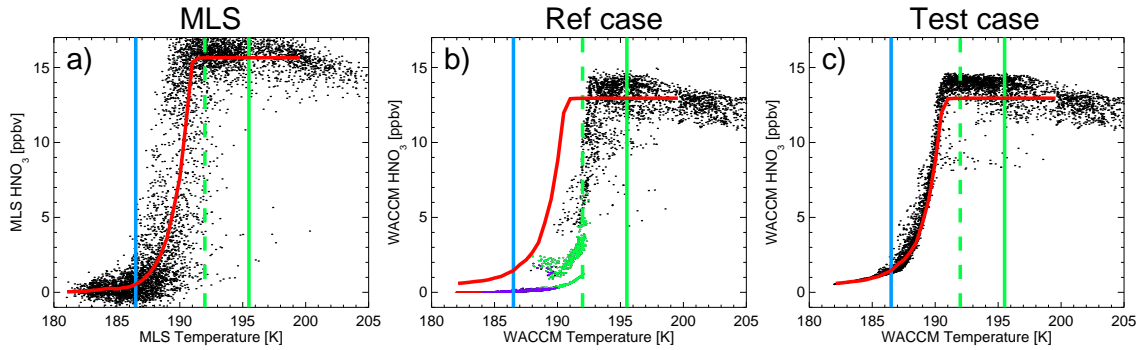


Figure 6.2.: a) All MLS gas-phase HNO_3 observations on 475 K between 1 May and 1 July 2005 over Antarctica correlated with temperature. b) Reference simulation output on the locations of the observations described in a). c) Same as b) for the test simulation. Green marks PSCs mainly composed of NAT, with more than 50 % of total HNO_3 in NAT and less than 10 % in STS; Red PSCs with high STS content, more than 50 % of HNO_3 in STS and less than 10 % in NAT; and purple mixed PSCs with more than 20 % HNO_3 in NAT and more than 20 % in STS. Solid green line marks T_{NAT} , dashed green line $T_{\text{S,NAT}}$ and solid blue T_{ICE} .

tions of liquid PSCs follow the thermodynamic equilibrium function for STS. No model data points coincide with this function, since STS only forms after gas-phase HNO_3 has already been completely depleted by the preceding formation of NAT.

Observations of the entire vortex show a similar dependence of gas-phase HNO_3 on temperature like the 475 K isentrope shown in Figure 6.2a. Removal from the gas-phase starts between T_{NAT} and $T_{\text{S,NAT}}$ and reaches its maximum around T_{ICE} (Figure 6.3b). The theoretical maximum uptake of HNO_3 on STS (Figure 6.3c) is calculated with the STS equilibrium function from Carslaw et al. (1995b). This theoretically possible uptake starts between $T_{\text{S,NAT}}$ and T_{ICE} . Figure 6.3d shows the difference between observed removal of gas-phase HNO_3 and the theoretical uptake by STS. Removal of HNO_3 before the uptake by STS may be due to the formation of NAT particles (Figure 6.3d). Assuming that this decrease is caused by NAT particles, NAT formation begins at temperatures around $T_{\text{S,NAT}}$ between 500 and 550 K. Outside this area, depletion of gas-phase HNO_3 can be explained by the formation of STS. SD-WACCM cannot reproduce this kind of distribution.

In the model gas-phase HNO_3 drops sharply as soon as the specified supersaturation, $T_{\text{S,NAT}}$, for NAT is reached (Figure 6.4b). At this temperature the model partitions all available HNO_3 into NAT without forming any STS (Figure 6.4c). When temperatures

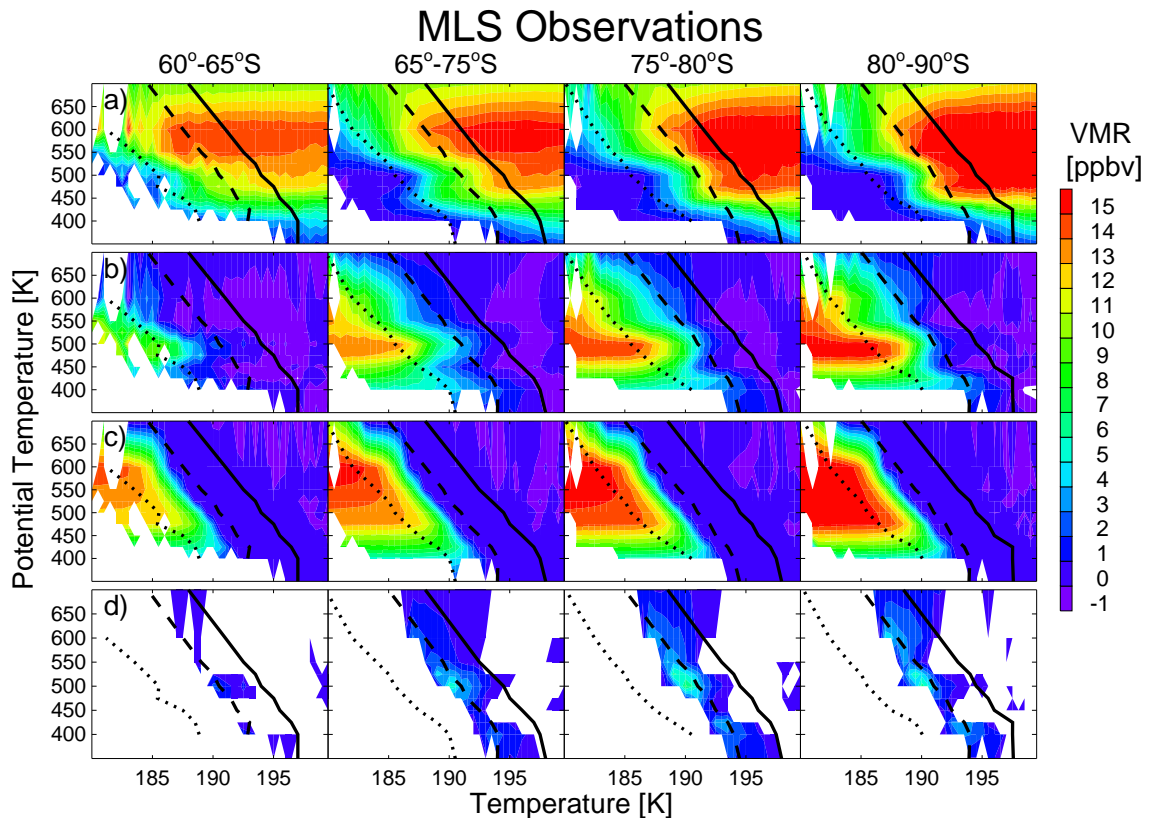


Figure 6.3.: a) Observations of gas-phase HNO_3 by MLS as function of temperature over Antarctica from 1 May to 1 July 2005 for four equivalent latitude regions. b) Condensed HNO_3 assuming no irreversible denitrification. c) Theoretical uptake of HNO_3 by STS. d) Difference of observed HNO_3 removal from the gas-phase and theoretical uptake by STS. Solid line is T_{NAT} , dashed $T_{\text{S-NAT}}$ and dotted T_{ICE} .

decrease further, STS becomes more abundant, and below the frost point STS is the only PSC type present (Figure 6.4d). This is contrary to the PSC behavior described in Pitts et al. (2009). Pitts et al. (2009) show that STS forms first and transitions into mix 2 PSCs (STS and high particle number density NAT) as temperatures decrease. At the end of winter, when temperatures increase, mix 2 transitions back into STS. Pitts et al. (2009) do not report a transition from NAT to STS with decreasing temperature. Mixed PSCs only exist to a minor extent in the model, between $T_{\text{S-NAT}}$ and T_{ICE} . In the model denitrification occurs in this narrow temperature range and shuts off once the vortex cools down to the frost point as NAT is no longer present. Nonetheless, denitrification is very efficient in this simulation, with NO_y dropping from 13 to 5 ppbv in the vortex core on 500 K once temperatures have reached the frost point.

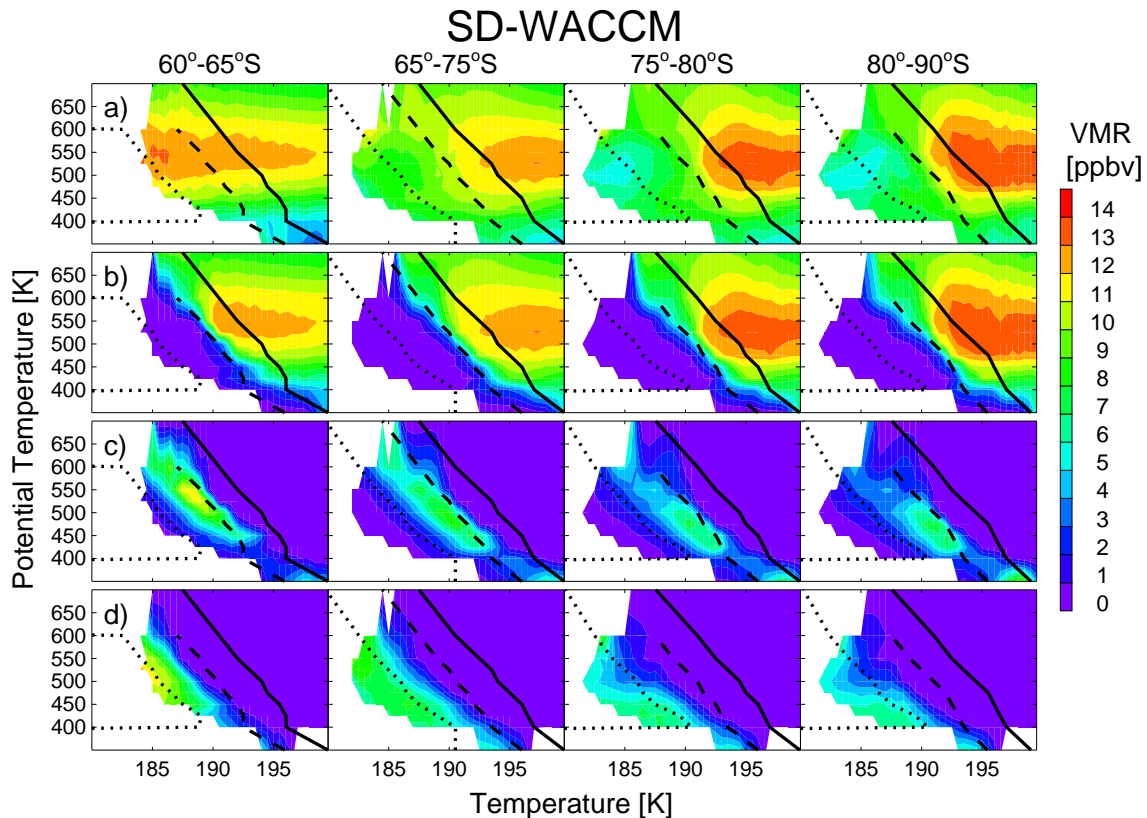


Figure 6.4.: a) SD-WACCM reference simulation NO_y as function of temperature over Antarctica from 1 May to 1st July 2005 for four equivalent latitude regions. b) Gas-phase HNO_3 . c) HNO_3 in NAT. d) HNO_3 in STS. Solid line is T_{NAT} , dashed $T_{\text{S_NAT}}$ and dotted T_{ICE} .

This comparison of modeled and observed gas-phase HNO_3 shows that overall the model gives a fairly good representation of denitrification. This is an important factor since the abundance of gas-phase HNO_3 can influence the speed of chlorine deactivation and therefore the extent of ozone depletion. However, the model's representation of HNO_3 containing PSCs is very different from the observations. In the model mixed phase PSCs form only rarely, and it has an unphysical transition from solid to liquid particles with decreasing temperatures.

6.1.2. Test Simulation

Since the model's main shortcoming is the representation of mixed PSCs, a test simulation is conducted in which the way the model partitions HNO_3 between the different PSC types is altered. CALIPSO observations suggest that most mixed phase PSCs

occur at backscatter and depolarization ratios between the Pitts et al. (2009) classification of mix 1 and mix 2. Mix 1 clouds are composed of STS and low particle number density NAT ($3 \cdot 10^{-4} \text{ cm}^{-3}$ - 10^{-3} cm^{-3}), and mix 2 of STS and high particle number density NAT ($> 10^{-3} \text{ cm}^{-3}$). The boundary between mix 1 and mix 2 corresponds to clouds containing NAT particles with an effective radius between $2 \mu\text{m}$ and $7 \mu\text{m}$, and a particle number density between 10^{-2} cm^{-3} and 10^{-3} cm^{-3} . When a NAT particle density of $1.62 \text{ g} \cdot \text{cm}^{-3}$ is assumed (Drdla et al., 1993), between 2 and 10 ppbv HNO_3 are present in NAT. This corresponds to 15-75% of the total available HNO_3 , assuming no irreversible denitrification. In addition, Biele et al. (2001) reported that ground based LIDAR observations of PSCs over Ny Alesund (located at 79°N) can best be explained when only 5% of the total available HNO_3 is allowed to condense onto solid particles.

Therefore, in the test simulation of SD-WACCM the amount of total available HNO_3 that is allowed to form NAT is limited. Best agreement with observed denitrification is achieved when 20% of total available HNO_3 is allowed to form NAT at a supersaturation of 10 and a particle number density of 10^{-2} cm^{-3} . Such a particle number density is also more in agreement with CALIPSO observations than the 10^{-1} cm^{-3} , which are assumed in the reference case, since Pitts et al. (2009, 2011) show that most NAT PSCs have a particle number density between 10^{-2} and 10^{-3} cm^{-3} . STS droplets still form according to Tabazadeh et al. (1994b), but only HNO_3 that has not been taken up by NAT is allowed to form STS.

With this approach NAT PSCs occur at $T_{\text{S,NAT}}$. But instead of transitioning into STS with decreasing temperature, both PSC types can coexist throughout the entire temperature range, with STS becoming more abundant at lower temperatures (Figure 6.5c and d). This is consistent with Lambert et al. (2012), who have shown that liquid PSCs occur more frequently than mixed PSCs at temperatures around the frost point. While the reference simulation shows a sharp drop in gas-phase HNO_3 when it is partitioned into NAT at $T_{\text{S,NAT}}$, HNO_3 is now gradually removed from the gas-phase beginning at $T_{\text{S,NAT}}$ and completely removed around the frost point (Figure 6.5b).

The model still cannot reproduce the sharp decrease which is observed at 190 K around 500 K potential temperature. Pitts et al. (2009) show increases in mix 2 PSCs at the beginning of June around 20 km, which would be consistent with this observed removal of HNO_3 from the gas-phase, suggesting that this depletion of gas-phase HNO_3 may be driven by the formation of PSCs with high NAT particle number density. Since the model forms NAT at only one prescribed number density and one specified supersaturation, this behavior cannot be represented with the current PSC scheme.

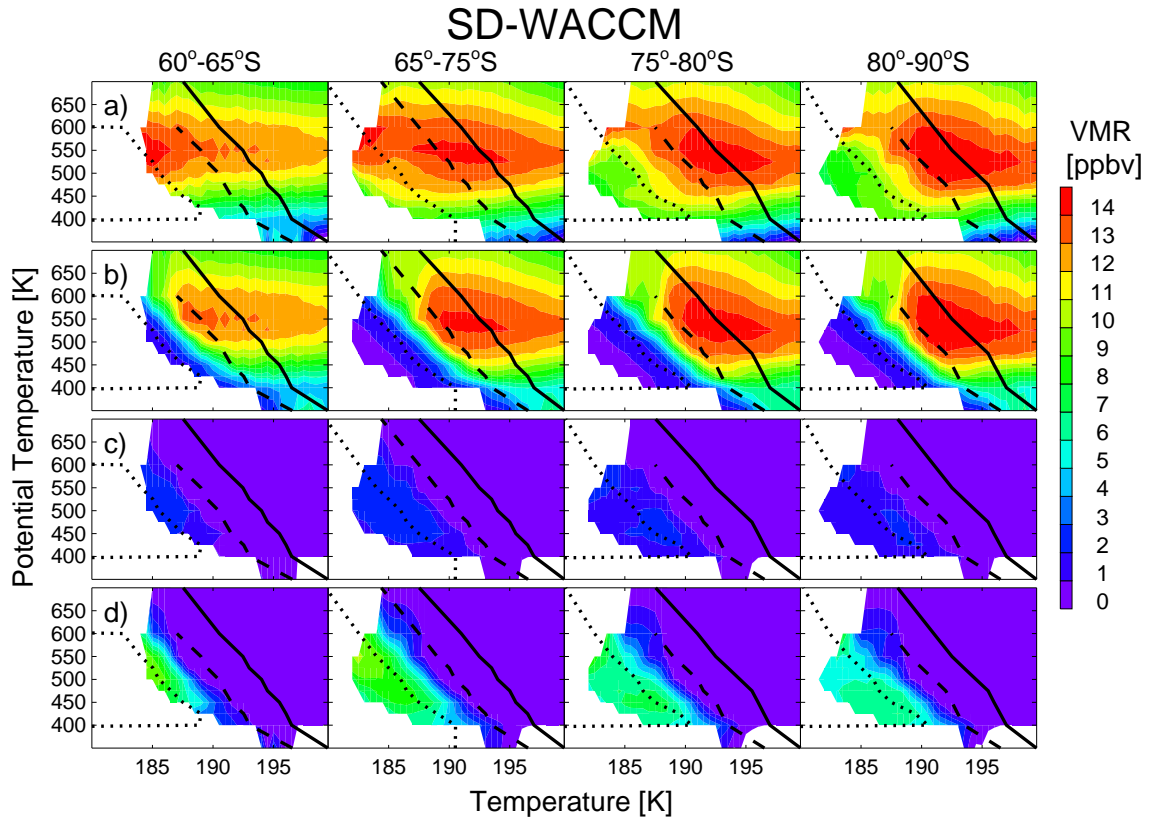


Figure 6.5.: a) SD-WACCM test simulation NO_y as function of temperature over Antarctica from 1 May to 1 July 2005 for four equivalent latitude regions. b) Gas-phase HNO_3 . c) HNO_3 in NAT. d) HNO_3 in STS. Solid line is T_{NAT} , dashed $T_{\text{S_NAT}}$ and dotted T_{ICE} .

The temperature dependence of HNO_3 on the 475 K isentrope now shows better agreement with the observations (Figure 6.2c). The removal of HNO_3 from the gas-phase is more compact than the reference simulation and the sharp drop at $T_{\text{S_NAT}}$ has been removed. Gas-phase HNO_3 now follows the STS equilibrium function, in good agreement with observations. STS is the most abundant modeled PSC type but the model is missing mix 2 PSCs which lead to very low gas-phase HNO_3 at temperatures between T_{NAT} and the STS function (Lambert et al., 2012).

The model shows significantly less scatter than the satellite observations due to the simplification that all PSCs are in thermodynamic equilibrium and exist at only one prescribed size distribution. In the real atmosphere an air parcel's history, especially the cooling rate, will have a crucial influence on PSC composition and size distribution. Therefore, air masses sampled at the same temperature can have very different parti-

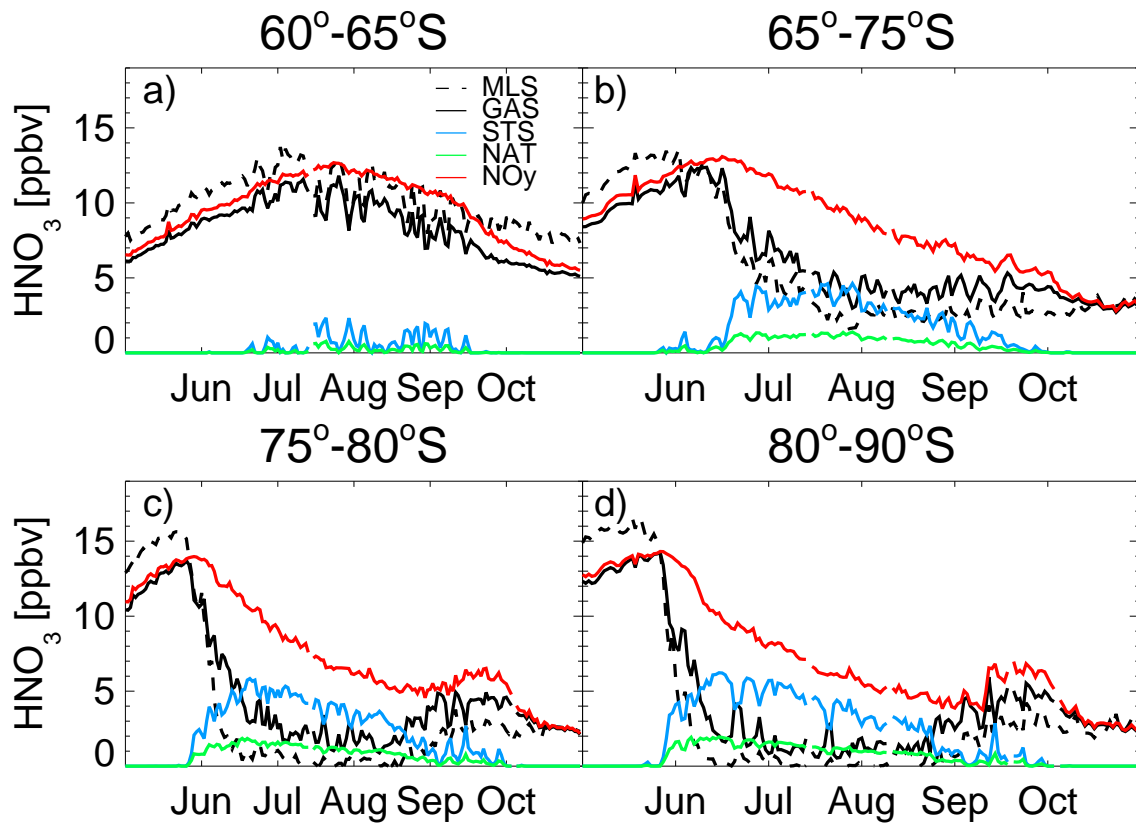


Figure 6.6.: Observations of gas-phase HNO_3 and modeled partitioning of HNO_3 between the gas-phase and PSCs on 475 K over Antarctica 2005 for four equivalent latitude regions. Dashed lines are observations of gas-phase HNO_3 by MLS and solid lines model output from the test simulation.

tioning of HNO_3 between gas-phase and the different PSC types, and do not necessarily have to be in thermodynamic equilibrium, as assumed in the model.

In the test case denitrification is a continuous process which slows down gradually as HNO_3 is irreversibly removed from the lower stratosphere (Figure 6.6). The maximum allowed amount of 20% of total available HNO_3 is partitioned into NAT from end of May for almost four months poleward of 65°S equivalent latitude. Gas-phase HNO_3 is never completely removed, and throughout the winter it is about 1-2 ppbv higher than observations. Still, the test simulation achieves a similar denitrification as the reference case and good agreement with observations.

The vertical distribution of HNO_3 shows improvement in the test simulation compared to the reference, especially in early winter (Figure 6.7). The reference simulation is only from August onward and below 500 K in better agreement with the observations than

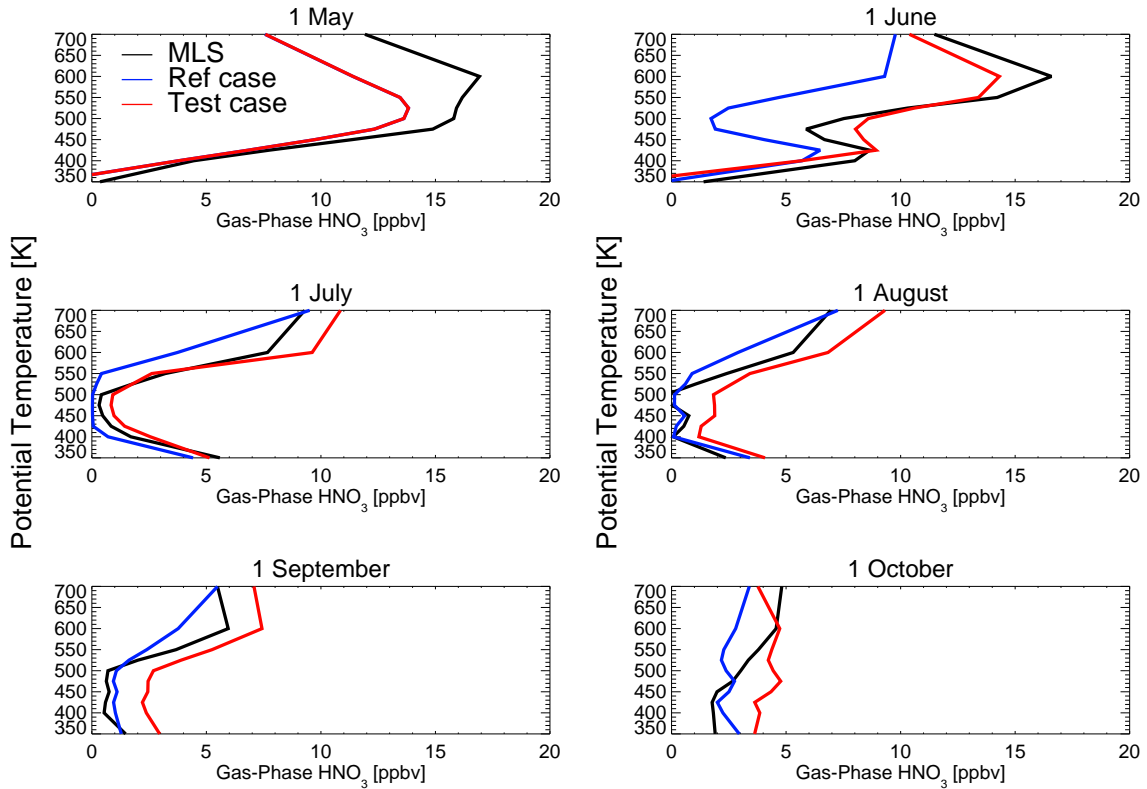


Figure 6.7.: Vertical distribution of gas-phase HNO_3 over Antarctica 2005 for six different days poleward of 80°S . Solid black lines are MLS measurements, blue lines are the reference simulation and red lines are the test simulation with updated PSC scheme.

the test case. Although gas-phase HNO_3 in the test simulation tends to be higher than the observations, the shape of the vertical distribution agrees with observations. Gas-phase HNO_3 in the test simulation is, except for the initialization on 1 May, always within 2 ppbv of the observations while the reference simulation is, temporarily, more than 5 ppbv lower than observations. Overall, the test simulation is in better agreement with observations than the reference, although HNO_3 in the test case is never completely removed from the gas-phase.

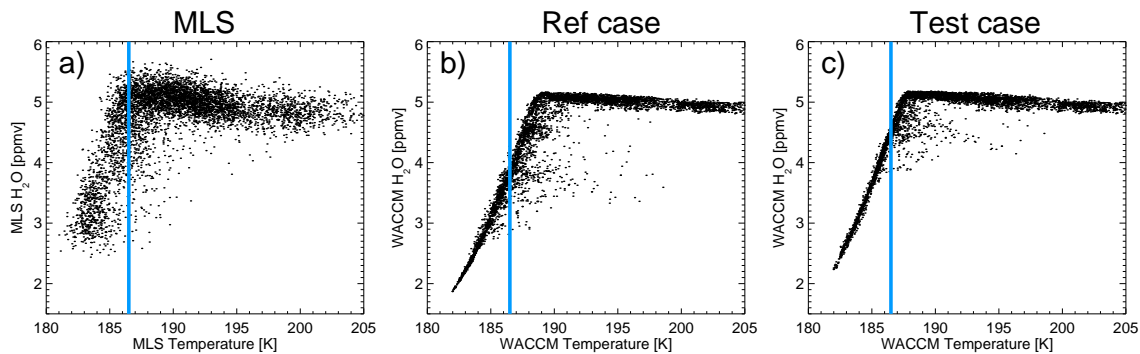


Figure 6.8.: a) All MLS gas-phase H_2O observations on 475 K between 1 May and 1 July 2005 over Antarctica correlated with temperature. b) Reference simulation output on the location of the observations described in a). c) Same as b) for the test simulation. Solid blue line marks T_{ICE} .

6.2. Type II PSCs

6.2.1. Observations and Reference Simulation

A second type of PSCs are ice clouds which can form at temperatures below the frost point (T_{ICE}). Just as HNO_3 removal from the gas-phase is an indicator for STS and NAT formation, a decrease in water vapor indicates the formation of ice clouds.

The temperature-dependence of observed water vapor (Figure 6.8a) shows that water vapor starts to decrease around the frost point. In the reference simulation, on the other hand, water vapor starts to decrease about 2 K above the frost point, which leads to faster dehydration than is observed. This faster dehydration has strong implications for the solubility of trace gases in STS particles, which primarily depends on ambient water vapor concentrations. The solubility of HNO_3 and HCl , as parameterized in Carslaw et al. (1995a), is primarily a function of water activity. With water vapor tied up in ice, less water condenses onto STS which causes a drastic decrease in HCl and HNO_3 solubility. For example, at 186 K and 50 hPa a drop in gas-phase water vapor from 4.5 to 2 ppmv, which commonly occurs in the Antarctic, causes the fraction of dissolved HNO_3 to drop from 99 to 75% and HCl from 76 to 1%.

Water vapor observations from MLS show ice formation between 400 and 550 K poleward of 65°S equivalent latitude (Figure 6.9a and b). Calculating the frost point according to Marti and Mauersberger (1993) indicates that ice formation below 500 K begins around T_{ICE} , which means that no or only little supersaturation is needed for ice clouds to form. With increasing altitude, a decrease in water vapor is only observed at

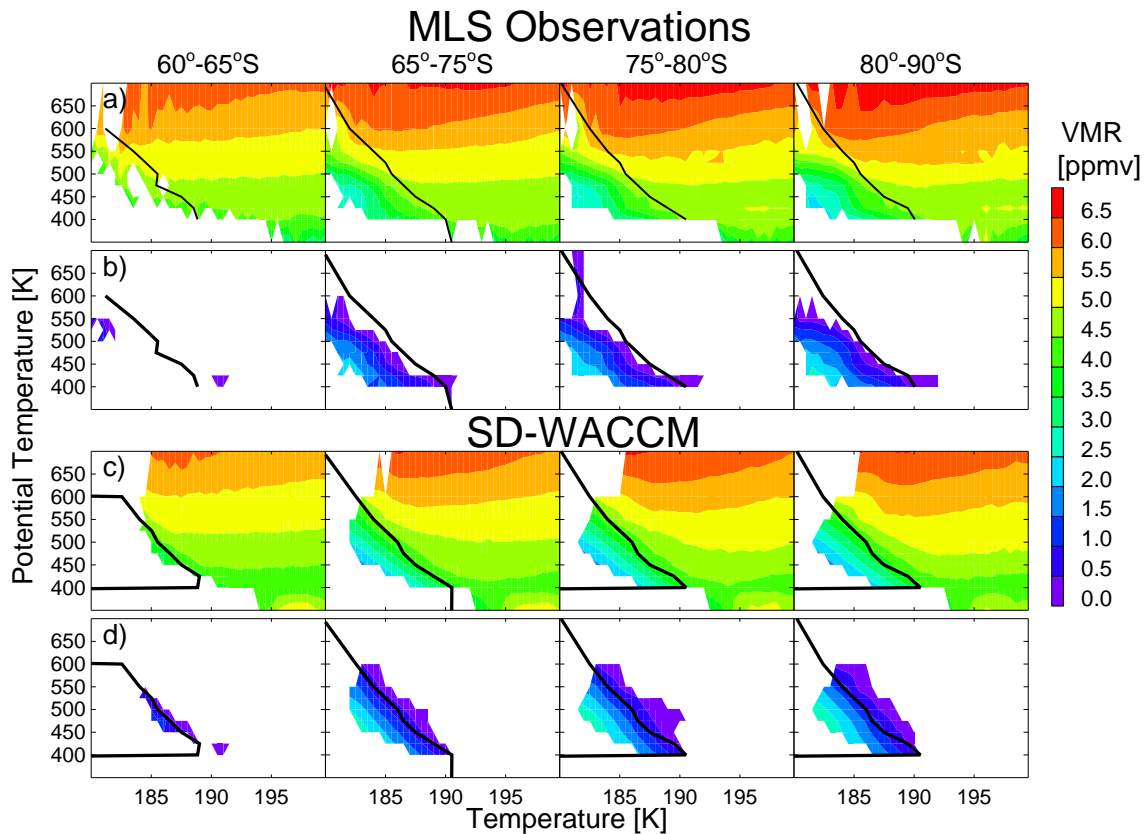


Figure 6.9.: a) Observations of gas-phase H_2O by MLS as function of temperature over Antarctica from 1 May to 1 July 2005 for four equivalent latitude regions. b) Condensed H_2O assuming no irreversible dehydration c) SD-WACCM reference gas-phase H_2O d) SD-WACCM H_2O in ice. Solid line is T_{ICE} .

temperatures well below the frost point, indicating that here a certain supersaturation is needed before ice clouds form, and the highest altitude for ice formation appears to be between 550 and 600 K. SD-WACCM assumes that ice clouds are always in equilibrium with gas-phase water vapor and form at a specified supersaturation. In the reference simulation ice clouds form at up to 600 K, and cause significantly higher dehydration than is observed. Observations show dehydration until the end of June of up to 50% (2 ppmv) in the vortex core (Figure 6.4b), while in the model water vapor decreases by up to 3 ppmv.

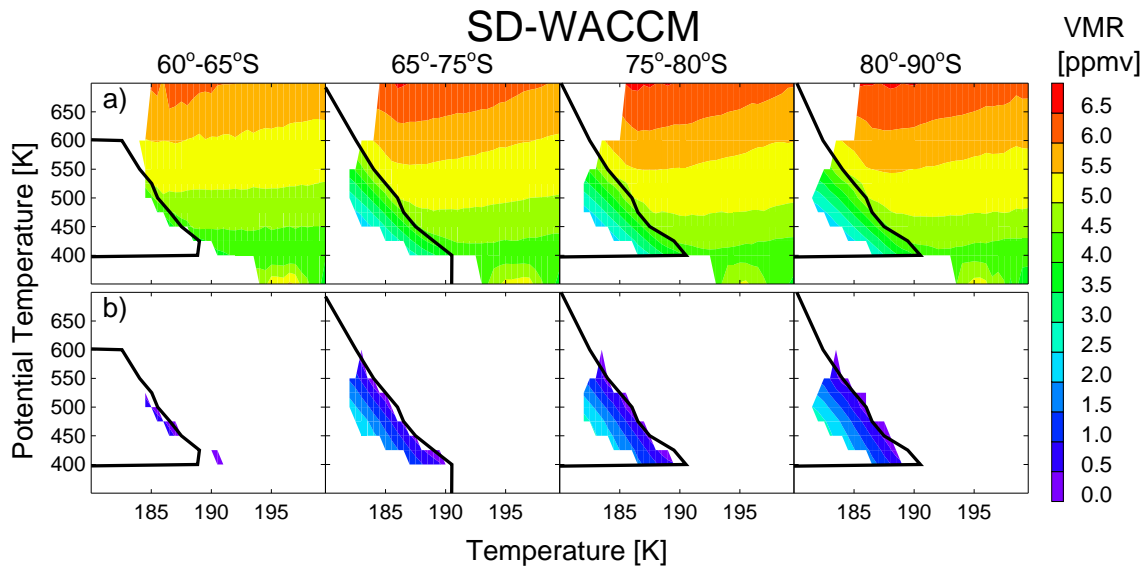


Figure 6.10.: a) SD-WACCM test simulation gas-phase H_2O b) SD-WACCM H_2O in ice. Solid line is T_{ICE} .

6.2.2. Test Simulation

The parameter controlling the supersaturation for ice clouds in the reference simulation was set, so modeled upwelling of water vapor through the cold point near the tropical tropopause agrees with observations. To achieve an improved representation of ice clouds in the Antarctic vortex, this parameter is tuned in the test case so ice clouds would form at temperatures close to the frost point.

With the new supersaturation, the test simulation produces very good agreement with observations (Figure 6.8c). Dehydration still starts at temperatures slightly above the frost point, but the modeled temperature dependence is similar to observations. The modeled temperature dependence of water vapor shows less scatter than the observations, due to the assumption that all ice clouds are in instant thermodynamic equilibrium with the gas-phase. In the real atmosphere ice formation, just like NAT formation, probably depends on more factors than just the equilibrium temperature, leading to variable attributes of the ice cloud (e.g. size distribution and number density), which causes the scatter of the temperature dependence.

The onset of dehydration in the test simulation occurs close to the frost point over the entire vertical range (Figure 6.10b), in agreement with observations. But the gradient of water vapor with decreasing temperature is stronger in the model than in the observations. At the minimum temperature on 500 K, observations show a decrease in water

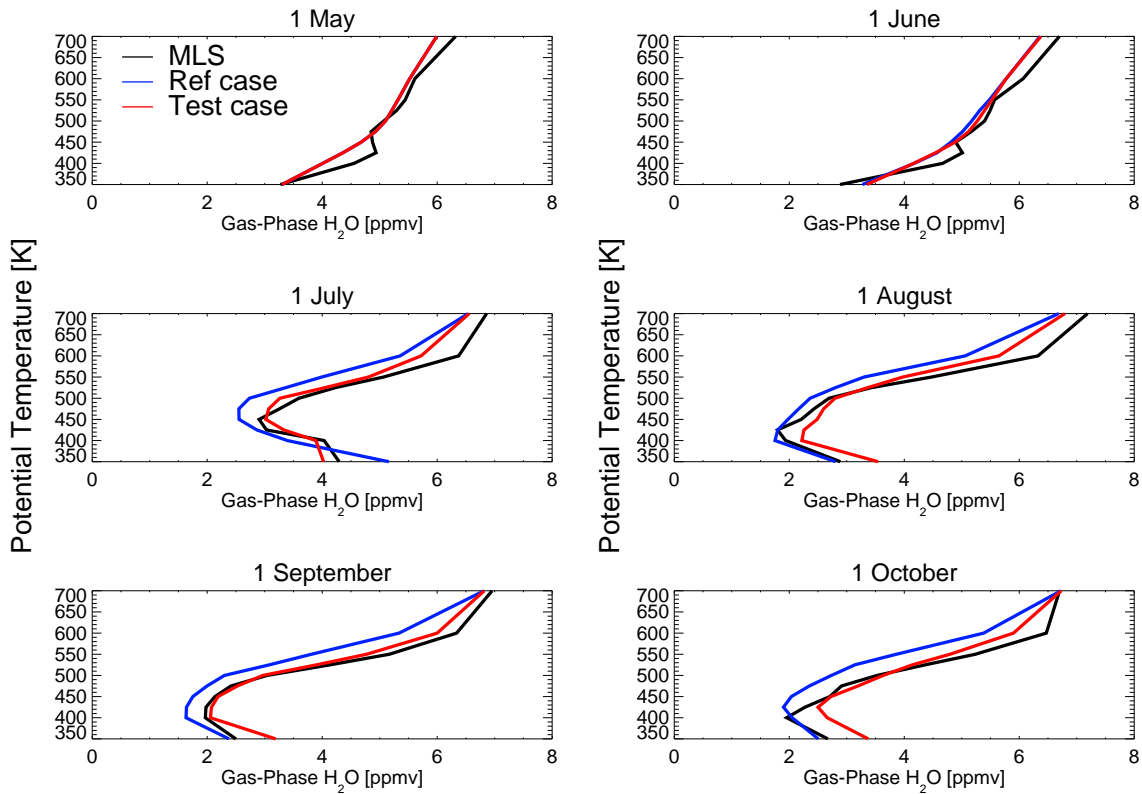


Figure 6.11.: Vertical distribution of gas-phase H_2O over Antarctica 2005 for six different days poleward of 80°S . Solid black lines are MLS measurements, blue lines are the reference simulation and red lines are the test simulation with updated PSC scheme.

vapor of 1.5 ppmv (Figure 6.9b). The test simulation shows a decrease of 2.5 ppmv, although temperatures in the model are about 1.5 K higher than observations indicate.

The vertical distribution of water vapor over the Antarctic winter 2005 for the simulations and observations is shown in Figure 6.11. The test simulation cannot only reproduce the shape of the observations, but is also in good agreement with the absolute values. The reference simulation overestimates the extent of dehydration over the whole vertical range by about 0.5-1 ppmv. Overall, the test case gives a very good representation of observed water vapor over the entire lower stratosphere and throughout the entire winter.

6.3. Conclusions

Observations from MLS provide important constraints on the occurrence of PSCs in the Antarctic 2005 and their representation in climate models. The analysis presented in this chapter focuses on the months of May and June, which provide information on the beginning of the PSC formation phase. Observations show that gas-phase HNO_3 decreases between $T_{\text{S_NAT}}$ and T_{ICE} . Most of this decrease can be explained with condensation of HNO_3 on the background aerosol and the formation of STS. But around 500 K, HNO_3 decreases at temperatures where no significant uptake of HNO_3 on the background aerosol is expected. At this altitude, HNO_3 is probably nucleating to NAT, forming PSCs with high NAT particle number density. In addition to STS and NAT, the observations also provide constraints for ice clouds. These observations show that the occurrence of ice clouds coincides with temperatures around the frost point.

The skill of SD-WACCM's thermodynamic equilibrium scheme for PSCs in representing the observed removal of HNO_3 and H_2O from the gas-phase has been analyzed in this chapter. The reference simulation has a fairly good representation of overall denitrification but cannot reproduce the temperature-dependent distribution of PSCs. The reference simulation shows a sharp transition from NAT to STS with decreasing temperature, with almost no occurrence of mixed PSCs. In contrast, observations show that PSCs transition from STS to NAT with decreasing temperature, with liquid PSCs being the dominant type and a large fraction consisting of mixed phase PSCs (Pitts et al., 2009, 2011; Lambert et al., 2012). For the test simulation NAT is set to be the preferred modeled PSC type, but at the same time the fraction of total HNO_3 to form NAT is limited, which forces the formation of mixed PSCs in the model. This approach significantly improves the agreement of modeled gas-phase HNO_3 with observations. In particular, the temperature dependence of HNO_3 removal from the gas-phase now shows good resemblance with observations. With a NAT particle number density of 10^{-2} cm^{-3} , modeled denitrification still agrees with observations while also giving an improved representation of HNO_3 containing PSCs. Most important, the unphysical transition from solid to liquid particles with decreasing temperature is removed in the test case, and mixed phase PSC occur throughout the entire winter.

MLS observations of water vapor show that ice formation occurs around the frost point, which suggests that no or only slight supersaturation is needed to form ice PSCs in the polar stratosphere. The reference simulation uses a global parameter, which was derived according to the upwelling of water vapor through the tropopause, to specify

the needed supersaturation for ice clouds. But this approach forms ice clouds at temperatures well above the frost point, which causes too severe dehydration compared to observations. In the test case, ice clouds form closer the frost point, which gives good agreement with the observed temperature-dependence and vertical distribution of water vapor and dehydration.

Since ice clouds near the tropical cold point and the polar stratosphere appear to require different supersaturation for their formation, ice clouds in these two regions seem to have different nucleation mechanisms. But without coupling SD-WACCM to a micro-physical model, this behavior cannot be accurately represented. Overall, the model gives a good representation not only of PSCs but also of denitrification and dehydration with the changes in parameterization described here, despite the simplified assumption that all PSCs are in thermodynamic equilibrium.

7. Chlorine Partitioning in SD-WACCM

In the previous chapters heterogeneous reaction rates were validated and the influence of the various aerosol types on chlorine activation elucidated. Furthermore, the ability of the chemistry-climate model SD-WACCM to represent PSCs with the updated scheme was demonstrated. This chapter focuses on chlorine activation and partitioning in SD-WACCM. Complete depletion of gas-phase HCl is regularly observed in the Antarctic vortex and for very cold winters in the Arctic (Manney et al., 2011), but is difficult to reconcile with the limited availability of reaction partners for HCl. Moreover, Brakebusch et al. (2012) have shown that the early decrease of gas-phase HCl, which is limited by the availability of ClONO₂, cannot be explained by heterogeneous chemistry alone. In this chapter possible sources of NO_x in the lower stratosphere are constrained, and additional sinks for gas-phase HCl beside heterogeneous chemistry are explored. The focus is again on the Antarctic winter season of 2005.

7.1. Description of SD-WACCM Simulations

Figure 7.1 shows results from a standard SD-WACCM simulation (BASE). Here, HNO₃ and H₂O are in good agreement with observations. The model tends to remove HNO₃ and H₂O slightly earlier compared to observation, this prompted modifications to the scheme for Polar Stratospheric Clouds (PSCs) which are discussed in detail in Chapter 6. However, the standard PSC scheme already gives an excellent account of the observed denitrification and a reasonably well for dehydration. While model HNO₃ and H₂O are in agreement with observations, HCl shows a great discrepancy to observations.

Modeled HCl is significantly higher than the observations throughout the entire winter, with the largest differences in June and July. It is important to note that there is no indication for irreversible removal of HCl in the observations, unlike HNO₃ and H₂O. Actually, HCl shows a super-recovery since the partitioning between the chlorine

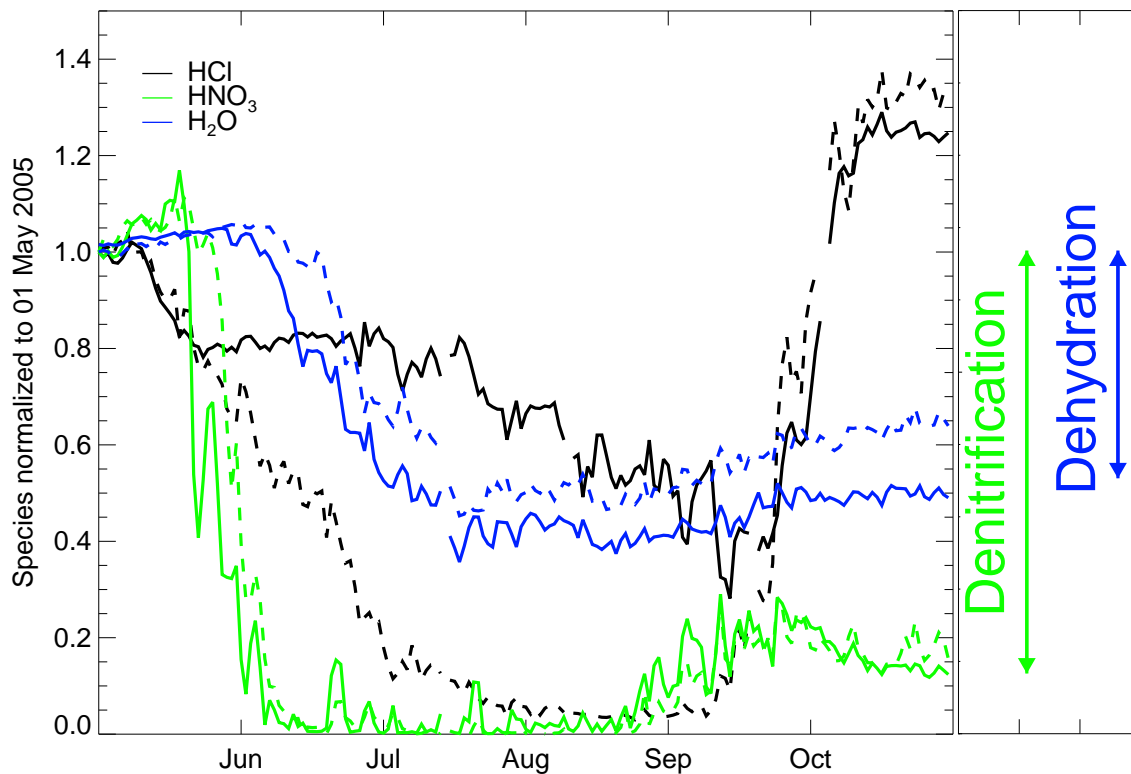


Figure 7.1.: Model (solid) and MLS observations (dashed) of gas-phase HCl, HNO₃ and H₂O poleward of 80°S from May through October 2005. Species are normalized to 1st May 2005 values.

reservoir species changes between formation and breakup of the polar vortex. Therefore, HCl is most likely removed by chemical or physical processes within an air mass and not by the sedimentation of HCl containing particles.

In addition to the BASE simulation, four model test cases are created, which include novel processes to analyze the loss of gas-phase HCl. All the test cases use the new PSC scheme, and an overview of the processes included in each case is given in Table 7.1. H_{HCl} denotes the Henry's law constant which describes the solubility of HCl in STS. In these cases HCl is actively partitioned between gas and condensed phase. Cases with $J_{\text{HNO}_3(c)}$ include the photolysis of HNO₃ that is condensed in PSC particles.

In addition, the sensitivity to temperature is tested by applying a temperature bias to the heterogeneous chemistry module of SD-WACCM. This temperature bias affects the heterogeneous reaction rates, HCl solubility, and the formation of STS and NAT particles. This temperature bias is based on the work by Brakebusch et al. (2012), who reported a warm bias of SD-WACCM in the Arctic vortex compared to observations, and

Table 7.1.: Overview of model cases and included processes.

case label	new PSC scheme	H_{HCl}	$J_{\text{HNO}_3(\text{c})}$	-2 K T-Bias
BASE	-	-	-	-
H_{HCl}	x	x	-	-
$H_{\text{HCl}} - 2 \text{ K}$	x	x	-	x
$J_{\text{HNO}_3(\text{c})}$	x	-	x	-
$J_{\text{HNO}_3(\text{c})} - 2 \text{ K}$	x	x	x	x

found improved agreement between modeled and observed HCl when applying a -1.5 K bias to the heterogeneous chemistry module. A similar bias of around 1 K is visible when modeled temperatures are compared to observations in the 2005 Antarctic vortex. Thus, a -2 K bias is applied to two test cases, this bias also includes the uncertainty of the temperature dependence of HCl solubility in STS and PSC formation (Lowe and MacKenzie, 2008).

7.2. Depletion of Gas-Phase HCl

7.2.1. Observations and the BASE Simulation

HCl and ClONO₂ are the main inorganic chlorine reservoir species in the stratosphere. The initial mixing ratios of those two species, as observed by ACE-FTS, are shown in Figure 7.2. Additionally, Figure 7.2 shows N₂O₅, the nighttime reservoir for NO_x. Only observations between 20th April and 1st May poleward of 70°S for the years 2004 to 2011 are shown in Figure 7.2. The Antarctic vortex starts to form during this period, and it conserves the initial ratio between HCl and ClONO₂ until temperatures drop low enough for these species to react heterogeneously (Solomon et al., 1986).

The initial ratio ClONO₂:HCl has a maximum of 0.3 at 20 km and a minimum of 0.15 at 15 and 35 km, respectively (Figure 7.2). This ratio would be expected to limit the effectiveness of chlorine activation. The bottleneck for the heterogeneous reactions responsible for the depletion of HCl is mainly the availability of ClONO₂. ClONO₂ is formed through reaction 2.11 with NO₂ being the limiting partner. HCl can also be depleted by the reaction with HOCl. The formation of HOCl is limited by the availability of OH; therefore, as long as ozone does not reach very low values (Grooß et al., 2011), this reaction is of only minor importance. Despite this imbalance, observations show that HCl is completely removed from the gas-phase in the lower stratosphere by July in the

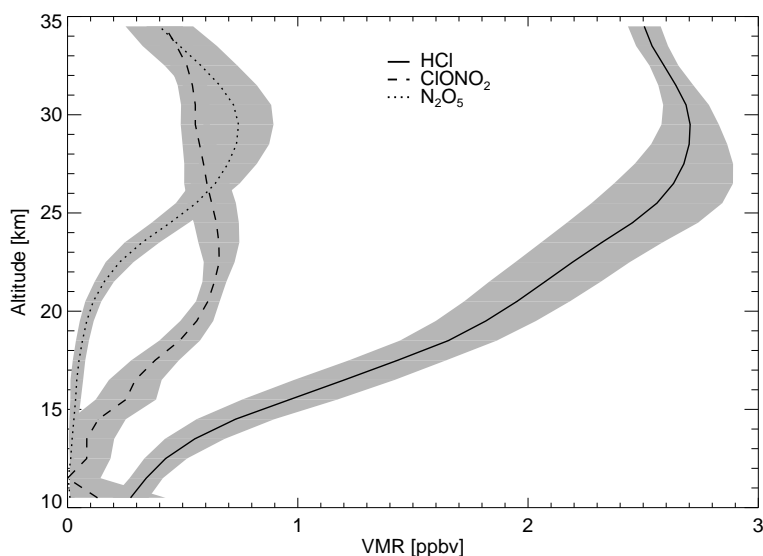


Figure 7.2.: Averaged ACE-FTS profiles of HCl (solid), ClONO₂ (dashed) and N₂O₅ (dotted) between 20th April and 1st May from 2004 to 2011 poleward of 70°S. Grey shading indicates the standard deviation.

Antarctic, and January in the Arctic for cold winters (e.g. Santee et al., 2008; Brakebusch et al., 2012). From the ACE-FTS observations it can be assumed that heterogeneous reactions with the initially available ClONO₂ can at most explain a depletion of 30% in gas-phase HCl. If the complete depletion of gas-phase HCl is caused by heterogeneous chemistry, ClONO₂ needs to be reformed during the polar night.

Figure 7.3 shows the distribution of gas-phase HCl on three different days for the BASE case and MLS observations. The meridional structures in gas-phase HCl are a clear indicator for the dependence of the supply of NO_x on the solar zenith angle. On 15th June the model and observations show three distinct regions of gas-phase HCl concentrations. The region between 60° and 50°S has HCl mixing ratios of up to 1.5 ppbv. This region is located just outside the polar vortex; hence, HCl concentrations in this region are unperturbed by heterogeneous chemistry. Here, the model is in good agreement with observations.

The second region is a ring at the vortex edge region between 70° and 60°S, that shows slightly depleted HCl concentrations in the model, but already complete depletion in the observations. While the model can reproduce the spatial extent of the inner ring, it overestimates HCl mixing ratios there by up to 1 ppbv. This region is exposed to some sunlight, providing a limited supply of NO_x. However, this process is too slow in the BASE case to regenerate sufficient ClONO₂ by the middle of June to cause a ring of air

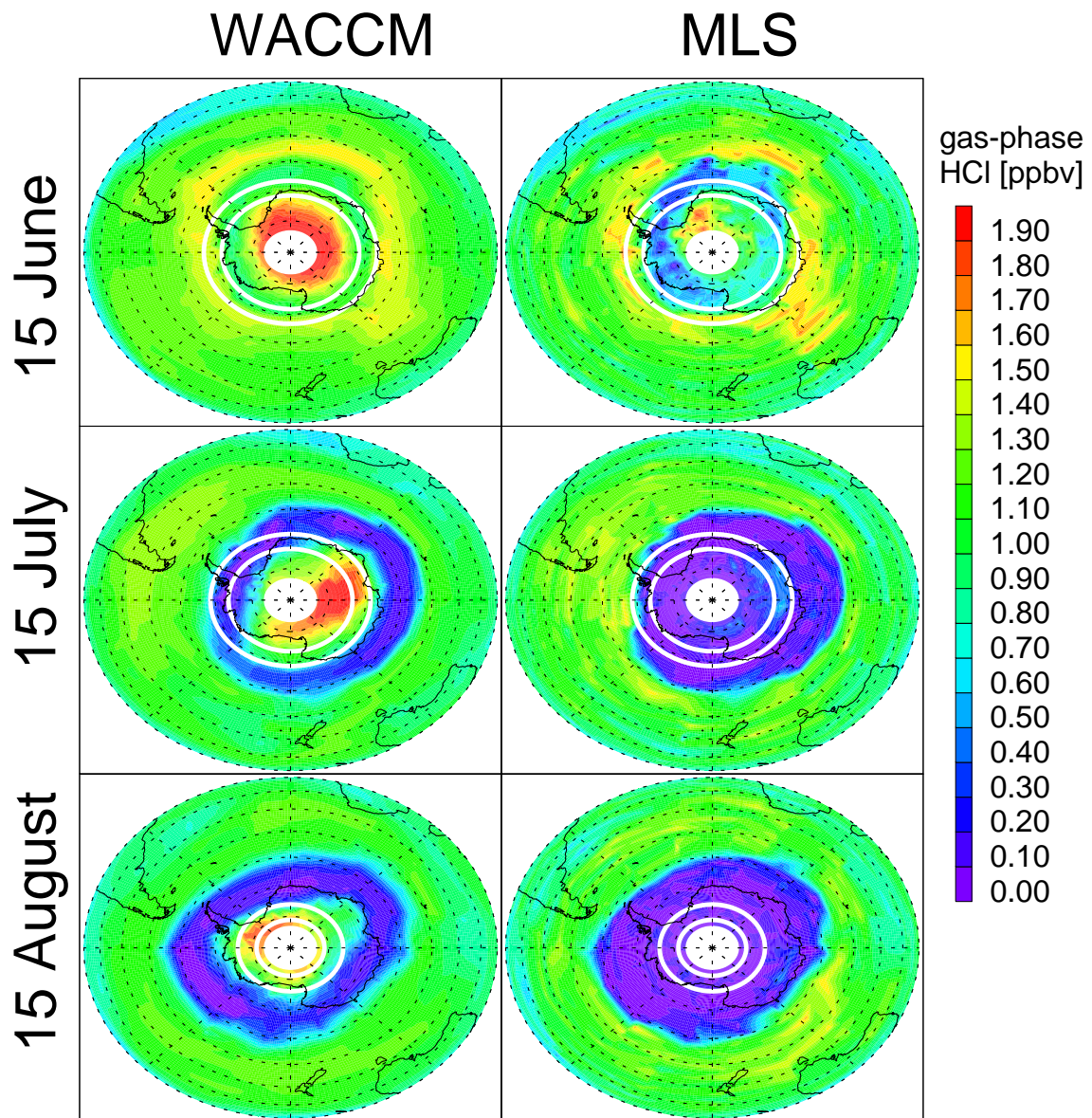


Figure 7.3.: BASE simulation (left) and observed (right) gas-phase HCl over Antarctica 2005 on 475 K. The white circles mark noontime solar zenith angles of 95° and 90° , respectively.

masses which are almost completely depleted in gas-phase HCl. This ring of depleted HCl suggests limitations in current photochemical schemes.

The third region is the vortex core where HCl concentrations are the greatest. This region is confined to darkness, effectively shutting off all photochemistry. The high HCl concentrations are caused by descent of HCl-rich air from higher altitudes, but the heterogeneous reaction of HCl with ClONO₂ is limited to the initially available ClONO₂. Just like in the inner ring the model overestimates HCl concentrations in this region, but observed and modeled maximum HCl concentrations of up to 2 ppbv are in agreement.

By 15th July, however, the BASE case shows little resemblance with observations (Figure 7.3, middle row). Satellite observations no longer show distinct regions of different HCl concentrations inside the vortex, but rather near-complete removal of gas-phase HCl throughout the entire polar vortex. The simulation eventually achieves complete depletion of gas-phase HCl, but only in the ring region. Poleward of this region HCl gas-phase concentrations steadily increase and remain practically unchanged in the vortex core compared to 15th June. While observations indicate that gas-phase HCl decreases by almost 2 ppbv in the vortex core between 15th June and 15th July, the model completely fails to reproduce this behavior.

On 15th August (Figure 7.3, bottom row) the meridional structure of gas-phase HCl, compared to one month earlier, has barely changed in the model and observations. MLS still indicates complete removal of gas-phase HCl, while modeled values in the vortex core remain essentially unchanged. The only change in the model compared to 15 July is the poleward expansion of the inner ring, that shows complete removal of gas-phase HCl. This expansion coincides with sunlight returning to higher latitudes, as indicated by the 90° and 95° boundaries for the noontime solar zenith angle. With more sunlight available, ClONO₂ is regenerated, driving the depletion of gas-phase HCl through heterogeneous chemistry.

The depletion in the ring region can be explained by photochemistry creating enough NO_x to steadily regenerate ClONO₂. The model indicates that in the vortex edge region ClONO₂ is never completely depleted (Figure 7.4a). This resupply of ClONO₂ then drives the depletion of HCl, leading to excellent agreement between model and observations as shown in Figure 7.4a.

However, the farther inside the vortex one looks, the stronger the difference between model and observations becomes. Poleward of 65°S standard photochemistry does not appear to be efficient enough to produce sufficient NO_x to keep up with the depletion of ClONO₂ through heterogeneous chemistry. Here, ClONO₂ is completely depleted in

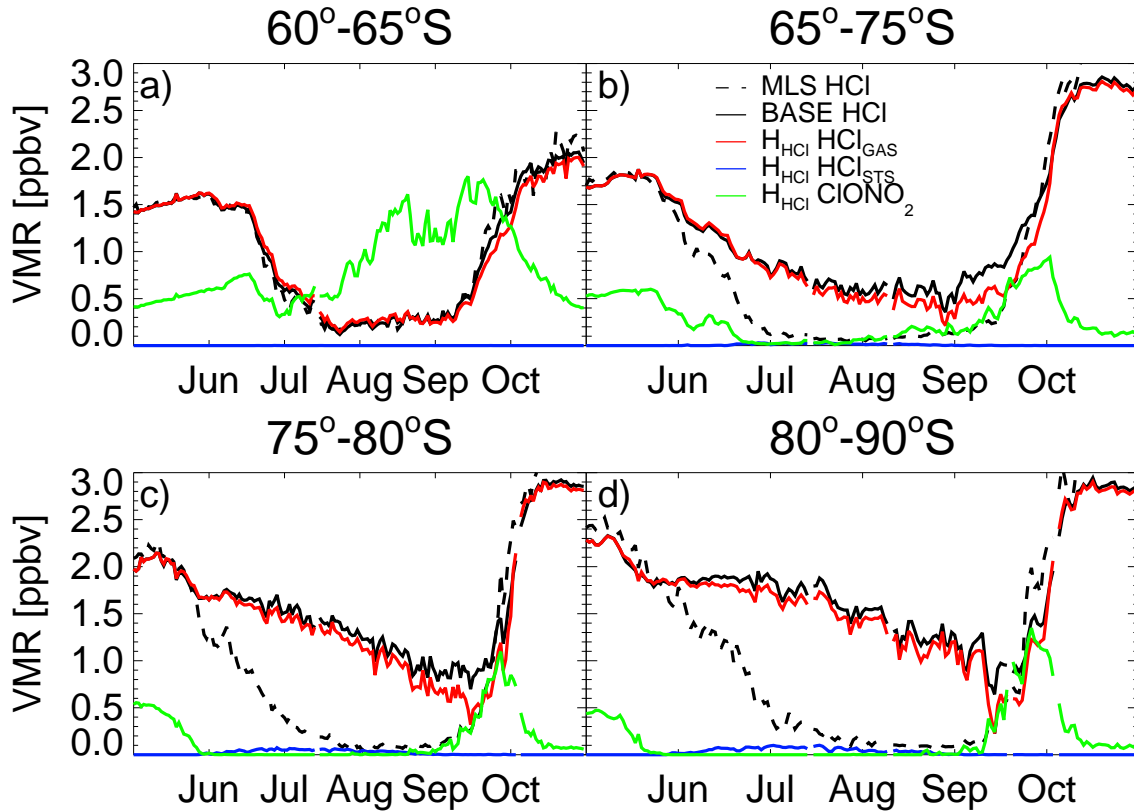


Figure 7.4.: Gas-phase HCl observations by MLS and chlorine partitioning for the BASE and H_{HCl} case for four equivalent latitude regions on 475 K.

the model, slowing down heterogeneous chemistry and the depletion of HCl. Poleward of 80°S , however, modeled HCl remains almost constant in June once initial ClONO_2 has been depleted, since no sunlight reaches these air masses until the end of July.

In contrast to the meridional structure of the depletion of gas-phase HCl, as seen in the model, observations indicate a steady decline of gas-phase HCl throughout the entire vortex. Poleward of 80°S gas-phase HCl declines at a rate of about $1000 \text{ molec}\cdot\text{cm}^{-3}\cdot\text{s}^{-1}$ ($50 \text{ pptv}\cdot\text{day}^{-1}$) on 15th June, whereas the model shows near constant gas-phase HCl mixing ratios. As the observed depletion rate of gas-phase HCl is constant in time and throughout the polar vortex, the process responsible for the depletion appears to be independent of solar zenith angle. However, the chemical regeneration of HCl, which begins in the middle of September, is accurately captured in the model and shows excellent agreement in timing and speed with the observations. The solubility of HCl in STS does not significantly improve the agreement between model and observations. The removal of gas-phase in the H_{HCl} case is only slightly higher compared to the BASE

simulation. At the beginning of the winter about 0.1 ppbv HCl are simulated to be partitioned into STS, and in late winter more HCl is removed from the gas-phase in the H_{HCl} case since the new PSC scheme produces slightly less denitrification than the BASE simulation. But overall both simulations are very similar. Having established the discrepancy between model and observations, the following sections are going to examine possible mechanisms that can account for the disappearance of HCl in and around the vortex core.

7.2.2. Photolysis of Gas-Phase HNO_3

With current JPL recommendations (Sander et al., 2011) for gas-phase HNO_3 photolysis, NO_x production of more than $50 \text{ pptv}\cdot\text{day}^{-1}$ on 1st June, at 20 km altitude and 15 ppbv HNO_3 only occurs at latitudes equator-ward of 57°S . At 80°S this rate of NO_x production is not reached until 19th September. For an undisturbed vortex these calculations yield the maximum possible photolysis rate of gas-phase HNO_3 , as in reality PSCs will denitrify the Antarctic stratosphere, suppressing NO_x production. Photolysis can increase further if the vortex is dynamically disturbed, which can cause excursions of vortex core air to lower latitudes. Fifteen-day backward trajectories, initialized on 15th June between 80°S - 90°S , indicate that the lowest latitude excursion is to 60°S . But most of the time the trajectories remain poleward of 70°S . Due to the stability of the Antarctic vortex, it does not appear that excursions to lower latitudes can produce enough NO_x to explain the observed HCl depletion. However, the amplitudes of the wave disturbances are uncertain, as are smaller scale mixing processes that may be unresolved in the model.

7.2.3. Galactic Cosmic Rays

Another source of NO_x , beside photolysis, is the production by Galactic Cosmic Rays (GCR). GCR flux is modulated by the heliosphere and strongest during solar minimum (Bazilevskaya et al., 2008). With the magnetic field lines perpendicular to the ground at the poles, the flux of magnetic particles is highest at high latitudes. Studies (Nicolet, 1975; Jackman et al., 1980; Vitt and Jackman, 1996) agree that NO_x production at the high latitudes by GCRs is in the range of $10\text{-}50 \text{ molec}\cdot\text{cm}^{-3}\cdot\text{s}^{-1}$, which can explain at most 5% of the observed HCl loss inside the vortex core in June. Müller and Crutzen (1993) explored in more detail the idea of GCRs accelerating the depletion of HCl. Their work represents an upper limit for the possible influence of GCRs on HCl loss.

However, with their assumptions GCRs make only a small difference in HCl loss during the polar night, and only after the end of polar night did Müller and Crutzen (1993) see a significant impact of GCRs on HCl depletion. Since total depletion of gas-phase HCl is already observed by the end of June in the vortex core, the reactions explored by Müller and Crutzen (1993) cannot explain the observed loss. Thus, it appears that neither vortex air excursions to lower latitudes nor GCRs can produce enough NO_x to regenerate sufficient ClONO_2 to explain the observed depletion of gas-phase HCl.

7.2.4. Photolysis of Condensed Phase HNO_3

The photolysis of gas-phase HNO_3 is a well established process (Sander et al., 2011); though, during the polar night a substantial fraction of HNO_3 is either tied up in Polar Stratospheric Clouds (PSCs) or has already sedimented out of the lower stratosphere, which prevents significant regeneration of ClONO_2 through gas-phase photolysis even in the presence of sunlight. However, photolysis of the condensed phase should also be considered. Particularly since recent studies have shown that nitrate photolysis from snow surfaces is a significant source of NO_x at Earth's surface (e.g. Honrath et al., 1999; Dominé and Shepson, 2002), and that nitrate photolysis in the quasi-liquid layer in aerosols is enhanced in the presence of halide ions due to a reduced solvent cage effect (Wingen et al., 2008; Richards et al., 2011). These and other studies indicate that photolysis of dissolved HNO_3 in PSC particles, including STS droplets is certainly feasible.

To probe photolysis of condensed HNO_3 in the model, the $J_{\text{HNO}_3(c)}$ test cases use the cross-section for the NO_3^- ion with a quantum yield of 0.3, similar to what has been adopted in recent studies of nitrate photolysis on snow surfaces (e.g. Richards et al. (2011)). The high quantum yield attempts to account for an increase in light intensity due to an increased path length caused by refraction at the air-liquid interface (Mayer and Madronich, 2004) and morphology dependent resonances (Johnson, 1993; Cappa et al., 2004), and for the fact that nitrate photolysis is further enhanced in highly acidic solutions (Abida et al., 2011). Nissenon et al. (2006) have shown that these effects can increase the photolysis rate in liquid aerosol droplets by three orders of magnitude over bulk-liquid solutions.

When this process is included the actinic flux rather than the availability of gas-phase HNO_3 is the limiting factor for NO_x production. However, even this process does not produce NO_x early enough to explain the HCl depletion. In particular, poleward of 80°S photolysis of NO_3^- in PSCs does not have any effect on chlorine partitioning until

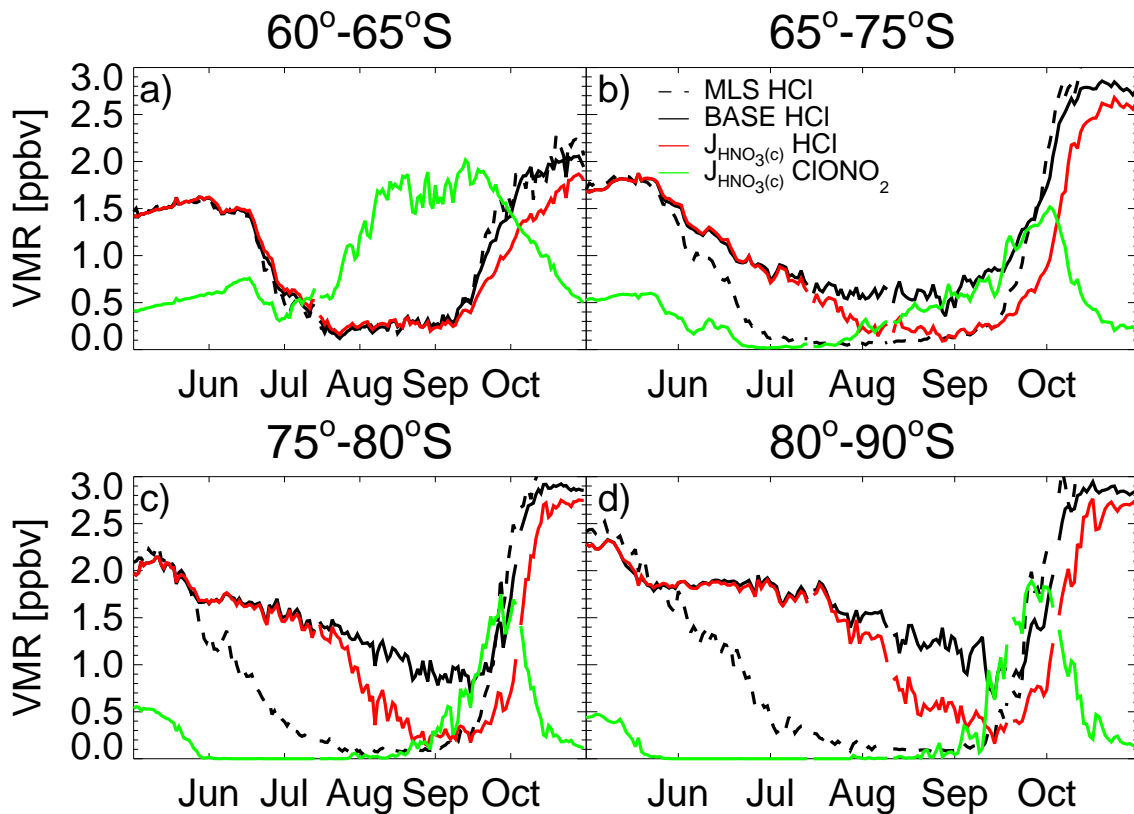


Figure 7.5.: Gas-phase HCl observations by MLS and chlorine partitioning for the BASE and $J_{\text{HNO}_3(c)}$ case for four equivalent latitude regions on 475 K.

the middle of July. Until then the $J_{\text{HNO}_3(c)}$ and the BASE case are virtually identical and differ significantly from the observations. Once the vortex is illuminated, $J_{\text{HNO}_3(c)}$ produces sufficient NO_x to completely deplete HCl in the vortex core, but not until August and September, about one month later than observations indicate.

Based on the simple assumptions that the photolysis of condensed HNO_3 occurs in a constant manner throughout fall, winter, and spring, sufficient NO_x is produced to cause total depletion of gas-phase HCl, as indicated in Figure 7.5, and it strongly perturbs NO_x in the lower stratosphere. While initially more ClONO_2 becomes available to react with HCl, once HCl is depleted any surplus of NO_x could result in a deactivation of ClO_x into ClONO_2 . Early deactivation into ClONO_2 could cause less ozone loss and prevent the buildup of HCl via reaction 2.20, resulting in slower regeneration of HCl in the model compared to observations. Such delay of HCl regeneration indicates that the simple assumptions for the photolysis of condensed phase HNO_3 produce too much NO_x . However, in the real atmosphere the rate of photolysis in spring could well be

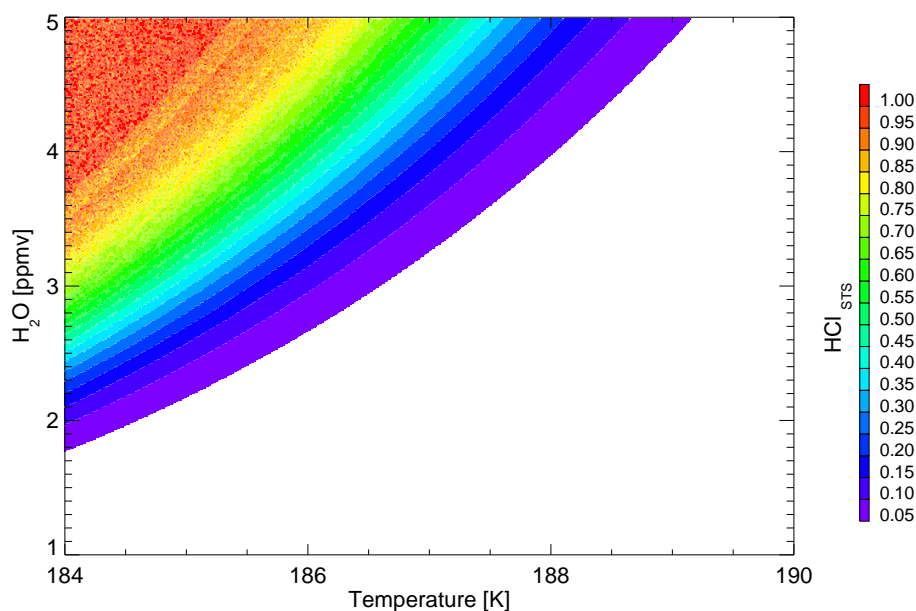


Figure 7.6.: Fraction of total HCl condensed in STS as a function of ambient water vapor and temperature.

slower, as any STS particles would become less acidic upon warming, and particles may not remain STS throughout the entire season.

7.2.5. Constraining HCl Solubility from Observations

The thermodynamic model for STS by Carslaw et al. (1995a) predicts that HCl is highly soluble in STS at temperatures below the frost point. The solubility of HCl in STS is governed by the Henry's law constant which is highly sensitive to temperature and ambient water vapor (Figure 7.6). Significant uptake of HCl in STS is only expected below the frost point and decreases rapidly with decreasing water vapor concentration. Murphy and Thomson (2000) provided observational evidence for Cl^- ions in stratospheric aerosols and the temperature dependence of their solubility. But these observations have received surprisingly little attention to date.

Therefore, the possibility that the decrease in gas-phase HCl in the vortex core is mainly due to the uptake of HCl into the aerosol, essentially forming Supercooled Quaternary Solution droplets, is considered here. Lambert et al. (2012) showed that Supercooled Ternary Solutions can be frequently observed at temperatures below the frost point, usually in mixtures with Nitric Acid Trihydrate (NAT), which agrees with laboratory studies by Song (1994); Koop et al. (1995), who have shown that STS can be

cooled below the frost point without freezing. Observations by Pitts et al. (2009, 2011) also indicate that STS droplets are present throughout the entire winter, a prerequisite to explain the removal of gas-phase HCl by uptake in STS throughout the entire winter season.

Figure 7.7a shows all MLS observations from May and June 2005 of gas-phase HCl as function of temperature ($\text{HCl}_{\text{gas}}(T)$) for four different equivalent latitude regions, from the vortex edge to the core. Since the Antarctic vortex cools gradually through the early months of winter, the temperature abscissa is equivalent to using a temporal scale, with higher temperatures corresponding to observations in May and the lowest temperatures occurring at the end of June.

Poleward of 65°S gas-phase HCl shows a similar dependence on temperature for all equivalent latitude regions. A decrease of gas-phase HCl can first be observed at temperatures between T_{NAT} and $T_{\text{S_NAT}}$ and is most severe below the frost point above 550 K potential temperature. Figure 7.7b shows the amount of depleted gas-phase HCl, which may be expressed as:

$$\text{HCl}(T) = \text{HCl}_0 - \text{HCl}_{\text{gas}}(T) \quad (7.1)$$

where HCl_0 represents the average profile of observations between temperatures of 195-200 K, and $\text{HCl}_{\text{gas}}(T)$ is the HCl present in the gas-phase at a given temperature T .

Interestingly, depletion of gas-phase HCl plateaus between 450-550 K and between $T_{\text{S_NAT}}$ and T_{ICE} , a behavior that is most prominent poleward of 80°S . There, gas-phase HCl decreases by 0.6 ppbv until temperatures reach $T_{\text{S_NAT}}$, remains fairly constant between $T_{\text{S_NAT}}$ and T_{ICE} , and decreases rapidly by an additional 1 ppbv just below the frost point. Assuming that HCl is only removed from the gas-phase by heterogeneous reactions with ClONO_2 , and that the abundance of this species is limited to the amount initially available $\text{ClONO}_{2,0}$, plus assuming that all N_2O_5 is also converted to ClONO_2 , then the residual HCl that cannot be explained by loss due to reaction with ClONO_2 is:

$$\text{HCl}_{\text{res1}}(T) = \text{HCl}(T) - (\text{ClONO}_{2,0} + 2 \cdot \text{N}_2\text{O}_{5,0}) \quad (7.2)$$

where $\text{ClONO}_{2,0}$ and $\text{N}_2\text{O}_{5,0}$ are the vertical profiles of these species when the vortex formed. This residual represents the upper limit of potential HCl removal by the reaction with ClONO_2 , as in reality N_2O_5 will also hydrolyze on stratospheric aerosols (Reaction 2.18) and remove NO_x . $\text{HCl}_{\text{res1}}(T)$ is shown in Figure 7.7c, which suggests that the

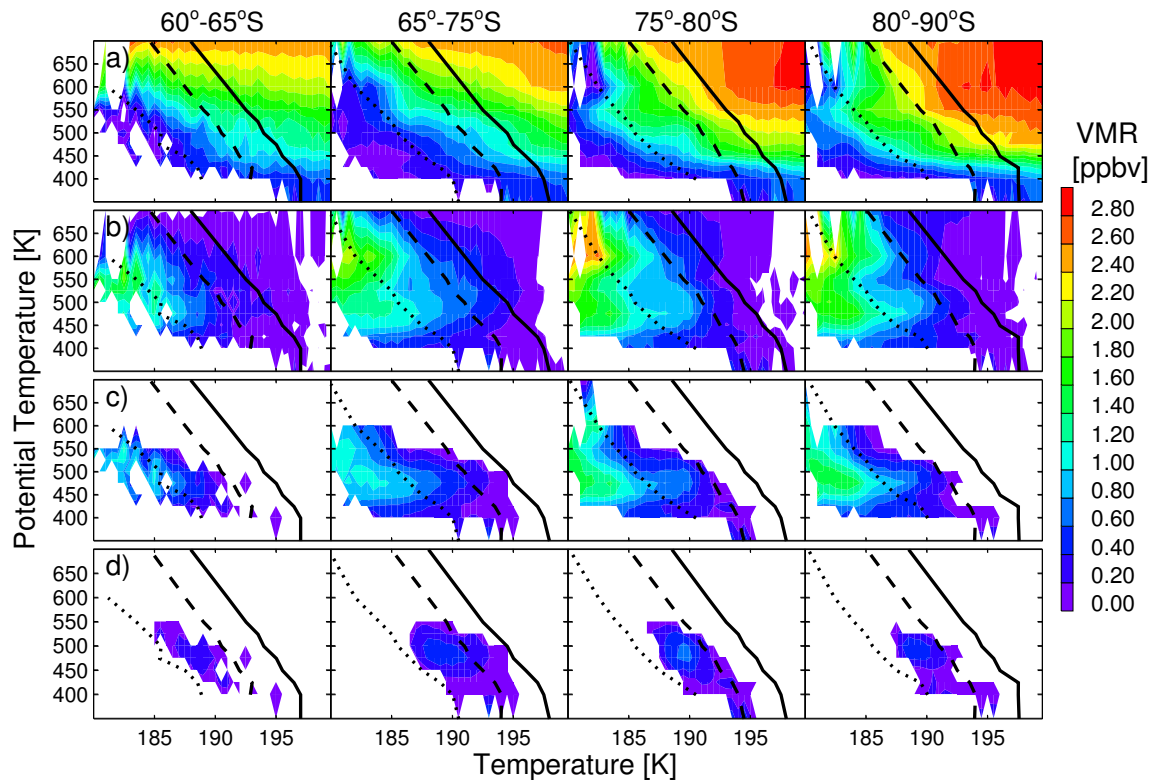


Figure 7.7.: a) MLS gas-phase HCl as function of temperature for May and June 2005 Poleward of 80°S. b) Removed gas-phase HCl, HCl_0 is defined as the mean between 195–200 K. c) Removed gas-phase HCl that cannot be explained by the reaction with ClONO_2 . d) Residual of removed gas-phase HCl after H_{HCl} is taken into account. Solid line is T_{NAT} , dashed $T_{\text{S_NAT}}$ and dotted T_{ICE} .

reaction with ClONO_2 can explain much of the depletion between $T_{\text{S_NAT}}$ and T_{ICE} . However, below the frost point the residual increases drastically, especially poleward of 75°S, where only a small fraction of the depleted HCl can be explained by loss through reaction with ClONO_2 .

In an effort to explain the residual below the frost point the solubility of HCl in STS is calculated. The model of Carslaw et al. (1995a) allows the calculation of HCl uptake into the aerosol for a given temperature if H_2O , HNO_3 , and pressure are known. While STS takes up more H_2O with decreasing temperature, this H_2O uptake is negligible compared to the amount of water sequestered in ice PSCs. On the other hand, any decrease of gas-phase HNO_3 is assumed to be by condensation on STS. Thus, to calculate the uptake of HCl into the aerosol, MLS gas-phase water vapor profiles averaged into 1 K temperature

bins and a mean gas-phase HNO_3 profile from the temperature range 200-205 K is used. With these quantities, the theoretical uptake of HCl into STS is derived. The solubility of HCl in STS increases rapidly below the frost point. Just 1-2 K below the frost point as much as 2 ppbv HCl can be taken up by STS. At temperatures above the frost point the model by Carslaw et al. (1995a) predicts negligible uptake of HCl into STS.

ClONO_2 regeneration in the vortex core is severely limited until the middle of July, and heterogeneous reactions of HCl with ClONO_2 will come to a stop once the initial supply of ClONO_2 and N_2O_5 has been depleted. Therefore, the solubility of HCl in STS at temperatures below the frost point offers an explanation for the decrease of gas-phase HCl even in the absence of a reaction partner in dark air masses. In Figure 7.7d the residual HCl ($\text{HCl}_{\text{res2}}(\text{T})$), assuming it is removed from the gas-phase both by heterogeneous reactions with ClONO_2 and by the uptake on STS aerosols, is shown. This residual HCl can be expressed by:

$$\begin{aligned} \text{HCl}_{\text{res2}}(\text{T}) &= \text{HCl}(\text{T}) - (\text{ClONO}_{2,0} + 2\text{N}_2\text{O}_{5,0}) - \text{H}_{\text{HCl}}(\text{T}) \\ &\equiv \text{HCl}_{\text{res1}}(\text{T}) - \text{H}_{\text{HCl}}(\text{T}) \end{aligned} \quad (7.3)$$

where H_{HCl} denotes the HCl taken up by STS. When the solubility of HCl in STS is added, the overall residual of gas-phase HCl is drastically reduced, and completely removed below the frost point. Thus, the depletion of gas-phase HCl below the frost point appears to be well explainable by the uptake on STS aerosol. Only a small residual of less than 0.5 ppbv remains between $\text{T}_{\text{S_NAT}}$ and T_{ICE} .

From the MLS observations of gas-phase HCl and the calculation of the theoretical solubility of HCl in STS, it can be shown that the majority of HCl depletion in May and June can be attributed to the uptake of HCl in STS, especially below the frost point. Key to the analysis presented here are the observations of mixed phase PSCs by Pitts et al. (2009, 2011), who demonstrated that some STS particles are present throughout the entire winter. It is important to emphasize that the STS droplets are small enough to be unaffected by gravitational settling over the considered timescales. Thus, HCl can be temporarily bound inside these particles without causing a vertical redistribution or irreversible removal of inorganic chlorine. While denitrification is important for nitrogen, dechlorination will not occur as long as the HCl is taken up into STS rather than ice or NAT particles. When NO_x becomes available in polar spring and ClONO_2 is regenerated, HCl will again react heterogeneously to form ClO_x .

Figure 7.8 shows HCl observations from MLS inside the vortex core (80-82°S) for May and June 2005 on the 475 K isentrope. The temperature-dependence of the observed

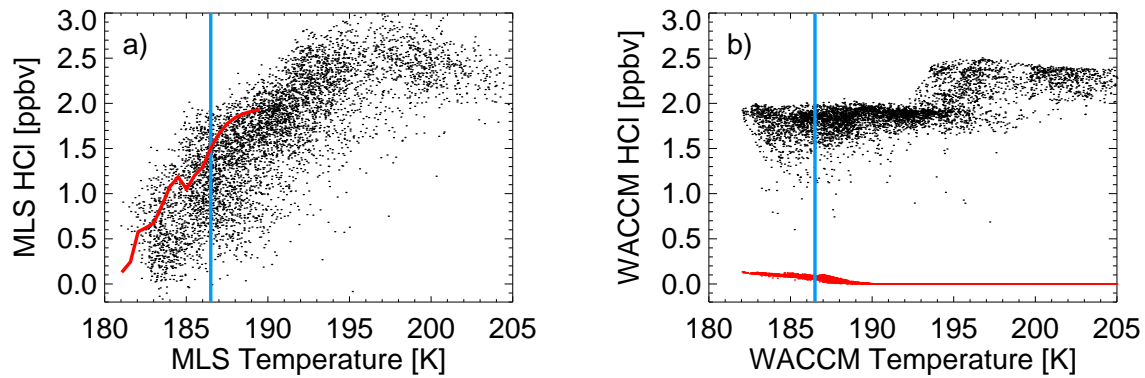


Figure 7.8.: a) MLS gas-phase HCl for May and June 2005 poleward of 80°S on 475 K, frost point (blue), theoretical uptake of HCl calculated with MLS H_2O and HNO_3 (red). b) gas-phase HCl for the H_{HCl} case (black) and condensed HCl (red).

HCl removal reveals that HCl depletion is not a continuous process but happens in two phases. The first phase occurs around the end of May when temperatures reach about 193 K, and is due to heterogeneous reactions with the initially available ClONO_2 . Once ClONO_2 is depleted HCl mixing ratios remain constant for about two weeks before decreasing further around the frost point and approaching zero several Kelvin below the frost point, this is the second phase. The theoretical uptake of HCl (Figure 7.8, red line) shows reasonable agreement with the temperature dependence of the observed decrease of gas-phase HCl during the second phase.

The H_{HCl} case (Figure 7.8b, black dots) does not completely remove HCl from the gas-phase even at temperatures well below the frost point. Only a small amount of HCl is partitioned into STS (Figure 7.8b, red dots). The only visible decrease of gas-phase HCl occurs around 193 K when HCl reacts with ClONO_2 . The model under predicts the uptake of HCl in STS, as the lower stratosphere in the model is drier than observations suggest, drastically reducing the solubility of HCl. Since H_{HCl} is so sensitive to water vapor, a small dry bias is sufficient to prevent the model from partitioning HCl into the condensed phase.

7.3. Modeling HCl Solubility in STS

Following Brakebusch et al. (2012) temperature in the heterogeneous chemistry submodule in SD-WACCM is lowered by 2 K. The effect is twofold, it accelerates heterogeneous

chemistry, and increases the solubility of HCl. The results for this simulation ($H_{\text{HCl-2 K}}$) are shown in Figure 7.9. Comparable to Figure 7.7 it shows the temperature dependence of HCl depletion for the $H_{\text{HCl-2 K}}$ case. Figure 7.9a indicates modeled gas-phase HCl and panel b) HCl that has been removed from the gas-phase for four different equivalent latitude regions between 1st May and 30th June.

Lowest values of gas-phase HCl are modeled at the vortex edge region (60° - 65° S). Here, gas-phase HCl is completely depleted at up to 5 K above the frost point up to 600 K altitude, due to the abundance of ClONO_2 . Farther poleward less gas-phase HCl is depleted even at temperatures below the frost point, since the ClONO_2 supply is severely limited.

Uptake of HCl into the aerosol begins around the frost point (Figure 7.9c) and reaches a maximum of 1 ppbv in the model. The amount of HCl in STS increases farther poleward. At the vortex edge, between 60° - 65° S, no HCl is in STS at all, since temperatures do not fall below the frost point. Between 65° - 75° S the model indicates complete depletion of HCl below the frost point and above 500 K. Again, this is mainly due to the reaction with ClONO_2 , since there is only little uptake of HCl by STS under these conditions. Poleward of 80° S up to 1 ppbv HCl are partitioned into STS at the lowest temperatures.

A comparison (Figure 7.9d) between the observed and simulated temperature dependence of gas-phase HCl generally reveals good agreement, especially poleward of 65° S. The largest discrepancies between model and observations occur between 60° - 65° S, in the vortex edge region. Since ClONO_2 in the model is readily available in this region, the temperature bias shows its largest effect here. The faster heterogeneous chemistry, due to the temperature bias, depletes HCl faster than the observations indicate. The maximum discrepancy occurs on 550 K below $T_{\text{S,NAT}}$, where the model underestimates gas-phase HCl by up to 1 ppbv. Farther poleward the comparison with observations indicates that the model underestimates gas-phase HCl above about 475 K, and overestimates it below 475 K. But overall differences between model and observations do not exceed ± 0.5 ppbv poleward of 65° S.

The most interesting region in this comparison is the vortex core, since the previous cases showed the strongest discrepancies with observations there. The two equivalent latitude regions poleward of 75° S exhibit a similar structure when compared to observations. Between T_{NAT} and $T_{\text{S,NAT}}$ the model underestimates gas-phase HCl due to faster heterogeneous chemistry. With decreasing temperatures the model starts to overestimate gas-phase HCl between $T_{\text{S,NAT}}$ and T_{ICE} below 500 K. This is similar to the

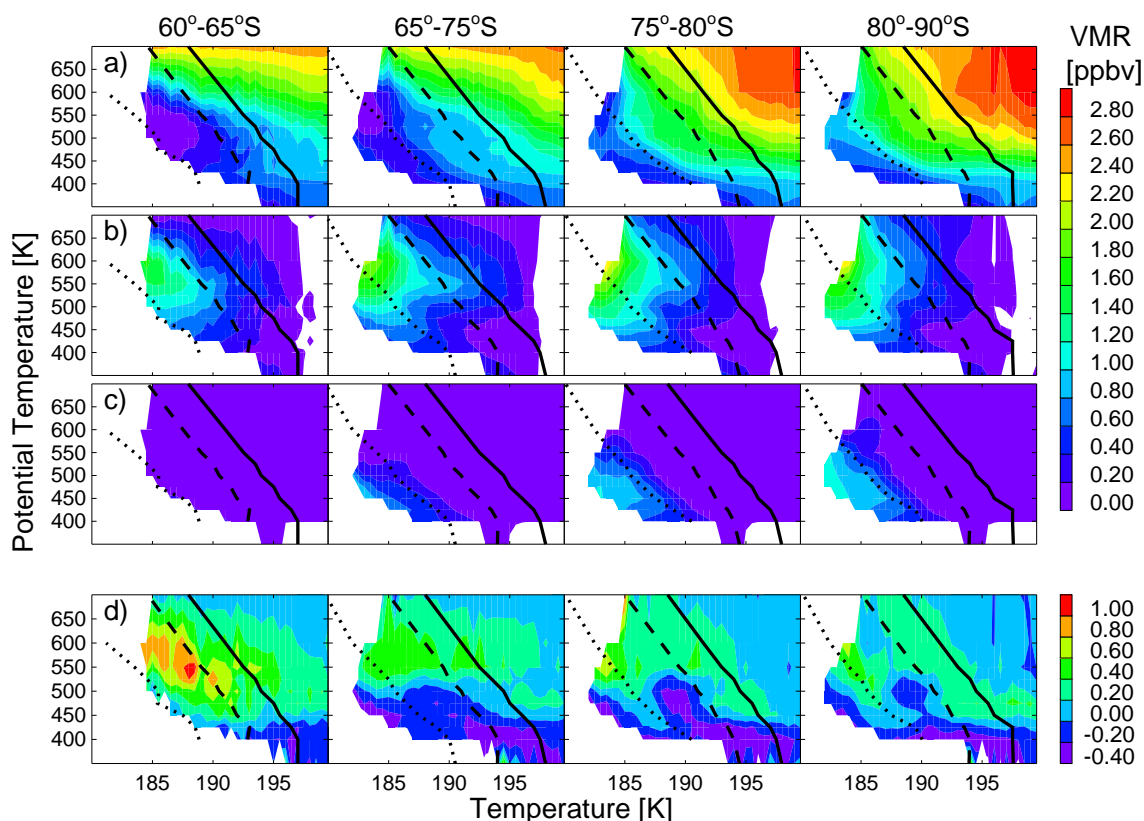


Figure 7.9.: a) Simulation $H_{\text{HCl}-2\text{K}}$ gas-phase HCl as function of temperature for May and June 2005 Poleward of 80°S . b) Removed gas-phase HCl, HCl_0 is defined as the mean between 195-200 K. c) Condensed phase HCl d) Difference between observations and model (observed minus modeled gas-phase HCl).

unexplained residual in Figure 7.7d, suggesting that the uptake of HCl into STS might start at higher temperatures than predicted by the model. This would be consistent with the findings of Murphy and Thomson (2000), who reported evidence for Cl^- in stratospheric aerosols at higher temperatures than the Carslaw et al. (1995a) model predicts.

Overall, when the temperature bias is applied a significant amount of HCl is partitioned into the condensed phase, which is the most prominent sink for gas-phase HCl until July in the Antarctic vortex. However, the agreement between model and observations degrades when ClONO_2 is readily available, because the acceleration of the heterogeneous reaction rates, due to the temperature bias, is too strong. This implies that the temperature bias may not be uniform over the entire vortex, but stronger in the core than at the edges. However, further studies are needed to constrain such a

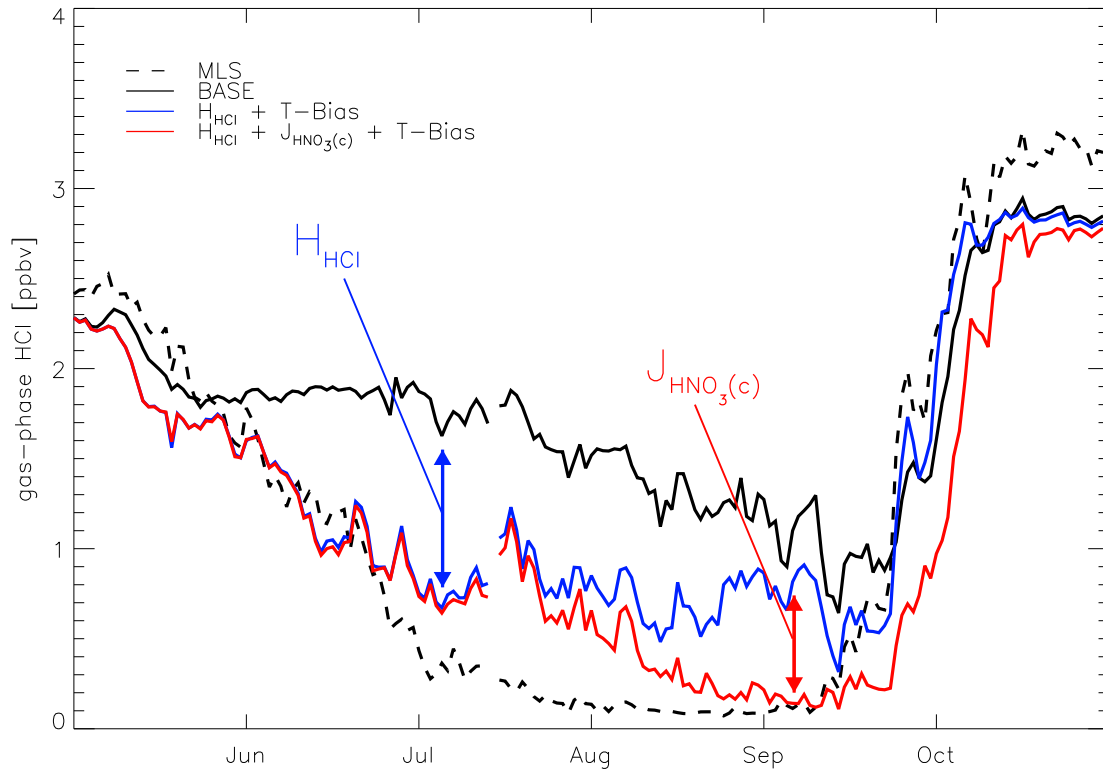


Figure 7.10.: Evolution of gas-phase HCl on 475 K poleward of 80°S for different model simulations (BASE, $H_{\text{HCl}}-2$ K and $J_{\text{HNO}_3(\text{c})}-2$ K) and MLS observations.

temperature bias.

7.4. The Combined Effect of $J_{\text{HNO}_3(\text{c})}$, H_{HCl} and the Temperature Bias

A simulation which combines the increase in solubility of HCl and heterogeneous reactions rate by applying the temperature bias, and takes into account the photolysis of HNO_3 in the condensed phase ($J_{\text{HNO}_3(\text{c})}-2$ K), yields very good agreement in the temporal evolution of gas-phase HCl inside the vortex core (Figure 7.10).

Until July modeled gas-phase HCl follows the observations and compared to the BASE simulation up to 1 ppbv HCl is taken up by the STS aerosol. However, without $J_{\text{HNO}_3(\text{c})}$ modeled gas-phase HCl is never fully depleted, due to the dry bias in the model, and also minimum temperatures in the model appear to be higher than the observations by

MLS indicate. Both factors reduce the solubility of HCl in STS. The effect of $J_{\text{HNO}_3(\text{c})}$ becomes visible at the end of July, completely depleting HCl by September, and the maximum additional depletion by $J_{\text{HNO}_3(\text{c})}$ is about 0.7 ppbv HCl at the beginning of September.

A polar-stereographic view of the simulations that include the temperature bias (Figure 7.11) shows significantly better agreement with observations compared to the BASE case (Figure 7.3). By 15th August gas-phase HCl is completely removed in the $J_{\text{HNO}_3(\text{c})}$ -2 K case throughout the entire polar vortex, in excellent agreement with observations. Before this date the H_{HCl} -2 K and $J_{\text{HNO}_3(\text{c})}$ -2 K cases show only little differences as the vortex core is confined to darkness.

As previously pointed out the effect of $J_{\text{HNO}_3(\text{c})}$, based on the assumptions adopted here, is only visible in late winter and beginning of spring. By 15th August $J_{\text{HNO}_3(\text{c})}$ causes almost complete depletion of HCl in the vortex core, in agreement with observations. Without $J_{\text{HNO}_3(\text{c})}$ a small residual of gas-phase HCl remains in the vortex core. However, the area where the simulation without $J_{\text{HNO}_3(\text{c})}$ shows higher concentrations of gas-phase HCl is very small compared to the rest of the vortex. Thus, when considering the total mass of gas-phase HCl in the polar vortex the difference with respect to observations is very small.

7.4.1. Observations of Active Chlorine

Since a major part of gas-phase HCl can be taken up into the STS aerosol, a depletion of gas-phase HCl should not be used as indicator for chlorine activation. To assess whether the test cases agree with observed chlorine activation, measurements of ClO by MLS are analyzed.

A quantitative comparison between model and observations is difficult, since ClO is in equilibrium with its dimer (Cl_2O_2), which is not observed by MLS, and the parameters describing this equilibrium are still subject to some uncertainty (von Hobe et al., 2007; Kawa et al., 2009; Sumińska-Ebersoldt et al., 2012). Nevertheless, MLS observations allow a qualitative comparison of chlorine activation in the model and observations. Figure 7.12 shows observations of ClO for 15th September, a time when the highest ClO values are observed for this Antarctic season, together with the results of four model test cases (BASE, H_{HCl} , H_{HCl} -2 K and $J_{\text{HNO}_3(\text{c})}$ -2 K).

Overall, the four shown simulations tend to underestimate ClO compared to observations. Best agreement is achieved for the H_{HCl} -2 K case. This suggests that, at this point in spring the availability of NO_x is no longer the limiting factor for chlorine activation,

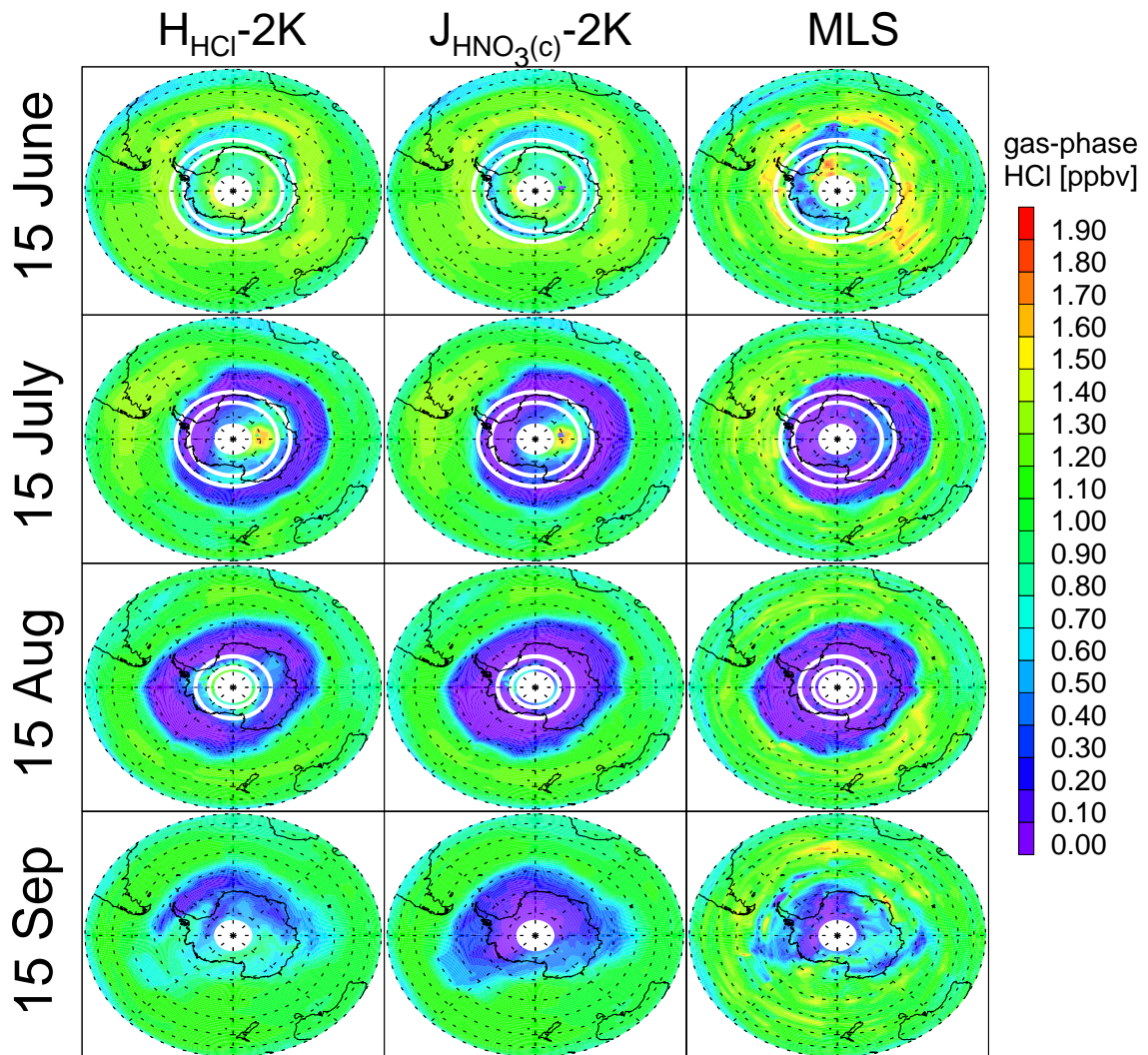


Figure 7.11.: Distribution of gas-phase HCl over Antarctica 2005 on 475 K for the $H_{\text{HCl}}-2\text{K}$ case (left), $J_{\text{HNO}_3(\text{c})}-2\text{K}$ case (center) and MLS observations (right). The white circles mark noontime solar zenith angles of 95° and 90° , respectively.

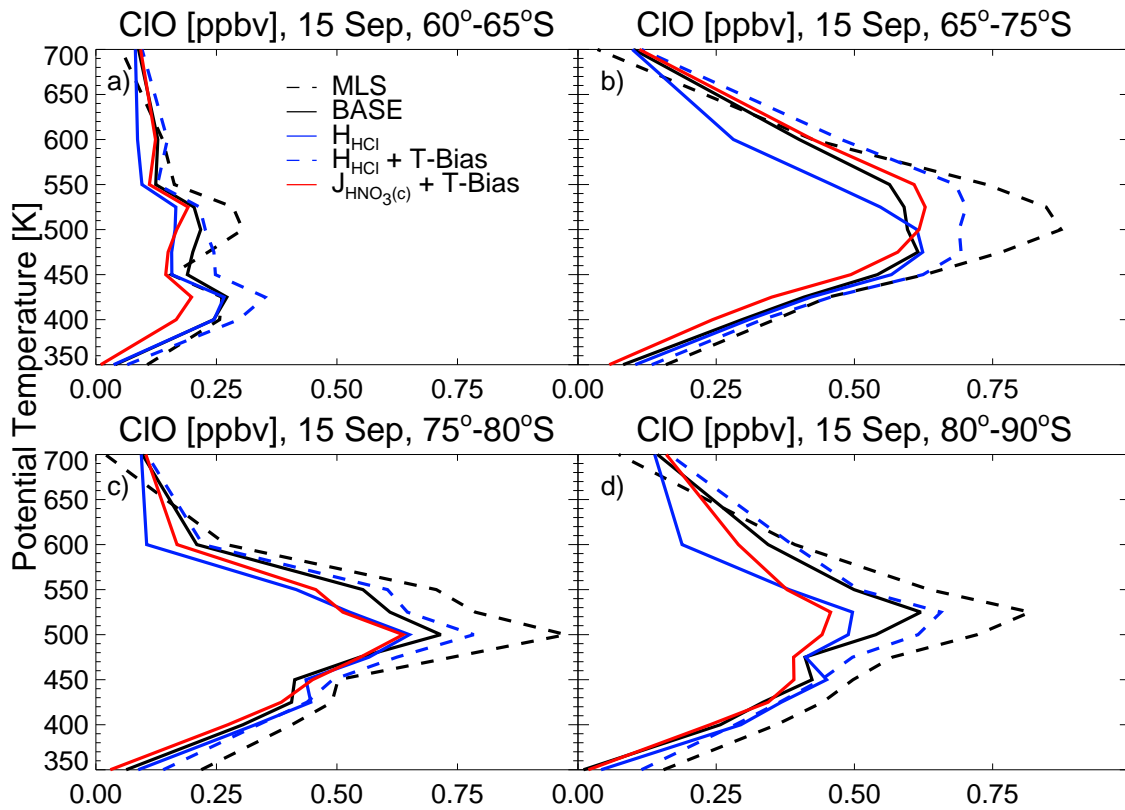


Figure 7.12.: Vertical profiles of modeled and observed ClO (dashed black) for 15th September 2005 for four equivalent latitude bins. BASE case (solid black), H_{HCl} (solid blue), $H_{\text{HCl}}-2\text{ K}$ (dashed blue) and $J_{\text{HNO}_3(c)}-2\text{ K}$ (solid red).

as in the H_{HCl} case without the temperature bias the same amount of NO_x is available. The difference in chlorine activation between the H_{HCl} and $H_{\text{HCl}}-2\text{ K}$ case results from the faster heterogeneous chemistry due to the temperature bias. Despite higher NO_x concentrations, the $J_{\text{HNO}_3(c)}-2\text{ K}$ case shows less chlorine activation than the $H_{\text{HCl}}-2\text{ K}$ case. Especially poleward of 80°S ClO is underestimated in this case, which indicates that the deactivation of ClO_x is too far advanced compared to observations; therefore, the parameters describing $J_{\text{HNO}_3(c)}$ still need further refinement.

7.5. Ozone Loss

Table 7.2 shows the calculated loss in the ozone column between 350-700 K for four equivalent latitude bins for the model test cases and observations. This loss includes

Table 7.2.: Column ozone loss between 350-700 K in Dobson Units between 1st May and 15th October.

	60-65°S	65-75°S	75-80°S	80-90°S
MLS	35	143	141	130
BASE	38	141	150	130
H _{HCl}	36	142	138	130
H _{HCl} - 2 K	60	158	150	142
J _{HNO₃(c)}	9	114	114	108
J _{HNO₃(c)} - 2 K	29	140	137	130

chemical and dynamical processes; thus, the comparison with observations has to be considered with caution. But since all simulations use the same atmospheric dynamics, differences in ozone loss between the model test cases can be attributed to the various new processes. The BASE simulation is already in very good agreement with the observations in terms of ozone loss, but its evolution of gas-phase HCl does not resemble observations at all. While the inclusion of HCl solubility and photolysis of condensed phase HNO₃ appear to be important for winter season composition, and for understanding the chemical processes, the effect on ozone depletion is limited in the Antarctic. For the H_{HCl} case ozone loss slightly decreases compared to the BASE simulation, which is caused by the changed PSC scheme. When the -2 K temperature bias is added, the faster heterogeneous reaction rates increase the modeled ozone loss, but the H_{HCl}-2 K case is still in agreement with observations. Only the model case including J_{HNO₃(c)} without the temperature bias results in significantly less ozone loss than the observations suggest, due to increased production of NO_x and subsequent faster deactivation of chlorine. When J_{HNO₃(c)} is used in combination with H_{HCl} and the temperature bias, ozone loss barely changes compared to the H_{HCl} case and is in agreement with the observations. Despite the large influence of J_{HNO₃(c)}, H_{HCl} and the temperature bias on the evolution of gas-phase HCl, the effect on ozone loss is limited as long as sufficient ClO_x is available in polar spring. This is because ozone loss is not sensitive to the partitioning of Cl_y during the polar night.

7.6. Conclusions

The evolution of gas-phase HCl during polar night in the Antarctic stratosphere has been analyzed with satellite observations and model simulations. In the core of the Antarctic

vortex observations show a steady decrease of gas-phase HCl starting in the middle of May, and complete depletion at the end of June. The BASE simulation cannot reproduce this development as the model can only remove gas-phase HCl through heterogeneous reactions, particularly with ClONO₂. Since production of ClONO₂ is severely limited during the polar night, model gas-phase HCl stabilizes once all ClONO₂ has reacted with HCl. The calculations have shown that the known mechanisms that regenerate ClONO₂ are by orders of magnitude too slow to explain the subsequent removal of gas-phase HCl.

Laboratory and field observations suggest that condensed phase HNO₃ may photolyze, with the potential to affect NO_x and ClONO₂. This process has not been considered in current stratospheric ozone depletion simulations to date. A test case including photolysis of condensed phase HNO₃ cannot produce enough NO_x to explain all of the depletion of gas-phase HCl at the beginning of the polar night, based on the assumptions included here. Once the polar vortex is illuminated again, this photolysis process produces sufficient NO_x to quickly deplete all gas-phase HCl. However, with the assumptions regarding the condensed phase photolysis of HNO₃ in the model, too much NO_x is produced in polar spring, which disturbs the regeneration of the chlorine reservoir species, HCl and ClONO₂. Although gas-phase HCl is eventually completely depleted in agreement with observations, its regeneration lags behind observations by two weeks in this test case. Further studies are needed to constrain the parameters controlling the photolysis of condensed phase HNO₃.

Laboratory and field measurements have also shown that HCl can be taken up by the STS aerosol; thus, effectively removed from the gas-phase. This process has also not generally been considered in stratospheric ozone modeling. It is only effective at temperatures below the frost point, and the correct representation of the solubility of HCl is strongly dependent on ambient water vapor and temperature. When using observed ambient water vapor and temperatures for calculating HCl solubility in STS, the evolution of gas-phase HCl in May and June can be explained with the uptake of HCl in STS, leaving only a small residual between T_{S_NAT} and T_{ICE}. Once temperatures are below the frost point up to 75% (1.5 ppbv) of HCl removed from the gas-phase is due to the uptake in STS. Therefore, the solubility of HCl in STS can act as the major, albeit temporary sink for gas-phase HCl during polar night.

Since this process is highly sensitive to temperature and water vapor, the model only partitions a significant amount of HCl into STS once a -2 K temperature bias is applied. When this temperature bias is applied, the model shows very good agreement with the observations of gas-phase HCl at the beginning of the polar night, until July. Since

the solubility of HCl in STS particles is only a temporary sequestering, the results show that a reduction in gas-phase HCl cannot be considered as equivalent to the formation of reactive chlorine, representing a major change in paradigm regarding the specific chemistry of the Antarctic stratosphere. While the processes identified here are chemically intriguing, they do not influence the amount of ozone lost since they affect the details of behavior in fall and winter, but do not significantly affect the reactive chlorine available to destroy ozone in the spring.

8. Summary

This work examined heterogeneous reactions on stratospheric sulfate particles and PSCs. It was shown that the parameterizations for heterogeneous chemistry used in atmospheric models yield good agreement with observations in terms of chlorine activation. With realistic assumptions about PSC composition (NAT particle number density, sulfuric acid content,...) the parameterizations predict reaction rates on liquid aerosols that are always faster than on NAT. Only with the formation of STS are reaction rates on PSCs faster than on the background aerosol. However, at the low temperatures when STS droplets form, reaction rates on the background aerosol are already fast enough that the additional surface area provided by STS is found to have only little impact on chlorine activation. This was confirmed by in-situ measurements from 2005 and 2010 where simulations show STS to cause a maximum of 10% more chlorine activation over the background aerosol. But accurate knowledge about the prevailing temperatures has proven to be vital to model chlorine activation, since heterogeneous reactions rates strongly depend on temperature and less on surface area density. Although this work could not irrefutably prove or disprove the hypothesis by Drdla and Müller (2012), observational evidence strongly suggests that the rate of chlorine activation is not linked to PSC. While chlorine activation usually coincides with the occurrence of PSCs, a multi-annual analysis of space-borne observations does not show any correlation between PSC occurrence and the rate of chlorine activation. But, PSCs control the NO_y budget in the stratosphere, and the deactivation of chlorine and ozone loss.

With PSCs being vital to correctly predict ozone loss, the representation of PSCs in SD-WACCM was examined and improved. The old scheme had a physically impossible phase transition from the solid to liquid phase with decreasing temperature, which was corrected. The new scheme in SD-WACCM forms mixed phase PSCs in agreement with observations, while still giving a good representation of denitrification. The most important change in the PSC scheme was to ice PSCs. Observations show the formation of ice at the frost point, while in the model ice formed several Kelvin above the frost point. By changing the required supersaturation for ice PSC, ice in the model now forms

closer to the frost point, which increases ambient water vapor during the polar night inside the vortex.

This increase in ambient water vapor influences the solubility of HCl in STS droplets. With decreasing ambient water vapor, HCl becomes less soluble in STS. Since SD-WACCM could not reproduce the observed decrease in HCl over the Antarctic in 2005, additional sinks for HCl in the polar vortex were explored. So far, a decrease in gas-phase HCl was assumed to be solely due to heterogeneous reactions, but during the polar night these reactions are limited by the availability of NO_x . This work showed that no known process can produce enough NO_x to explain the observed loss of gas-phase HCl. Even the photolysis of in STS condensed HNO_3 , at a rate about 10 times faster than gas-phase photolysis, cannot generate sufficient NO_x to explain the decrease of gas-phase HCl. While there are no observational constraints for the photolysis of condensed HNO_3 in STS, this work suggests that such a photolysis reaction is unlikely to be faster than photolysis of gas-phase HNO_3 .

However, it could be shown that the decrease of gas-phase HCl can be explained by the uptake of HCl into STS droplets. When calculating the solubility of HCl with a thermodynamic model for STS with observed temperatures and ambient water vapor, the entire removal of HCl from the gas-phase below the frost point can be explained. Modeling this process in SD-WACCM is difficult, since it strongly depends on temperature and ambient water vapor, but with the improved PSC scheme the model successfully reproduced the decrease of observed gas-phase HCl by partitioning it into STS during polar night. This has important implications for constraining chlorine activation. Since a large fraction of HCl may only be temporarily removed from the gas-phase by the sequestering into STS, a decrease in gas-phase HCl cannot be used as indicator for chlorine activation.

The results presented in this work are currently in review (Wegner et al., 2012a) or are in preparation and will be submitted to a scientific journal soon (Wegner et al., 2012b,c).

A. Appendix

A.1. Model Descriptions

A.1.1. Chemical Lagrangian Model of the Stratosphere

The Chemical Lagrangian Model of the Stratosphere (CLaMS) is an off-line chemical transport model, driven by externally provided wind fields. Advection, mixing and chemistry are described in McKenna et al. (2002a,b), and the extension to three-dimensions in Konopka et al. (2004). The latest CLaMS simulations include 48 chemical species, 144 chemical reactions including 36 photolytic and 11 heterogeneous processes (Grooß et al., 2011). The standard resolution for CLaMS simulations with full chemistry is 100 km with an orography following pressure/potential temperature hybrid vertical coordinate. Polar Stratospheric Clouds are simulated with a hybrid scheme (Grooß et al., 2005). Large NAT particles, which are responsible for denitrification, are represented by particle boxes. Within these boxes growth and evaporation are calculated according to Carslaw et al. (2002) with the fixed nucleation rate reported by Voigt et al. (2005). STS and the mode of small NAT particles are calculated with the thermodynamic equilibrium scheme described in Carslaw et al. (1995b) at a fixed supersaturation and particle number density. Ice particles are simulated to form at the frost point at a fixed number density. Figure A.1 shows an exemplary distribution of air parcels in CLaMS over the Arctic 2010/11.

A.1.2. Specified Dynamics - Whole Atmosphere Community Climate Model

The Whole Atmosphere Community Climate Model, Version 4 (WACCM4) is a fully interactive chemistry climate model, where the radiatively active gases affect heating and cooling rates and therefore dynamics (Garcia et al.; Marsh et al., 2007; Tilmes et al., 2007; Eyring et al., 2010). Recently, a new version of the WACCM4 model has been developed that allows the model to be run with external specified dynamical

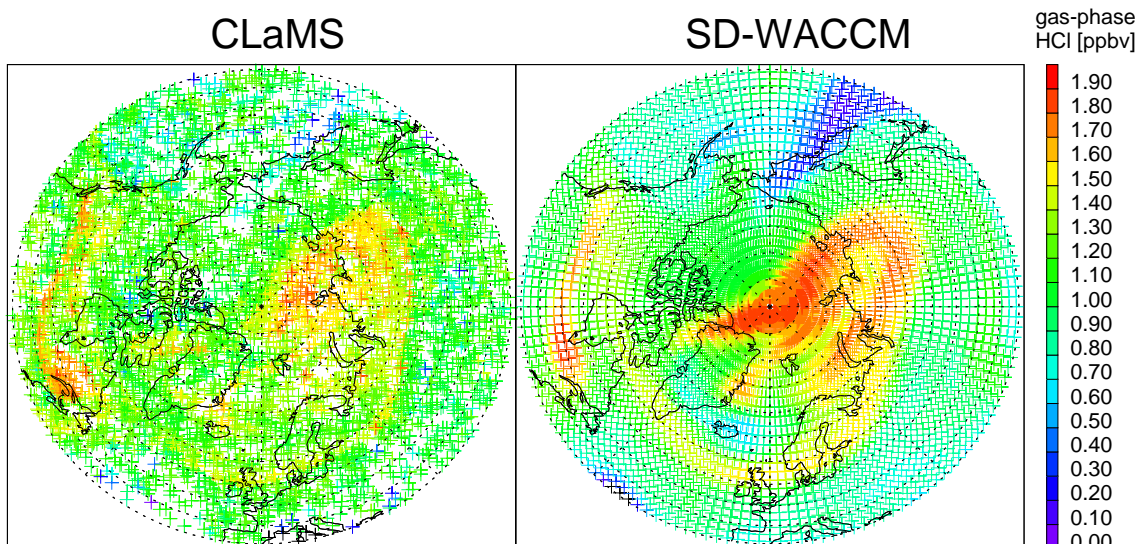


Figure A.1.: Irregular CLaMS grid (left) and regular SD-WACCM grid (right) for gas-phase HCl on 22nd December 2010 on the 475 K isentrope. For CLaMS all air parcels between 470 and 480 K are plotted.

(SD) fields (Lamarque et al., 2012). This version of WACCM leads to an improved representation of atmospheric dynamics and temperatures compared to its free running counterpart. These meteorological fields come from the NASA Global Modeling and Assimilation Office (GMAO) Modern-Era Retrospective Analysis for Research and Applications (MERRA; Rienecker et al. (2011)). Temperature, zonal and meridional winds, and surface pressure are used to drive the physical parameterization that control boundary layer exchanges, advective and convective transport, and the hydrological cycle. In this study, the WACCM4 meteorological fields are relaxed towards the MERRA reanalysis fields using the approach described in Kunz et al. (2011). The chemical module of WACCM4 is based upon the 3-D chemical transport Model of Ozone and Related Tracers, Version 3 (MOZART-3; Kinnison et al., 2007). It includes a detailed representation of the chemical and physical processes from the troposphere through the lower thermosphere. The species included within this mechanism are contained within the O_x , NO_x , HO_x , ClO_x , and BrO_x chemical families, along with CH_4 and its degradation products. In addition, fourteen primary non-methane hydrocarbons and related oxygenated organic compounds are included (Emmons et al., 2010). This mechanism contains 122 species, more than 220 gas-phase reactions, 71 photolytic processes, and 18 heterogeneous reactions on multiple aerosol types. The heterogeneous chemistry uses the approach described in chapter 6 to simulate Polar Stratospheric Clouds (PSCs).

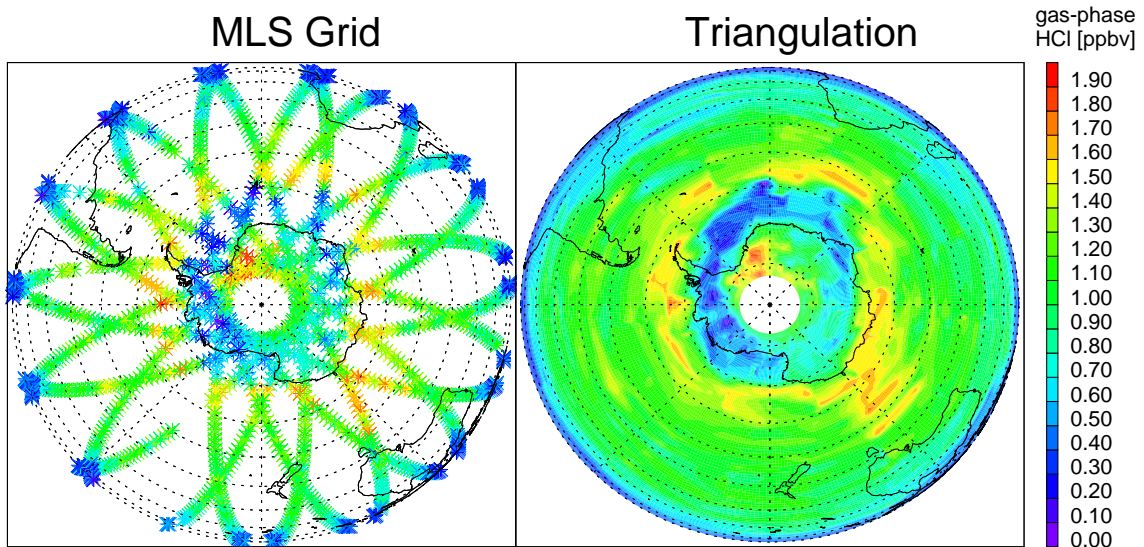


Figure A.2.: Native MLS data points (left) and the triangulation on a regular grid (right) for gas-phase HCl on 15th June 2005 on 475 K.

Supercooled Ternary Solution (STS) droplets are simulated according to the thermodynamic equilibrium model described in Tabazadeh et al. (1994a). Nitric Acid Trihydrate (NAT) forms at a supersaturation of 10, about 3 K below the thermodynamic equilibrium temperature. The thermodynamic equilibrium temperature for NAT and the temperature at a supersaturation of 10 are referred to as T_{NAT} and S_{NAT} respectively.

The SD-WACCM/MERRA simulation employed here corresponds to the time period from 1 May 2005 through November 2005. For this simulation the model used a SD-WACCM/MERRA simulation that started in January 1988 through April 2005. The horizontal resolution is $1.9^\circ \times 2.5^\circ$, with a vertical resolution of <1 km in the troposphere, 1 km in the lower stratosphere, and about ~ 2 km in the upper stratosphere. The model grid is shown in figure A.1. To allow for a direct comparison with satellite observations the model output is co-located in space and time with the satellite observations. Maps of trace gas distributions are generated with a Delaunay triangulation to a regular $1^\circ \times 1^\circ$ grid.

Table A.1.: Vertical resolution, range and precision for the MLS measured species used in this work.

species	vert. resolution [km]	vert. range [hPa]	precision
Temperature	4	261-0.001	1 K
HNO ₃	3.5-4.5	215-1.5	0.7 ppbv
H ₂ O	3	316-0.002	15%
HCl	3	100-0.32	0.2-0.4 ppbv
ClO	3-4.5	147-1	0.3 ppbv
O ₃	3	261-0.02	0.04-0.5 ppmv

A.2. Instrument Descriptions

A.2.1. Microwave Limb Sounder

The Microwave Limb Sounder (MLS) is an instrument on the EOS AURA satellite which flies in a polar orbit of 705 km at an inclination of 98°, and has provided continuous measurements since 2004 (Waters et al., 2006). MLS provides about 3500 profiles from Earth's surface to 90 km altitude between 82°N and 82°S. The daily coverage of MLS and results for the triangulation on a regular grid are shown in figure A.2. The high spatial coverage over the polar regions allows to identify even small scale structures as in this case the ring of low gas-phase HCl. This work uses observations of gas-phase HNO₃ (Santee et al., 2007a), H₂O (Lambert et al., 2007), HCl (Froidevaux et al., 2008), ClO (Santee et al., 2007b), O₃ (Froidevaux et al., 2008) and temperature from retrieval version 3.3. An overview of the vertical resolution, vertical range and precision for these species is given in table A.1.

A.2.2. Atmospheric Chemistry Experiment - Fourier Transform Spectrometer

The Atmospheric Chemistry Experiment - Fourier Transform Spectrometer (ACE-FTS) is a solar occultation instrument on SCISAT-1, flying in a circular orbit at 650 km at an inclination of 74°, and has provided measurements since 2004 (Bernath et al., 2005). ACE-FTS provides daily vertical profiles for up to 15 sunrises and 15 sunsets with latitudinal coverage exhibiting an annual cycle between 85°S to 85°N. ACE-FTS has better vertical and spectral resolution than MLS but lacks the spatial coverage. Figure A.3 shows ACE-FTS observations for June and August. Due to its orbit it has only

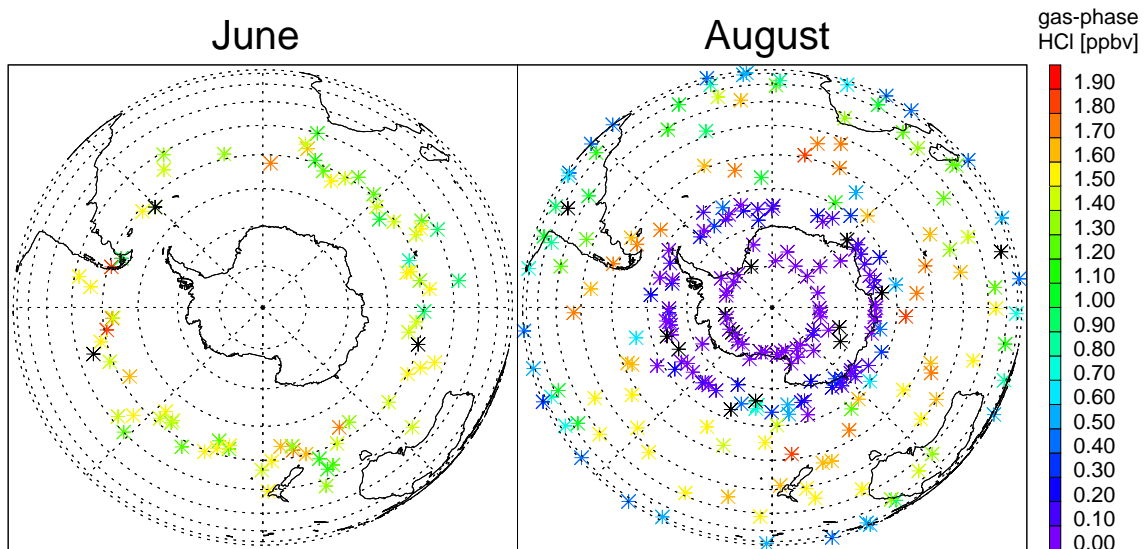


Figure A.3.: All ACE-FTS observations of gas-phase HCl in June (left) and August (right) on 20.5 km.

limited coverage of the polar regions in June. This work uses observations of ClONO_2 , N_2O_5 , HNO_3 (Wolff et al., 2008) and HCl (Mahieu et al., 2008) from retrieval version 3 and 2.2update with a vertical resolution of about 4 km.

List of Figures

3.1.	Top: STS composition as function of temperature; Solid red marks the fraction of H_2SO_4 and solid blue the fraction of HNO_3 . Bottom: Surface area density as function of temperature; Dashed red line marks the SAD for binary aerosol and blue dashed for STS. Solid black line marks the condensed fraction of HNO_3 . Composition and SAD are calculated with the thermodynamic model of Carslaw et al. (1995b) for typical stratospheric conditions (50 hPa, 15 ppbv HNO_3 , 4.5 ppbv H_2O and 0.15 ppbv H_2SO_4).	18
4.1.	Schematic of the heterogeneous processes between a gas molecule and a liquid droplet.	22
4.2.	γ -values calculated with parameterizations by Shi et al. (2001) (blue) and Hanson (1998) (red) for liquid aerosols. γ for NAT by Hanson and Ravishankara (1993) (green) and Abbatt and Molina (1992) (orange) as formulated by Carslaw and Peter (1997). Current JPL recommendations (Sander et al., 2011) are fixed γ -values for NAT (black).	24
4.3.	First order loss rates for $\text{HCl}+\text{ClONO}_2$ and $\text{ClONO}_2+\text{H}_2\text{O}$ for typical stratospheric conditions (50 hPa, 2 ppbv HCl , 1 ppbv ClONO_2 , 15 ppbv HNO_3 , 5 ppmv H_2O and 0.15 ppbv H_2SO_4).	26
5.1.	Top: HAGAR CH_4 as function of potential temperature and equivalent latitude. Bottom: Derived initialization of chlorine species as function of potential temperature.	30
5.2.	Temperatures interpolated from ERA-INTERIM data on the flightpath versus TDC temperature measurements on board the Geophysica as function of potential temperature.	31

- 5.3. Temperature history (a), simulated condensation of HNO_3 on STS (b), NAT (c) and corresponding enhancement of the surface area density over the background aerosol (d) along 92 h back-trajectories ending on the Geophysica flightpath. Areas under T_{NAT} are enclosed by the black line. 32
- 5.4. Comparison of HALOX in-situ data and CLaMS simulations. Solid black line marks the HALOX ClO_x measurement with its accuracy shaded gray and the dashed black line initial ClO_x . Solid red line marks results from the “Full PSC” and dashed blue from the “Binary only” simulation. Error bars show model uncertainty. 33
- 5.5. Top: Temperature history along seven-day backward trajectories from HALOX measurements for 3 flights in January 2010. Middle: ClO_x initialization (black) and modeled ClO_x on the flightpath with full PSC surface area density (red) and background aerosol only (blue dashed). Bottom: Measured (black) and modeled values of ClO (red). 35
- 5.6. HCl and HNO_3 observations by MLS for the Arctic winters 2004/05 to 2010/11 on 500 K potential temperature in the vortex core (equivalent latitude $> 75^\circ\text{N}$). 37
- 5.7. Probability density distribution of maximum surface area density enhancement by STS along seven-day back-trajectories starting on MLS observations poleward of 75°N equivalent latitude in 2004, 2008 and 2009. 39
- 6.1. Observations of gas-phase HNO_3 and modeled partitioning of HNO_3 between the gas-phase and PSCs on 475 K over Antarctica 2005 for four equivalent latitude regions. Dashed line are observations of gas-phase HNO_3 by MLS and solid lines model output from the reference simulation. 43
- 6.2. a) All MLS gas-phase HNO_3 observations on 475 K between 1 May and 1 July 2005 over Antarctica correlated with temperature. b) Reference simulation output on the locations of the observations described in a). c) Same as b) for the test simulation. Green marks PSCs mainly composed of NAT, with more than 50 % of total HNO_3 in NAT and less than 10 % in STS; Red PSCs with high STS content, more than 50 % of HNO_3 in STS and less than 10 % in NAT; and purple mixed PSCs with more than 20 % HNO_3 in NAT and more than 20 % in STS. Solid green line marks T_{NAT} , dashed green line $T_{\text{S_NAT}}$ and solid blue T_{ICE} 45

6.3.	a) Observations of gas-phase HNO_3 by MLS as function of temperature over Antarctica from 1 May to 1 July 2005 for four equivalent latitude regions. b) Condensed HNO_3 assuming no irreversible denitrification. c) Theoretical uptake of HNO_3 by STS. d) Difference of observed HNO_3 removal from the gas-phase and theoretical uptake by STS. Solid line is T_{NAT} , dashed $T_{\text{S_NAT}}$ and dotted T_{ICE}	46
6.4.	a) SD-WACCM reference simulation NO_y as function of temperature over Antarctica from 1 May to 1st July 2005 for four equivalent latitude regions. b) Gas-phase HNO_3 . c) HNO_3 in NAT. d) HNO_3 in STS. Solid line is T_{NAT} , dashed $T_{\text{S_NAT}}$ and dotted T_{ICE}	47
6.5.	a) SD-WACCM test simulation NO_y as function of temperature over Antarctica from 1 May to 1 July 2005 for four equivalent latitude regions. b) Gas-phase HNO_3 . c) HNO_3 in NAT. d) HNO_3 in STS. Solid line is T_{NAT} , dashed $T_{\text{S_NAT}}$ and dotted T_{ICE}	49
6.6.	Observations of gas-phase HNO_3 and modeled partitioning of HNO_3 between the gas-phase and PSCs on 475 K over Antarctica 2005 for four equivalent latitude regions. Dashed line are observations of gas-phase HNO_3 by MLS and solid lines model output from the test simulation. . .	50
6.7.	Vertical distribution of gas-phase HNO_3 over Antarctica 2005 for six different days poleward of 80°S . Solid black lines are MLS measurements, blue lines are the reference simulation and red lines are the test simulation with updated PSC scheme.	51
6.8.	a) All MLS gas-phase H_2O observations on 475 K between 1 May and 1 July 2005 over Antarctica correlated with temperature. b) Reference simulation output on the location of the observations described in a). c) Same as b) for the test simulation. Solid blue line marks T_{ICE}	52
6.9.	a) Observations of gas-phase H_2O by MLS as function of temperature over Antarctica from 1 May to 1 July 2005 for four equivalent latitude regions. b) Condensed H_2O assuming no irreversible dehydration c) SD-WACCM reference gas-phase H_2O d) SD-WACCM H_2O in ice. Solid line is T_{ICE} . . .	53
6.10.	a) SD-WACCM test simulation gas-phase H_2O b) SD-WACCM H_2O in ice. Solid line is T_{ICE}	54

6.11. Vertical distribution of gas-phase H ₂ O over Antarctica 2005 for six different days poleward of 80°S. Solid black lines are MLS measurements, blue lines are the reference simulation and red lines are the test simulation with updated PSC scheme.	55
7.1. Model (solid) and MLS observations (dashed) of gas-phase HCl, HNO ₃ and H ₂ O poleward of 80°S from May through October 2005. Species are normalized to 1st May 2005 values.	59
7.2. Averaged ACE-FTS profiles of HCl (solid), ClONO ₂ (dashed) and N ₂ O ₅ (dotted) between 20th April and 1st May from 2004 to 2011 poleward of 70°S. Grey shading indicates the standard deviation.	61
7.3. BASE simulation (left) and observed (right) gas-phase HCl over Antarctica 2005 on 475 K. The white circles mark noontime solar zenith angles of 95° and 90°, respectively.	62
7.4. Gas-phase HCl observations by MLS and chlorine partitioning for the BASE and H _{HCl} case for four equivalent latitude regions on 475 K.	64
7.5. Gas-phase HCl observations by MLS and chlorine partitioning for the BASE and J _{HNO₃(c)} case for four equivalent latitude regions on 475 K.	67
7.6. Fraction of total HCl condensed in STS as a function of ambient water vapor and temperature.	68
7.7. a) MLS gas-phase HCl as function of temperature for May and June 2005 Poleward of 80°S. b) Removed gas-phase HCl, HCl ₀ is defined as the mean between 195-200 K. c) Removed gas-phase HCl that cannot be explained by the reaction with ClONO ₂ . d) Residual of removed gas-phase HCl after H _{HCl} is taken into account. Solid line is T _{NAT} , dashed T _{S,NAT} and dotted T _{ICE}	70
7.8. a) MLS gas-phase HCl for May and June 2005 poleward of 80°S on 475 K, frost point (blue), theoretical uptake of HCl calculated with MLS H ₂ O and HNO ₃ (red). b) gas-phase HCl for the H _{HCl} case (black) and condensed HCl (red).	72
7.9. a) Simulation H _{HCl} -2 K gas-phase HCl as function of temperature for May and June 2005 Poleward of 80°S. b) Removed gas-phase HCl, HCl ₀ is defined as the mean between 195-200 K. c) Condensed phase HCl d) Difference between observations and model (observed minus modeled gas-phase HCl).	74

7.10. Evolution of gas-phase HCl on 475 K poleward of 80°S for different model simulations (BASE, H _{HCl} -2 K and J _{HNO₃(c)} -2 K) and MLS observations.	75
7.11. Distribution of gas-phase HCl over Antarctica 2005 on 475 K for the H _{HCl} -2 K case (left), J _{HNO₃(c)} -2 K case (center) and MLS observations (right). The white circles mark noontime solar zenith angles of 95° and 90°, respectively.	77
7.12. Vertical profiles of modeled and observed ClO (dashed black) for 15th September 2005 for four equivalent latitude bins. BASE case (solid black), H _{HCl} (solid blue), H _{HCl} -2 K (dashed blue) and J _{HNO₃(c)} -2 K (solid red).	78
A.1. Irregular CLaMS grid (left) and regular SD-WACCM grid (right) for gas-phase HCl on 22nd December 2010 on the 475 K isentrope. For CLaMS all air parcels between 470 and 480 K are plotted.	85
A.2. Native MLS data points (left) and the triangulation on a regular grid (right) for gas-phase HCl on 15th June 2005 on 475 K.	86
A.3. All ACE-FTS observations of gas-phase HCl in June (left) and August (right) on 20.5 km.	88

List of Tables

7.1. Overview of model cases and included processes.	60
7.2. Column ozone loss between 350-700 K in Dobson Units between 1st May and 15th October.	79
A.1. Vertical resolution, range and precision for the MLS measured species used in this work.	87

Glossary

ACE – FTS Atmospheric Chemistry Experiment - Fourier Transform Spectrometer.

CALIPSO Cloud-Aerosol Lidar and Infrared Pathfinder Satellite Observations.

CCM Coupled Climate Model.

CFCs chlorofluorocarbons.

CLaMS Chemical Lagrangian Model of the Stratosphere.

ClO_x ClO + 2 · Cl₂O₂.

Cl_y HCl + ClONO₂.

CTM Chemistry Transport Model.

γ uptake coefficient.

GCR Galactic Cosmic Rays.

H_{HCl} solubility of HCl in STS.

HO_x OH + HO₂.

J_{HNO₃(c)} photolysis of condensed phase *HNO*₃.

LIDAR LIght Detection And Ranging.

mix 1 PSCs composed of STS and low number density NAT ($3 \cdot 10^{-4} \text{ cm}^{-3}$ - 10^{-3} cm^{-3}).

mix 2 PSCs composed of STS and high number density NAT ($> 10^{-3} \text{ cm}^{-3}$).

MLS Microwave Limb Sounder.

NAT Nitric Acid Trihydrate.

NO_x $\text{NO} + \text{NO}_2 + \text{NO}_3 + 2 \cdot \text{N}_2\text{O}_5$.

NO_y $\text{NO}_x + \text{HNO}_3 + \text{ClONO}_2 + \text{HCN}$.

Φ equivalent latitude.

PSCs Polar Stratospheric Clouds.

SAD Surface Area Density.

SD – WACCM Specified Dynamics - Whole Atmosphere Community Climate Model.

T_{S,NAT} thermodynamic equilibrium temperature for Nitric Acid Trihydrate particles at a specified supersaturation.

STS Supercooled Ternary Solutions.

T_{ICE} thermodynamic equilibrium temperature for ice particles.

T_{NAT} thermodynamic equilibrium temperature for Nitric Acid Trihydrate particles.

WACCM Whole Atmosphere Community Climate Model.

Bibliography

- Abbatt, J. P. D. and Molina, M. J.: Heterogeneous interactions of ClONO₂ and HCl on nitric acid trihydrate at 202 K, *J. Phys. Chem.*, 96, 7674–7679, doi:10.1021/j100198a036, 1992.
- Abida, O., Mielke, L.-H., and Osthoff, H. D.: Observation of gas-phase peroxyxynitrous and peroxyxynitric acid during the photolysis of nitrate in acidified frozen solutions, *Chem. Phys. Lett.*, 511, 187–192, doi:10.1016/j.cplett.2011.06.055, 2011.
- Bates, D. R. and Nicolet, M.: Atmospheric hydrogen, *Publ. Astron. Soc. Pac.*, 62, 106–110, 1950.
- Bazilevskaya, G., Usoskin, I., Flückiger, E., Harrison, R., Desorgher, L., Bütikofer, R., Krainev, M., Makhmutov, V., Stozhkov, Y., Svirzhevskaya, A., Svirzhevsky, N., and Kovaltsov, G.: Cosmic Ray Induced Ion Production in the Atmosphere, *Space. Sci. Rev.*, 137, 149–173, doi:10.1007/s11214-008-9339-y, 2008.
- Bernath, P. F., McElroy, C., Abrams, M., Boone, C., Butler, M., Camy-Peyret, C., Carleer, M., Clerbaux, C., Coheur, P., Colin, R., DeCola, P., DeMazière, M., Drummond, J., Dufour, D., Evans, W., Fast, H., Fussen, D., Gilbert, K., Jennings, D., Llewellyn, E., Lowe, R., Mahieu, E., McConnell, J., McHugh, M., McLeod, S., Michaud, R., Midwinter, C., Nassar, R., Nichitiu, F., Nowlan, C., Rinsland, C., Rochon, Y., Rowlands, N., Semeniuk, K., Simon, P., Skelto, R., Sloan, J., Soucy, M.-A., Strong, K., Tremblay, P., Turnbull, D., Walker, K., Walkty, I., Wardle, D., Wehrle, V., Zander, R., and Zou, J.: Atmospheric Chemistry Experiment (ACE): Mission overview, *Geophys. Res. Lett.*, 32, L15S01, doi:10.1029/2005GL022386, 2005.
- Biele, J., Tsias, A., Luo, B. P., Carslaw, K. S., Neuber, R., Beyerle, G., and Peter, T.: Nonequilibrium coexistence of solid and liquid particles in Arctic stratospheric clouds, *J. Geophys. Res.*, 106, D19, doi:10.1029/2001JD900188, 2001.

- Brakebusch, M., Randall, C. E., Kinnison, D. E., Tilmes, S., Santee, M. L., and Manney, G. L.: Evaluation of Whole Atmosphere Community Climate Model simulations of ozone during Arctic winter 2004-2005, in preparation, 2012.
- Cappa, C. D., Wilson, K. R., Messer, B. M., Saykally, R. J., and Cohen, R. C.: Optical cavity resonances in water micro-droplets: Implications for shortwave cloud forcing, *Geophys. Res. Lett.*, 31, L10205, doi:10.1029/2004GL019593, 2004.
- Carslaw, K. S. and Peter, T.: Uncertainties in reactive uptake coefficients for solid stratospheric particles - 1. Surface chemistry, *Geophys. Res. Lett.*, 24, 1743–1746, 1997.
- Carslaw, K. S., Luo, B. P., Clegg, S. L., Peter, T., Brimblecombe, P., and Crutzen, P. J.: Stratospheric aerosol growth and HNO₃ gas phase depletion from coupled HNO₃ and water uptake by liquid particles, *Geophys. Res. Lett.*, 21, 2479–2482, 1994.
- Carslaw, K. S., Clegg, S. L., and Brimblecombe, P.: A thermodynamic model of the system HCl-HNO₃-H₂SO₄-H₂O, including solubilities of HBr, from <200 to 328 K, *J. Phys. Chem.*, 99, 11 557–11 574, doi:10.1021/j100029a039, 1995a.
- Carslaw, K. S., Luo, B., and Peter, T.: An analytic expression for the composition of aqueous HNO₃-H₂SO₄ stratospheric aerosols including gas phase removal of HNO₃, *Geophys. Res. Lett.*, 22, 1887–1880, 1995b.
- Carslaw, K. S., Wirth, M., Tsias, A., Luo, B. P., Dörnbrack, A., Leutbecher, M., Volkert, H., Renger, W., Bacmeister, J. T., and Peter, T.: Particle microphysics and chemistry in remotely observed mountain polar stratospheric clouds, *J. Geophys. Res.*, 103(D5), 5785–5796, doi:10.1029/97JD03626, 1998.
- Carslaw, K. S., Kettleborough, J. A., Northway, M. J., Davies, S., Gao, R., Fahey, D. W., Baumgardner, D. G., Chipperfield, M. P., and Kleinböhl, A.: A vortex-scale simulation of the growth and sedimentation of large nitric acid hydrate particles, *J. Geophys. Res.*, 107, 8300–8418, 2002.
- Chapman, S.: On ozone and atomic oxygen in the upper atmosphere, *Philosophical Magazine*, 10, 369–383, 1930.
- Considine, D. B., Douglass, A. R., Connell, P. S., Kinnison, D. E., and Rotman, D. A.: A polar stratospheric cloud parameterization for the global modeling initiative three-

- dimensional model and its response to stratospheric aircraft, *J. Geophys. Res.*, 105, 3955–3973, 2000.
- Cox, R. A., MacKenzie, A. R., Müller, R. H., Peter, T., and Crutzen, P. J.: Activation of stratospheric chlorine by reactions in liquid sulphuric acid, *Geophys. Res. Lett.*, 21, 1439–1442, 1994.
- Crutzen, P.: Albedo Enhancement by Stratospheric Sulfur Injections: A Contribution to Resolve a Policy Dilemma?, *Climatic Change*, 77, 211–220, doi:10.1007/s10584-006-9101-y, 2006.
- Crutzen, P. J.: The influence of nitrogen oxides on the atmospheric ozone content, *Q.J.R. Meteorol. Soc.*, 96, 320–325, doi:10.1002/qj.49709640815, 1970.
- Curtius, J., Weigel, R., Vössing, H.-J., Wernli, H., Werner, A., Volk, C.-M., Konopka, P., Krebsbach, M., Schiller, C., Roiger, A., Schlager, H., Dreiling, V., and Borrmann, S.: Observations of meteoric material and implications for aerosol nucleation in the winter Arctic lower stratosphere derived from in situ particle measurements, *Atmos. Chem. Phys.*, 5, 3053–3069, doi:10.5194/acp-5-3053-2005, 2005.
- Davies, S., Chipperfield, M. P., Carslaw, K. S., Sinnhuber, B.-M., Anderson, J. G., Stimpfle, R. M., Wilmouth, D. M., Fahey, D. W., Popp, P. J., Richard, E. C., von der Gaathen, P., Jost, H., and Webster, C. R.: Modeling the effect of denitrification on Arctic ozone depletion during winter 1999/2000, *J. Geophys. Res.*, 107, 10.1029/2001JD000445, 2003.
- Davies, S., Mann, G. W., Carslaw, K. S., Chipperfield, M. P., Remedios, J. J., Allen, G., Waterfall, A. M., Spang, R., and Toon, G. C.: Testing our understanding of Arctic denitrification using MIPAS-E satellite measurements in winter 2002/2003, *Atmos. Chem. Phys.*, 6, 3149–3161, 2006.
- Dee, D. P., Uppala, S. M., Simmons, A. J., Berrisford, P., Poli, P., Kobayashi, S., Andrae, U., Balmaseda, M. A., Balsamo, G., Bauer, P., Bechtold, P., Beljaars, A. C. M., van de Berg, L., Bidlot, J., Bormann, N., Delsol, C., Dragani, R., Fuentes, M., Geer, A. J., Haimberger, L., Healy, S. B., Hersbach, H., Hólm, E. V., Isaksen, L., Kållberg, P., Köhler, M., Matricardi, M., McNally, A. P., Monge-Sanz, B. M., Morcrette, J.-J., Park, B.-K., Peubey, C., de Rosnay, P., Tavolato, C., Thépaut, J.-N., and Vitart, F.: The ERA-Interim reanalysis: configuration and performance of

- the data assimilation system, *Q.J.R. Meteorol. Soc.*, 137, 553–597, doi:10.1002/qj.828, 2011.
- Deshler, T.: A Review of Global Stratospheric Aerosol: Measurements, Importance, Life Cycle, and Local Stratospheric Aerosol, *Atmos. Res.*, 90, 223–232, 2008.
- Dominé, F. and Shepson, P. B.: Air-Snow Interactions and Atmospheric Chemistry, *Science*, 297, 1506–1510, doi:10.1126/science.1074610, 2002.
- Douglass, A. R., Schoeberl, M. R., Stolarski, R. S., Waters, J. W., Russell III, J. M., Roche, A. E., and Massie, S. T.: Interhemispheric differences in springtime production of HCl and ClONO₂ in the polar vortices, *J. Geophys. Res.*, 100, 13 967–13 978, doi: 10.1029/95JD00698, 1995.
- Drdla, K. and Müller, R.: Temperature thresholds for chlorine activation and ozone loss in the polar stratosphere, *Ann. Geophys.*, 30, 1055–1073, doi:10.5194/angeo-30-1055-2012, 2012.
- Drdla, K., Turco, R. P., and Elliott, S.: Heterogeneous Chemistry on Antarctic Polar Stratospheric Clouds: A Microphysical Estimate of the Extent of Chemical Processing, *J. Geophys. Res.*, 98, 8965–8981, doi:10.1029/93JD00164, 1993.
- Drdla, K., and R. P. Turco, A. T., Jacobson, M. Z., Dye, J. E., Twohy, C., and Baumgardner, D.: Analysis of the physical state of one arctic polar stratospheric cloud based on observations, *Geophys. Res. Lett.*, 21, 2475–2478, 1994.
- Dye, J. E., Gandrud, B. W., Baumgardner, D., Chan, K. R., Ferry, G. V., Loewenstein, M., Kelly, K. K., and Wilson, J. C.: Observed particle evolution in the polar stratospheric cloud of January 24, 1989, *Geophys. Res. Lett.*, 17, 413–416, 1990.
- Dye, J. E., Baumgardner, D., Gandrud, B. W., Kawa, S. R., Kelly, K. K., Loewenstein, M., Ferry, G. V., Chan, K. R., and Gary, B. L.: Particle size distributions in arctic polar stratospheric clouds, growth and freezing of sulfuric acid droplets, and implications for cloud formation, *J. Geophys. Res.*, 97, 8015–8034, 1992.
- Emmons, L. K., Walters, S., Hess, P. G., Lamarque, J.-F., Pfister, G. G., Fillmore, D., Granier, C., Guenther, A., Kinnison, D. E., Laepple, T., Orlando, J., Tie, X., Tyndall, G., Wiedinmyer, C., Baughcum, S. L., and Kloster, S.: Description and evaluation of the Model for Ozone and Related chemical Tracers, version 4 (MOZART-4), *Geosci. Model Dev.*, 3, 43–67, doi:10.5194/gmd-3-43-2010, 2010.

- Engel, I., Luo, B. P., Hoyle, C. R., Pitts, M. C., Poole, L. R., Grooß, J.-U., and Peter, T.: Heterogeneous formation of polar stratospheric clouds. Part II: Ice nucleation, in preparation, 2012.
- Eyring, V., Sheperd, T. G., and Waugh, D. W.: SPARC report on the evaluation of chemistry-climate models, in: SPARC Rep. No. 5, WRCP-132, WMO-TD No. 1526, p. 434, World Meteorol. Organ., Geneva, 2010.
- Fahey, D. W., Gao, R. S., Carslaw, K. S., Kettleborough, J., Popp, P. J., Northway, M. J., Holecek, J. C., Ciciora, S. C., McLaughlin, R. J., Thompson, T. L., Winkler, R. H., Baumgardner, D. G., Gandrud, B., Wennberg, R. O., Dhaniyala, S., McKinney, K., Peter, T., Salawitch, R. J., Bui, T. P., Elkins, J. W., Webster, C. R., Atlas, E. L., Jost, H., Wilson, J. C., Herman, R. L., Kleinböhl, A., and von König, M.: The detection of large HNO₃-containing particles in the winter Arctic stratosphere, *Science*, 291, 1026–1031, doi:10.1126/science.1057265, 2001.
- Farman, J., Gardiner, B. G., and Shanklin, J. D.: Large losses of total ozone in Antarctica reveal seasonal ClO_x/NO_x interaction, *Nature*, 315, 207–210, 1985.
- Feng, W., Chipperfield, M. P., Davies, S., Mann, G. W., Carslaw, K. S., Dhomse, S., Harvey, L., Randall, C., and Santee, M. L.: Modelling the effect of denitrification on polar ozone depletion for Arctic winter 2004/2005, *Atmos. Chem. Phys.*, 11, 6559–6573, doi:10.5194/acp-11-6559-2011, 2011.
- Froidevaux, L., Jiang, Y. B., Lambert, A., Livesey, N. J., Read, W. G., Waters, J. W., Fuller, R. A., Marcy, T. P., Popp, P. J., Gao, R. S., Fahey, D. W., Jucks, K. W., Stachnik, R. A., Toon, G. C., Christensen, L. E., Webster, C. R., Bernath, P. F., Boone, C. D., Walker, K. A., Pumphrey, H. C., Harwood, R. S., Manney, G. L., Schwartz, M. J., Daffer, W. H., Drouin, B. J., Cofield, R. E., Cuddy, D. T., Jarnot, R. F., Knosp, B. W., Perun, V. S., Snyder, W. V., Stek, P. C., Thurstans, R. P., and Wagner, P. A.: Validation of Aura Microwave Limb Sounder HCl measurements, *J. Geophys. Res.*, 113, D15S25, doi:10.1029/2007JD009025, 2008.
- Garcia, R. R., Marsh, D., Kinnison, D. E., Boville, B., and Sassi, F.: Simulation of secular trends in the middle atmosphere, 1950-2003, *J. Geophys. Res.*, 112, D09301, doi:10.1029/2006JD007485.
- Goff, J. A. and Gratch, S.: Low-pressure properties of water from -160 to 212 F, in: *F. Trans. Am. Soc. Heating Air-Cond. Eng.*, vol. 52, pp. 95–122, 1946.

- Groß, J.-U. and Müller, R.: Simulation of ozone loss in Arctic winter 2004/2005, *Geophys. Res. Lett.*, 34, L05 804, doi:10.1029/2006GL028901, 2007.
- Groß, J.-U., Günther, G., Konopka, P., Müller, R., McKenna, D. S., Stroh, F., Vogel, B., Engel, A., Müller, M., Hoppel, K., Bevilacqua, R., Richard, E. and Webster, C. R., J. W. Elkins, Hurst, D. F., Romashkin, P. A., and Baumgardner, D. G.: Simulation of ozone depletion in spring 2000 with the Chemical Lagrangian Model of the Stratosphere (CLaMS), *J. Geophys. Res.*, 107, 8295, doi:10.1029/2001JD000456, 2002.
- Groß, J.-U., Günther, G., Müller, R., Konopka, P., Bausch, S., Schlager, H., Voigt, C., Volk, C. M., and Toon, G. C.: Simulation of denitrification and ozone loss for the Arctic winter 2002/2003, *Atmos. Chem. Phys.*, 5, 1437–1448, 2005.
- Groß, J.-U., Brautzsch, K., Pommrich, R., Solomon, S., and Müller, R.: Stratospheric ozone chemistry in the Antarctic: what determines the lowest ozone values reached and their recovery?, *Atmos. Chem. Phys.*, 11, 12 217–12 226, doi:10.5194/acp-11-12217-2011, 2011.
- Hanson, D. R.: Reaction of ClONO₂ with H₂O and HCl in sulfuric acid and HNO₃/H₂SO₄/H₂O mixtures, *J. Phys. Chem. A*, 102, 4794–4807, doi:10.1021/jp972767s, 1998.
- Hanson, D. R. and Lovejoy, E. R.: Heterogeneous Reactions in Liquid Sulfuric Acid: HOCl + HCl as a Model System, *J. Phys. Chem.*, 100, 6397–6405, doi:10.1021/jp953250o, 1996.
- Hanson, D. R. and Mauersberger, K.: Laboratory studies of the nitric acid trihydrate: Implications for the south polar stratosphere, *Geophys. Res. Lett.*, 15, 855–858, 1988.
- Hanson, D. R. and Ravishankara, A. R.: Reaction of ClONO₂ with HCl on NAT, NAD and frozen sulfuric acid and Hydrolysis of N₂O₅ and ClONO₂ on frozen sulfuric acid, *J. Phys. Chem.*, 97, 12 309–12 319, doi:10.1021/j100149a035, 1993.
- Hanson, D. R., Ravishankara, A. R., and Solomon, S.: Heterogeneous reactions in sulfuric acid aerosols: A framework for model calculations, *J. Geophys. Res.*, 99, 3615–3629, 1994.
- Hofmann, D. J. and Solomon, S.: Ozone destruction through heterogenous chemistry following the eruption of El Chichón, *J. Geophys. Res.*, 94, 5029–5041, 1989.

- Homan, C. D., Volk, C. M., Kuhn, A. C., Werner, A., Baehr, J., Viciani, S., Ulanovski, A., and Ravegnani, F.: Tracer measurements in the tropical tropopause layer during the AMMA/SCOUT-O3 aircraft campaign, *Atmos. Chem. Phys.*, 10, 3615–3627, doi:10.5194/acp-10-3615-2010, 2010.
- Honrath, R. E., Peterson, M. C., Guo, S., Dibb, J. E., Shepson, P. B., and Campbell, B.: Evidence of NO_x production within or upon ice particles in the Greenland snowpack, *Geophys. Res. Lett.*, 26, 695–698, doi:10.1029/1999GL900077, 1999.
- Hoyle, C. R., Engel, I., Luo, B. P., Pitts, M. C., Poole, L. R., Grooß, J.-U., and Peter, T.: Heterogeneous formation of polar stratospheric clouds. Part I: NAT nucleation, in preparation, 2012.
- IPCC; Working Group I: The Physical Science Basis, Cambridge University Press, Cambridge, UK and New York, NY, USA, 2007.
- Jackman, C. H., Frederick, J. E., and Stolarski, R. S.: Production of Odd Nitrogen in the Stratosphere and Mesosphere: An Intercomparison of Source Strengths, *J. Geophys. Res.*, 85, 7495–7505, doi:10.1029/JC085iC12p07495, 1980.
- Johnson, B. R.: Theory of morphology-dependent resonances: shape resonances and width formulas, *J. Opt. Soc. Am. A*, 10, 343–352, doi:10.1364/JOSAA.10.000343, 1993.
- Junge, C. E., Chagnon, C. W., and Manson, J. E.: Stratospheric aerosols, *Journal of Meteorology*, 18, 81–108, 1961.
- Kawa, S. R., Newman, P. A., Lait, L. R., Schoeberl, M. R., Stimpfle, R. M., Kohn, D. W., Webster, C. R., May, R. D., Baumgardner, D., Dye, J. E., Wilson, J. C., Chan, K. R., and Loewenstein, M.: Activation of chlorine in sulfate aerosol as inferred from aircraft observations, *J. Geophys. Res.*, 102, 3921–3933, 1997.
- Kawa, S. R., Stolarski, R. S., Newman, P. A., Douglass, A. R., Rex, M., Hofmann, D. J., Santee, M. L., and Frieler, K.: Sensitivity of polar stratospheric ozone loss to uncertainties in chemical reaction kinetics, *Atmos. Chem. Phys.*, 9, 8651–8660, 2009.
- Kelly, K. K., Tuck, A. F., Murphy, D. M., Proffitt, M. H., Fahey, D. W., Jones, R. L., McKenna, D. S., Loewenstein, M., Podolske, J. R., Strahan, S. E., Ferry, G. V., Chan, K. R., Vedder, J. F., Gregory, G. L., Hynes, W. D., McCormick, M. P.,

- Browell, E. V., and Heidt, L. E.: Dehydration In The Lower Antarctic Stratosphere During Late Winter And Early Spring, 1987, *J. Geophys. Res.*, 94, 11 317–11 357, doi:10.1029/JD094iD09p11317, 1989.
- Khosrawi, F., Urban, J., Pitts, M. C., Voelger, P., Achtert, P., Kaphlanov, M., Santee, M. L., Manney, G. L., Murtagh, D., and Fricke, K.-H.: Denitrification and polar stratospheric cloud formation during the Arctic winter 2009/2010, *Atmos. Chem. Phys.*, 11, 8471–8487, doi:10.5194/acp-11-8471-2011, 2011.
- Kinnison, D. E., Brasseur, G. P., Walters, S., Garcia, R. R., Marsh, D. R., Sassi, F., Harvey, V. L., Randall, C. E., Emmons, L., Lamarque, J. F., Hess, P., Orlando, J. J., Tie, X. X., Randel, W., Pan, L. L., Gettelman, A., Granier, C., Diehl, T., Niemeier, U., and Simmons, A. J.: Sensitivity of chemical tracers to meteorological parameters in the MOZART-3 chemical transport model, *J. Geophys. Res.*, 112, D20302, doi:10.1029/2006JD007879, 2007.
- Konopka, P., Steinhorst, H.-M., Groöß, J.-U., Günther, G., Müller, R., Elkins, J. W., Jost, H.-J., Richard, E., Schmidt, U., Toon, G., and McKenna, D. S.: Mixing and ozone loss in the 1999-2000 Arctic vortex: Simulations with the three-dimensional Chemical Lagrangian Model of the Stratosphere (CLaMS), *J. Geophys. Res.*, 109, 10.1029/2003JD003792, doi:D02315, 2004.
- Koop, T., Biermann, U. M., Raber, W., Luo, B. P., Crutzen, P. J., and Peter, T.: Do stratospheric aerosol droplets freeze above the ice frost point?, *Geophys. Res. Lett.*, 22, 917–920, doi:10.1029/95GL00814, 1995.
- Kunz, A., Pan, L., Konopka, P., Kinnison, D. E., and Tilmes, S.: Chemical and dynamical discontinuity at the extratropoical tropopause based on START08 and WACCM analysis, *J. Geophys. Res.*, 116, D24302, doi:10.1029/2011JD016686, 2011.
- Lamarque, J.-F., Emmons, L. K., Hess, P. G., Kinnison, D. E., Tilmes, S., Vitt, F., Heald, C. L., Holland, E. A., Lauritzen, P. H., Neu, J., Orlando, J. J., Rasch, P., and Tyndall, G.: CAM-chem: Description and evaluation of interactive atmospheric chemistry in CESM, *Geosci. Model Dev.*, 5, 369–411, doi:10.5194/gmd-5-369-2012, 2012.
- Lambert, A., Read, W. G., Livesey, N. J., Santee, M. L., Manney, G. L., Froidevaux, L., Wu, D. L., Schwartz, M. J., Pumphrey, H. C., Jimenez, C., Nedoluha, G. E., Cofield, R. E., Cuddy, D. T., Daffer, W. H., Drouin, B. J., Fuller, R. A., Jarnot, R. F.,

- Knosp, B. W., Pickett, H. M., Perun, V. S., Snyder, W. V., Stek, P. C., Thurstans, R. P., Wagner, P. A., Waters, J. W., Jucks, K. W., Toon, G. C., Stachnik, R. A., Bernath, P. F., Boone, C. D., Walker, K. A., Urban, J., Murtagh, D., Elkins, J. W., and Atlas, E.: Validation of the Aura Microwave Limb Sounder middle atmosphere water vapor and nitrous oxide measurements, *J. Geophys. Res.*, 112, D24S36, doi:10.1029/2007JD008724, 2007.
- Lambert, A., Santee, M. L., Wu, D. L., and Chae, J. H.: A-train CALIOP and MLS observations of early winter Antarctic polar stratospheric clouds and nitric acid in 2008, *Atmos. Chem. Phys.*, 12, 2899–2931, doi:10.5194/acp-12-2899-2012, 2012.
- Lien, C.-Y., Lin, W.-Y., Chen, H.-Y., Huang, W.-T., Jin, B., Chen, I.-C., and Lin, J. J.: Photodissociation cross sections of ClOOCl at 248.4 and 266 nm, *J. Chem. Phys.*, 131, 174301, doi:10.1063/1.3257682, 2009.
- Lowe, D. and MacKenzie, A. R.: Polar stratospheric cloud microphysics and chemistry, *J. Atmos. Solar-Terr. Phys.*, 70, 13–40, 2008.
- Luo, B. P., Voigt, C., Fueglistaler, S., and Peter, T.: Extreme NAT supersaturations in mountain wave ice PSCs: A clue to NAT formation, *J. Geophys. Res.*, 108, doi:10.1029/2002JD003104, 2003.
- Mahieu, E., Duchatelet, P., Demoulin, P., Walker, K. A., Dupuy, E., Froidevaux, L., Randall, C., Catoire, V., Strong, K., Booner, C. D., Bernath, P. F., Blavier, J.-F., Blumenstock, T., Coffey, M., Maziere, M. D., Griffith, D., Hannigan, J., Hase, F., Jones, N., Jucks, K. W., Kagawa, A., Kasai, Y., Mebarki, Y., Mikuteit, S., Nassar, R., Notholt, J., Rinsland, C. P., Robert, C., Schrems, O., Senten, C., Smale, D., Taylor, J., Tetard, C., Toon, G. C., Warneke, T., Wood, S. W., Zander, R., and Servais, C.: Validation of ACE-FTS v2.2 measurements of HCl, HF, CCl₃F and CCl₂F₂ using space-, balloon- and ground-based instrument observations, *Atmos. Chem. Phys.*, 8, 6199–6221, 2008.
- Manney, G. L., Santee, M. L., Rex, M., Livesey, N. J., Pitts, M. C., Veefkind, P., Nash, E. R., Wohltmann, I., Lehmann, R., Froidevaux, L., Poole, L. R., Schoeberl, M. R., Haffner, D. P., Davies, J., Dorokhov, V., Gernandt, H., Johnson, B., Kivi, R., Kyro, E., Larsen, N., Levelt, P. F., Makshtas, A., McElroy, C. T., Nakajima, H., Parrondo, M. C., Tarasick, D. W., von der Gathen, P., Walker, K. A., and Zi-

- noviev, N. S.: Unprecedented Arctic ozone loss in 2011, *Nature*, 478, 469–475, doi:doi:10.1038/nature10556, 2011.
- Marsh, D. R., Garcia, R. R., Kinnison, D. E., Boville, B. A., Walters, S., Matthes, K., and Solomon, S.: Modeling the whole atmosphere response to solar cycle changes in radiative and geomagnetic forcing, *J. Geophys. Res.*, 112, D23306, doi:10.1029/2006JD008306, 2007.
- Marti, J. and Mauersberger, K.: A survey and new measurements of ice vapor pressure at temperatures between 170 and 250K, *Geophys. Res. Lett.*, 20, 363–366, doi:10.1029/93GL00105, 1993.
- Matthey, R., Cacciani, M., Fiocco, G., Martinez, A. A., Martucci, G., Mitev, V., Pace, G., and Stefanutti, L.: Observations of aerosol and clouds with the ABLE and MAL lidars during the mid-latitude and Arctic ENVISAT validation campaigns, in: *European Rocket and Balloon Programmes and Related Research*, edited by Warmbein, B., vol. 530, pp. 579–584, ESA Special Publication, 2003.
- Mayer, B. and Madronich, S.: Actinic flux and photolysis in water droplets: Mie calculations and geometrical optics limit, *Atmos. Chem. Phys.*, 4, 2241–2250, doi:10.5194/acp-4-2241-2004, 2004.
- McElroy, M. B., Salawitch, R. J., Wofsy, S. C., and Logan, J. A.: Reductions of Antarctic ozone due to synergistic interactions of chlorine and bromine, *Nature*, 321, 759–762, doi:10.1038/321759a0, 1986.
- McKenna, D. S., Grooß, J.-U., Günther, G., Konopka, P., Müller, R., Carver, G., and Sasano, Y.: A new Chemical Lagrangian Model of the Stratosphere (CLaMS): 2. Formulation of chemistry scheme and initialization, *J. Geophys. Res.*, 107, 4256, doi:10.1029/2000JD000113, 2002a.
- McKenna, D. S., Konopka, P., Grooß, J.-U., Günther, G., Müller, R., Spang, R., Offermann, D., and Orsolini, Y.: A new Chemical Lagrangian Model of the Stratosphere (CLaMS): 1. Formulation of advection and mixing, *J. Geophys. Res.*, 107, 4309, doi:10.1029/2000JD000114, 2002b.
- Molina, J. M. and Rowland, F. S.: Stratospheric sink for chlorofluoromethanes: Chlorine-catalyzed destruction of ozone, *Nature*, 249, 810–812, 1974.

- Molina, L. T. and Molina, M. J.: Production of Cl_2O_2 from the self-reaction of the ClO radical, *J. Phys. Chem.*, 91, 433–436, doi:10.1021/j100286a035, 1987.
- Müller, R. and Crutzen, P. J.: A possible role of Galactic Cosmic Rays in chlorine activation during polar night, *J. Geophys. Res.*, 98, 20 483–20 490, doi:10.1029/93JD02455, 1993.
- Müller, R., Peter, T., Crutzen, P. J., Oelhaf, H., Adrian, G. P., v. Clarmann, T., Wegner, A., Schmidt, U., and Lary, D.: Chlorine chemistry and the potential for ozone depletion in the arctic stratosphere in the winter of 1991/1992, *Geophys. Res. Lett.*, 21, 1427–1430, 1994.
- Murphy, D. M. and Koop, T.: Review of the vapour pressures of ice and supercooled water for atmospheric applications, *Q. J. R. Meteorol. Soc.*, 131, 1539–1565, doi: 10.1256/qj.04.94, 2005.
- Murphy, D. M. and Thomson, D. S.: Halogen ions and NO^+ in the mass spectra of aerosols in the upper troposphere and lower stratosphere, *Geophys. Res. Lett.*, 27, 3217–3220, 2000.
- Newman, P. A., Oman, L. D., Douglass, A. R., Fleming, E. L., Frith, S. M., Hurwitz, M. M., Kawa, S. R., Jackman, C. H., Krotkov, N. A., Nash, E. R., Nielsen, J. E., Pawson, S., Stolarski, R. S., and Velders, G. J. M.: What would have happened to the ozone layer if chlorofluorocarbons (CFCs) had not been regulated?, *Atmos. Chem. Phys.*, 9, 2113–2128, doi:10.5194/acp-9-2113-2009, 2009.
- Nicolet, M.: On the production of nitric oxide by cosmic rays in the mesosphere and stratosphere, *Planet. Space Sci*, 23, 637–649, doi:10.1016/0032-0633(75)90104-X, 1975.
- Nissenon, P., Knox, C. J. H., Finlayson-Pitts, B. J., Phillips, L. F., and Dabdub, D.: Enhanced photolysis in aerosols: evidence for important surface effects, *Phys. Chem. Chem. Phys.*, 8, 10.1039/B609219E, 2006.
- Peter, T.: Microphysics and heterogeneous chemistry of polar stratospheric clouds, *Annu. Rev. Phys. Chem.*, 49, 785–822, 1997.
- Peter, T. and Grooß, J. U.: Polar Stratospheric Clouds and Sulfate Aerosol Particles: Microphysics, Denitrification and Heterogeneous Chemistry, chap. 4, RSC Publishing, Cambridge, 2012.

- Pitts, M. C., Poole, L. R., and Thomason, L. W.: CALIPSO polar stratospheric cloud observations: second-generation detection algorithm and composition discrimination, *Atmos. Chem. Phys.*, 9, 7577–7589, 2009.
- Pitts, M. C., Poole, L. R., Dörnbrack, A., and Thomason, L. W.: The 2009-2010 Arctic polar stratospheric cloud season: a CALIPSO perspective, *Atmos. Chem. Phys.*, 11, 2161–2177, doi:10.5194/acp-11-2161-2011, 2011.
- Plenge, J., Kühl, S., Vogel, B., Müller, R., von Hobe, M., Flesch, R., and Rühl, R.: Bond Strength of Chlorine Peroxide, *J. Phys. Chem. A*, 109, 6730–6734, doi:10.1021/jp044142h, 2005.
- Portmann, R. W., Solomon, S., Garcia, R. R., Thomason, L. W., Poole, L. R., and McCormick, M. P.: Role of aerosol variations in anthropogenic ozone depletion in the polar regions, *J. Geophys. Res.*, 101(D17), 22 991–23 006, 1996.
- Rex, M., Salawitch, R. J., Deckelmann, H., von der Gathen, P., Harris, N. R. P., Chipperfield, M. P., Naujokat, B., Reimer, E., Allaart, M., Andersen, S. B., Bevilacqua, R., Braathen, G. O., Claude, H., Davies, J., Backer, H. D., Dier, H., Dorokhov, V., Fast, H., Gerding, M., Godin-Beekmann, S., Hoppel, K., Johnson, B., Kyrö, E., Litynska, Z., Moore, D., Nakane, H., Parrondo, M. C., Jr., A. D. R., Skrivankova, P., Stübi, R., Viatte, P., Yushkov, V., and Zerefos, C.: Arctic winter 2005: Implications for stratospheric ozone loss and climate change, *Geophys. Res. Lett.*, 33, L23808, doi:10.1029/2006GL026731, 2006.
- Richards, N. K., Wingen, L.-M., Callahan, K. M., Nishino, N., Kleinman, M. T., Tobias, D. J., and Finlayson-Pitts, B. J.: Nitrate Ion Photolysis in Thin Water Films in the Presence of Bromide Ions, *J. Phys. Chem. A*, 115, 5810–5821, doi:10.1021/jp109560j, 2011.
- Rienecker, M. M., Suarez, M. J., Gelaro, R., Todling, R., Bacmeister, J., Liu, E., Bosilovich, M. G., Schubert, S. D., Takacs, L., Kim, G.-K., Bloom, S., Chen, J., Collins, D., Conaty, A., da Silva, A., Gu, W., Joiner, J., Koster, R. D., Lucchesi, R., Molod, A., Owens, T., Pawson, S., Pegion, P., Redder, C. R., Reichle, R., Robertson, F. R., Ruddick, A. G., Sienkiewicz, M., and Woollen, J.: MERRA: NASA's Modern-Era Retrospective Analysis for Research and Applications, *J. Climate*, 24, 3624–3648, doi:10.1175/JCLI-D-11-00015.1, 2011.

- Robinson, G. N., Worsnop, D. R., Jayne, J. T., Kolb, C. E., Swartz, E., and Davidovits, P.: Heterogeneous uptake of HCl by sulfuric acid solutions, *J. Geophys. Res.*, 103, 25 371–25 381, 1998.
- Rodriguez, J. M., Ko, M. K. W., and Sze, N. D.: Antarctic chlorine chemistry: Possible global implications, *Geophys. Res. Lett.*, 15, 257–260, 1988.
- Sander, S., Friedl, R. R., Golden, D. M., Kurylo, M. J., Moortgat, G. K., Wine, P. H., Ravishankara, A. R., Kolb, C. E., Molina, M. J., Finlyason-Pitts, B. J., Huie, R. E., and Orkin, V. L.: Chemical kinetics and photochemical data for use in atmospheric studies, evaluation number 17, JPL Publication, 10-6, 2006.
- Sander, S., Friedl, R. R., Barker, J. R., Golden, D. M., Kurylo, M. J., Moortgat, G. K., Wine, P. H., Abbatt, J. P. D., Burkholder, J. B., Kolb, C. E., Huie, R. E., and Orkin, V. L.: Chemical kinetics and photochemical data for use in atmospheric studies, evaluation number 15, JPL Publication, 06-2, 2011.
- Santee, M., MacKenzie, I. A., Manney, G. L., Chipperfield, M. P., Bernath, P. F., Walker, K. A., Boone, C. D., Froidevaux, L., Livesey, N. J., and Waters, J. W.: A study of stratospheric chlorine partitioning based on new satellite measurements and modeling, *J. Geophys. Res.*, 113, D12 307, doi:10.1029/2007JD009057, 2008.
- Santee, M. L., Lambert, A., Read, W., Livesey, N., Cofield, R., Cuddy, D., Daffer, W., Drouin, B., Froidevaux, L., Fuller, R., Jarnot, R., Knosp, B., Manney, G., Perun, V., Snyder, W., Stek, P., Thurstans, R., Wagner, P., Waters, J., Muscari, G., de Zafra, R., Dibb, J., Fahey, D. W., Popp, P., Marcy, T., Jucks, K., Toon, G., Stachnik, R., Bernath, P., Boone, C., Walker, K., Urban, J., and Murtagh, D.: Validation of the Aura Microwave Limb Sounder HNO₃ measurements, *J. Geophys. Res.*, 112, D24S40, doi:10.1029/2007JD008721, 2007a.
- Santee, M. L., Lambert, A., Read, W. G., Livesey, N. J., Manney, G. L., Cofield, R. R., Cuddy, D. T., Daffer, W. H., Froidevaux, L., Fuller, R. A., Jarnot, R. F., Knosp, B. W., Perun, V. S., Snyder, W. V., Stek, P. C., Thurstans, R. P., Wagner, P. A., Waters, J. W., Connor, B., Urban, J., Murtagh, D., Ricaud, P., Barret, B., Kleinböhl, A., J. K., Küllmann, H., von Hobe, M., Toon, G. C., and Stachnik, R. A.: Validation of the Aura Microwave Limb Sounder ClO measurements, *J. Geophys. Res.*, 113, D15S22, doi:10.1029/2007JD008762, 2007b.

- Shi, Q., Davidovits, P., Jayne, J. T., Worsnop, D. R., and Kolb, C. E.: Uptake of Gas-Phase Ammonia. 1. Uptake by Aqueous Surfaces as a Function of pH, *J. Phys. Chem.*, 14, 10.1021/jp991696p, 1999.
- Shi, Q., Jayne, T., Kolb, C. E., Worsnop, D. R., and Davidovits, P.: Kinetic model for reaction of ClONO₂ with H₂O and HCl and HOCl with HCl in sulfuric acid solutions, *J. Geophys. Res.*, 106, 24 259–24 274, 2001.
- Shur, G. N., Yushkov, V. A., Drynkov, A. V., Fadeeva, G. V., and Potertikova, G. A.: Study of Thermodynamics of the Stratosphere at High Latitudes of the Northern Hemisphere on the M- 55 Geofizika Flying Laboratory, *Russ. Meteorol. Hydrol.*, 8, 43–53, 2006.
- Solomon, S.: Stratospheric ozone depletion, A review of concepts and history, *Rev. Geophys.*, 37, 275–316, 1999.
- Solomon, S., Garcia, R. R., Rowland, F. S., and Wuebbles, D. J.: On the depletion of Antarctic ozone, *Nature*, 321, 755–758, 1986.
- Solomon, S., Portmann, R. W., Garcia, R. R., Thomason, L. W., Poole, L. R., and McCormick, M. P.: The role of aerosol variations in anthropogenic ozone depletion at northern midlatitudes, *J. Geophys. Res.*, 101, 6713–6727, doi:10.1029/95JD03353, 1996.
- Solomon, S., Daniel, J. S., Neely III, R. R., Vernier, J.-P., Dutton, E. G., and Thomason, L. W.: The Persistently Variable "Background" Stratospheric Aerosol Layer and Global Climate Change, *Science*, 333, 866–870, doi:10.1126/science.1206027, 2011.
- Song, N.: Freezing temperatures of H₂SO₄/HNO₃/H₂O mixtures: Implications for polar stratospheric clouds, *Geophys. Res. Lett.*, 21, 2709–2712, doi:10.1029/94GL02459, 1994.
- Spang, R., Remedios, J. J., Tilmes, S., and Riese, M.: MIPAS observation of polar stratospheric clouds in the Arctic 2002/2003 and Antarctic 2003 winters, *Adv. Space Sci.*, 36, 868–878, doi:10.1016/j.asr.2005.03.092, 2005.
- Stolarski, R. S., Krueger, A. J., Schoeberl, M. R., McPeters, R. D., Newman, P. A., and Alpert, J. C.: Nimbus 7 satellite measurements of the springtime Antarctic ozone decrease, *Nature*, 322, 808–811, 1986.

- Sumińska-Ebersoldt, O., Lehmann, R., Wegner, T., Grooß, J.-U., Hösen, E., Weigel, R., Frey, W., Griessbach, S., Mitev, V., Emde, C., Volk, C. M., Borrmann, S., Rex, M., Stroh, F., and von Hobe, M.: ClOOCl photolysis at high solar zenith angles: analysis of the RECONCILE self-match flight, *Atmos. Chem. Phys.*, 12, 1353–1365, doi:10.5194/acp-12-1353-2012, 2012.
- Swartz, E., Shi, Q., Davidovits, P., Jayne, J. T., Worsnop, D. R., and Kolb, C. E.: Uptake of gas-phase ammonia. 2. Uptake by sulfuric acid surfaces, *J. Phys. Chem. A*, 103, 8824–8833, 1999.
- Sweet, M., Kirkham, N., Bendall, M., Currey, L., Bythell, J., and Heupel, M.: Evidence of Melanoma in Wild Marine Fish Populations, *PLoS ONE*, 7, e41989, doi:10.1371/journal.pone.0041989, 2012.
- Tabazadeh, A., Turco, R. P., Drdla, K., Jacobson, M. Z., and Toon, O. B.: A study of type I polar stratospheric cloud formation, *Geophys. Res. Lett.*, 21, 1619–1622, 1994a.
- Tabazadeh, A., Turco, R. P., and Jacobson, M. Z.: A model for studying the composition and chemical effects of stratospheric aerosols, *J. Geophys. Res.*, 99, 12 897–12 914, 1994b.
- Tilmes, S., Kinnison, D. E., Garcia, R. R., Müller, R., Sassi, F., Marsh, D. R., and Boville, B. A.: Evaluation of heterogeneous processes in the polar lower stratosphere in the Whole Atmosphere Community Climate Model, *J. Geophys. Res.*, 112, D24 301, doi:10.1029/2006JD008334, 2007.
- Tilmes, S., Müller, R., Salawitch, R. J., Schmidt, U., Webster, C. R., Oelhaf, H., Camy-Peyret, C. C., and Russell III, J. M.: Chemical ozone loss in the Arctic winter 1991–1992, *Atmos. Chem. Phys.*, 8, 1897–1910, doi:10.5194/acp-8-1897-2008, 2008.
- Vernier, J.-P., Thomason, L. W., Pommereau, J.-P., Bourassa, A., Pelon, J., Garnier, A., Hauchecorne, A., Blanot, L., Trepte, C., Degenstein, D., and Vargas, F.: Major influence of tropical volcanic eruptions on the stratospheric aerosol layer during the last decade, *Geophys. Res. Lett.*, 38, L12807, doi:10.1029/2011GL047563, 2011.
- Vitt, F. M. and Jackman, C. H.: A comparison of sources of odd nitrogen production from 1974 through 1993 in the Earth’s middle atmosphere as calculated using a two-dimensional model, *J. Geophys. Res.*, 101, 6729–6739, doi:10.1029/95JD03386, 1996.

- Voigt, C., Schreiner, J., Kohlmann, A., Zink, P., Mauersberger, K., Larsen, N., Deshler, T., Kröger, C., Rosen, J., Adriani, A., Cairo, F., Di Donfrancesco, G., Viterbini, M., Ovarlez, J., Ovarlez, H., David, C., and Dörnbrack, A.: Nitric Acid Trihydrate (NAT) in Polar Stratospheric Clouds, *Science*, 290, 1756–1758, doi:10.1126/science.290.5497.1756, 2000.
- Voigt, C., Schlager, H., Luo, B. P., Dörnbrack, A., Roiger, A., Stock, P., Curtius, J., Vössing, H., Borrmann, S., Davies, S., Konopka, P., Schiller, C., Shur, G., and Peter, T.: Nitric acid trihydrate (NAT) formation at low NAT supersaturation in polar stratospheric clouds (PSCs), *Atmos. Chem. Phys.*, 5, 1371–1380, 2005.
- von Hobe, M., Ulanovsky, A., Volk, C. M., Groß, J.-U., Tilmes, S., Konopka, P., Günther, G., Werner, A., Spelten, N., Shur, G., Yushkov, V., Ravagnani, F., Schiller, C., Müller, R., and Stroh, F.: Severe ozone depletion in the cold Arctic winter 2004-05, *Geophys. Res. Lett.*, 33, L17815, doi:10.1029/2006GL026945, 2006.
- von Hobe, M., Salawitch, R. J., Canty, T., Keller-Rudek, H., Moortgat, G. K., Groß, J.-U., Müller, R., and Stroh, F.: Understanding the kinetics of the ClO dimer cycle, *Atmos. Chem. Phys.*, 7, 3055–3069, 2007.
- von Hobe, M., Stroh, F., Beckers, H., Benter, T., and Willner, H.: The UV/Vis absorption spectrum of matrix-isolated dichlorine peroxide, ClOOC1, *Phys. Chem. Chem. Phys.*, 11, 1571–1580, 2009.
- Waters, J. W., Froidevaux, L., Harwood, R. S., Jarnot, R. F., Pickett, H. M., Read, W. G., Siegel, P. H., Cofield, R. R., Filipak, M. J., Flower, D. A., Holden, J. R., Lau, G. K., Livesey, N. J., Manney, G. L., Pumphrey, H. C., Santee, M. L., Wu, D. L., Cuddy, D. T., Lay, R. R., Loo, M. S., Perun, C. S., Schwartz, M. J., Stek, P. C., Thurstans, R. P., Boyles, M. A., Chandra, K. M., Chavez, M. C., Chen, G.-S., Chudasama, B. V., Dodge, R., Fuller, R. A., Girard, M. A., Jiang, J. H., Jiang, Y., Knosp, B. W., LaBelle, R. C., Lam, J. C., Lee, K. A., Miller, D., Oswald, J. E., Patel, N. C., Pukala, D. M., Quintero, O., Scaff, D. M., Snyder, W. V., Tope, M. C., Wagner, P. A., and Walch, M. J.: The Earth Observing System Microwave Limb Sounder (EOS MLS) on the Aura Satellite, *IEEE Transactions on Geoscience and Remote Sensing*, 44, doi:10.1109/TGRS.2006.873771, 2006.
- Wegner, T., Groß, J.-U., von Hobe, M., Stroh, F., Sumińska-Ebersoldt, O., Volk, C. M., Hösen, E., Mitev, V., Shur, G., and Müller, R.: Chlorine activation on stratospheric

- aerosols: Uncertainties in parameterizations and surface area, *Atmos. Chem. Phys. Discuss.*, 12, 20 561–20 591, doi:10.5194/acpd-12-20561-2012, 2012a.
- Wegner, T., Kinnison, D. E., Garcia, R. R., Madronich, S., and Solomon, S.: Polar Stratospheric Clouds in SD-WACCM 4, in preparation, 2012b.
- Wegner, T., Kinnison, D. E., Garcia, R. R., Madronich, S., Solomon, S., and von Hobe, M.: On the depletion of HCl in the Antarctic polar vortex, in preparation, 2012c.
- Weigel, R., Hermann, M., Curtius, J., Voigt, C., Walter, S., Böttger, T., Lepukhov, B., Belyaev, G., and Borrmann, S.: Experimental characterization of the COndensation PArticle counting System for high altitude aircraft-borne application, *Atmos. Meas. Tech.*, 2, 243–258, doi:10.5194/amt-2-243-2009, 2009.
- Werner, A., Volk, C. M., Ivanova, E. V., Wetter, T., Schiller, C., Schlager, H., and Konopka, P.: Quantifying transport into the Arctic lowermost stratosphere, *Atmos. Chem. Phys.*, 10, 11 623–11 639, doi:10.5194/acp-10-11623-2010, 2010.
- Wingen, L. M., Moskun, A. C., Johnson, S. N., Thomas, J. L., Roeselová, M., Tobias, D. J., Kleinman, M. T., and Finlayson-Pitts, B. J.: Enhanced surface photochemistry in chloride-nitrate ion mixtures, *Phys. Chem. Chem. Phys.*, 10, 5668–5677, doi:10.1039/b806613b, 2008.
- WMO/ICSU/IOC World Climate Research Programme: Assesment of Stratospheric Aerosol Properties (ASAP), Stratospheric Processes And their Role in Climate (SPARC), Report No. 4, URL <http://www.atmosp.physics.utoronto.ca/SPARC/>, 2006.
- Wolff, M. A., Kerzenmacher, T., Strong, K., Walker, K. A., Toohey, M., Dupuy, E., Bernath, P. F., Boone, C. D., Brohede, S., Catoire, V., von Clarmann, T., Coffey, M., Daffer, W. H., De Mazière, M., Duchatelet, P., Glatthor, N., Griffith, D. W. T., Hannigan, J., Hase, F., Höpfner, M., Huret, N., Jones, N., Jucks, K., Kagawa, A., Kasai, Y., Kramer, I., Küllmann, H., Kuttippurath, J., Mahieu, E., Manney, G., McElroy, C. T., McLinden, C., Mébarki, Y., Mikuteit, S., Murtagh, D., Piccolo, C., Raspollini, P., Ridolfi, M., Ruhnke, R., Santee, M., Senten, C., Smale, D., Tétard, C., Urban, J., and Wood, S.: Validation of HNO₃, ClONO₂, and N₂O₅ from the Atmospheric Chemistry Experiment Fourier Transform Spectrometer (ACE-FTS), *Atmos. Chem. Phys.*, 8, 3529–3562, doi:10.5194/acp-8-3529-2008, 2008.

World Meteorological Organization: Scientific Assessment of Ozone Depletion: 2010, Global Ozone Research and Monitoring Project, Report No. 52, 516 pp., 2011.

Zöger, M., Afchine, A., Eicke, N., Gerhards, M.-T., Klein, E., McKenna, D., Mörschel, U., Schmidt, U., Tan, V., Tuitjer, F., Woyke, T., and Schiller, C.: Fast in situ stratospheric hydrometers: A new family of balloon-borne and airborne Lyman alpha photofragment fluorescence hygrometers, *J. Geophys. Res.*, 104(D1), 1807–1816, 1999.

Danksagung

Hier möchte ich allen Personen, die zum Entstehen dieser Arbeit beigetragen haben, danken.

Marc und Rolf für die Betreuung meiner Arbeit am IEK-7 und Thorsten für seine Bereitschaft, mein Doktorvater an der Universität Wuppertal zu sein.

Martin und Michael danke ich für ihre Gutachtertätigkeit. Michael und seiner Arbeitsgruppe möchte ich auch besonders für ihren HAGAR-Datensatz danken.

Doug möchte ich für meinen Aufenthalt am NCAR und die Bereitstellung der WACCM Simulationen danken.

Jens-Uwe, Susan, Rolando und Sasha danke ich für wertvolle Diskussionen, welche einen erheblichen Beitrag zu dieser Arbeit geleistet haben.

Fred und Olga danke ich für die HALOX Daten.

Dem gesamten RECONICLE Team danke ich für die erfolgreichen Kampagnen.

Dem MLS und ACE-FTS Teams möchte ich für die hochwertigen Satellitendaten danken.

Charlotte und Felix danke ich, dass sie es drei Jahre in einem Büro mit mir ausgehalten haben.

Den Mitarbeitern des IEK-7 und ACD danke ich für die hervorragende Arbeitsatmosphäre.

Für die Finanzierung dieser Arbeit danke ich dem Forschungszentrum Jülich, der Europäischen Kommission und dem Fulbright Programm.

Meinen Eltern und meiner Familie danke ich für die Unterstützung während Studium und Promotion.